Free-Space Optical Communication Systems Over Fading Channels

by

Fan Yang

B.Sc., South China University of Technology, 2010
M.Sc., Southeast University, 2012

A THESIS SUBMITTED IN PARTIAL FULFILLMENT OF
THE REQUIREMENTS FOR THE DEGREE OF

DOCTOR OF PHILOSOPHY

in

The College of Graduate Studies

(Electrical Engineering)

THE UNIVERSITY OF BRITISH COLUMBIA

(Okanagan)

January 2016

Abstract

Free-space optical (FSO) communication systems can provide larger bandwidth and rapid deployment for communication links. Such systems do not interfere with existing radio frequency (RF) systems and can make communication more secure. However, the performance of FSO communication systems is highly dependent on its channel conditions. The atmospheric channels can impose attenuation and scintillation effects on the communication link, and these effects can hinder the correct detection of information on receiver side.

In this thesis, we focus on the performance analysis of terrestrial FSO systems over atmospheric fading channels. One successful channel model to fit the experiment data is the lognormal-Rician model, but its widely adoption is impeded by its analytically intractable probability density function (PDF). Therefore we use Padé approximants method to obtain accurate approximations of the PDF, cumulative density function, and moment generating function of lognormal-Rician distribution. Simple closed-form bit-error rate (BER) expression are obtained for binary phase-shift keying (BPSK) modulation with maximum ratio combining (MRC) reception and for binary differential phase-shift keying (DPSK) with selection combing (SC) reception. Asymptotic error rate analysis for BPSK and DPSK is also presented to reveal the performance behavior in large signal-to-noise ratio regimes.

The pointing error effects in FSO systems can also contribute to channel impairments. In order to study the influence of pointing error on system performance, we propose a statistical model for pointing error with nonzero boresight error, which takes into account of laser beamwidth, detector aperture size, and jitter variance. A novel closed-form PDF is derived for this pointing error model. Furthermore, we obtain closed-form PDF and series PDF, respectively, for the composite lognormal and Gamma-Gamma turbulence channels with nonzero boresight pointing errors. We conduct error rate analysis of on-off keying signaling with intensity modulation and direct detection over the lognormal and Gamma-Gamma fading channels. The BER results are presented in highly accurate converging series. Asymptotic error rate analysis and outage probability of such a system are also presented

based on the derived composite PDFs. It is shown that the boresight error can only affect the coding gain, while the diversity order is determined by either the atmospheric fading effect or the pointing error effect, depending on which effect is more dominant.

For subcarrier intensity modulated FSO systems, the carrier phase estimation error (CPE) would degrade the system performance. We study the BER performance of subcarrier M-ary phase-shift keying systems with carrier phase errors (CPE) in lognormal turbulence channels. The CPE is modeled as a Tikhonov random variable. The CPE induced asymptotic noise reference losses for the studied systems are quantified analytically by introducing the lognormal-Nakagami fading as an auxiliary channel model.

One effective counter fading technique is spatial diversity, which requires multiple apertures at transmitter or receiver side. We first conduct a diversity analysis on single-branch FSO systems over atmospheric fading channels. We find that the diversity order of an FSO system is usually determined by small scale effects in its fading channels when the irradiance fluctuation can be modeled as a modulation process (K, lognormal-Rician, Gamma-Gamma and $\mathcal{M}$ distribution). Based on this observation and the fact that lognormal channel does not have valid diversity order, we propose a lognormal-Nakagami model to facilitate asymptotic analysis on lognormal channels. Using such an approach, we study different multi-branch FSO systems over correlated lognormal fading channels that may have nonidentical variance. We discover that the correlation among the lognormal channels can impose large signal-to-noise ratio (SNR) penalty to system bit-error rate performance, compared to that of a similar system with independent lognormal channels. This property is not shared with the other commonly used fading channels. In addition, we also derive a compact expression for the asymptotic relative diversity order (ARDO) between an L-branch combining system over correlated lognormal channels and a single-branch system. It is found that the ARDO is related to the number of diversity branches as well as entry-wise norm of the covariance matrix of the logarithm of the lognormal channel states. While maximal ratio combing (MRC), equal gain combining (EGC) and selection combining (SC) result in the same ARDO, we find that the coding gain difference between MRC and EGC is negligible, but SC suffers a $10\log(L)$ dB loss.

Preface

This thesis is based on the research work conducted in the School of Engineering at UBC Okanagan campus under the supervision of Dr. Julian Cheng.

Chapter 4 of this thesis is partially published in J5 and C4. In these publications, I proposed the research topic and conducted all the analysis and simulation. Dr. T. A. Tsiftsis helped with proofreading the manuscript.

Chapter 5 contains a part of the results in J2. In this journal paper, I conducted the system performance analysis and evaluation on asymptotic performance loss between binary phase-shift keying and quadrature phase-shift keying modulation scheme. Dr. X. Song established the system model and performed the analytical analysis and numerical evaluation of the system performance. In Chapter 5 of this thesis, we generalize the analysis to M-ary phase-shift keying.

Refereed Journal Publications

J1. B. Zhu, **F. Yang**, J. Cheng and L. Wu, "Performance Bounds for Diversity Receptions Over Arbitrarily Correlated Nakagami-m Fading Channels," Accepted for publication in *IEEE Trans. Wireless Commun.*, 2015.

J2. X. Song, **F. Yang**, J. Cheng, N. Al-Dhahir, and Z. Xu, "Subcarrier Phase-Shift Keying Systems With Phase Errors in Lognormal Turbulence Channels," *IEEE/OSA J. Lightwave Technol.*, vol.33, pp. 1896-1904, May 2015. (Part of Chapter 5)

J3. X. Song, **F. Yang**, J. Cheng, and M.-S. Alouini, "Asymptotic SER Performance Comparison of MPSK and MDPSK in Wireless Fading Channels," *IEEE Wireless Commun. Lett.*, vol. 4, pp. 18-21, Feb. 2015.

J4. X. Song, **F. Yang**, J. Cheng, and M.-S. Alouini, "BER of Subcarrier MPSK/MDPSK Modulated OWC Systems in Gamma-Gamma Turbu-

lence," *IEEE/OSA J. Lightwave Technol.*, vol. 33, no. 1, pp. 161-170, Jan. 2015.

J5. **F. Yang**, J. Cheng, and T. A. Tsiftsis, "Free-Space Optical Communication With Nonzero Boresight Pointing Errors," *IEEE Trans. Commun.*, vol. 62, pp. 713-725, Feb. 2014. (Part of Chapter 4)

J6. X. Song, **F. Yang**, and J. Cheng, "Subcarrier Intensity Modulated Optical Wireless Communications in Atmospheric Turbulence with Pointing Errors," *IEEE/OSA J. Opt. Commun. Netw.*, vol. 5, pp. 349-358, Apr. 2013.

J7. **F. Yang** and J. Cheng, "Coherent Free-Space Optical Communications in Lognormal-Rician Turbulence," *IEEE Commun. Lett.*, vol. 16, pp. 1872-1875, Nov. 2012. (Part of Chapter 3)

Refereed Conference Publications

C1. **F. Yang** and J. Cheng, "Recent Results on Correlated Lognormal Fading Channels," Accepted for publication in *International Conference on Computing, Networking and Communications (ICNC)*, 2015. (Part of Chapter 6)

C2. B. Zhu, **F. Yang**, J. Cheng and L. Wu, "Performance Bounds for MRC and SC Over Nakagami-m Fading Channels With Arbitrary Correlation," Accepted for publication in *International Conference on Computing, Networking and Communications (ICNC)*, 2015.

C3. X. Song, **F. Yang**, J. Cheng, and M.-S. Alouini, "Subcarrier MPSK/MDPSK Modulated Optical Wireless Communications in Lognormal Turbulence," *Proceedings of 2015 IEEE Wireless Communications and Networking Conference (WCNC)*, New Orleans, LA, Mar. 9-12, 2015.

C4. **F. Yang**, J. Cheng, and T. A. Tsiftsis, "Free-Space Optical Communications With Generalized Pointing Errors," *Proceedings of the IEEE International Conference on Communications (ICC)*, Budapest, Hungary, June 9-13, 2013. (Part of Chapter 4)

C5. X. Song, **F. Yang**, and J. Cheng, "Subcarrier BPSK Modulated FSO Communications With Pointing Errors," *Proceedings of the IEEE Wireless Communications and Networking Conference (WCNC)*, Shanghai, China, Apr. 7-10, 2013.

Refereed Journal Publications (submitted)

SJ1. **F. Yang** and J. Cheng, "Asymptotic Performance Analysis of Free-Space Optical Communication over Correlated Lognormal Channels," Submitted to *IEEE Trans. Wireless Commun.*, 2015. (Part of Chapter 6)

Table of Contents

List of Tables

List of Figures

List of Acronyms

ARDO Asymptotic Relative Diversity Order

AWGN Additive White Gaussian Noise

BER Bit-Error Rate

BPSK Binary Phase-Shift Keying

CDF Cumulative Distribution Function

CPE Carrier Phase Error

DPSK Differential Phase-Shift Keying

EGC Equal Gain Combining

FSO Free-Space Optical

i.i.d. Independent and Identically Distributed

IM/DD Intensity Modulation with Direct Detection

LOS Line-of-Sight

MGF Mmoment Generating Function

MIMO Multiple-Input Multiple-Output

MPSK M-ary Phase-Shift Keying

MRC Maximum Ratio Combining

OOK On-Off Keying

PA Padé Approximants

PDF Probability Density Function

PPM Pulse Position Modulation

RF	Radio Frequency
RV	Random Variable
SC	Selection Combinig
SIM	Subcarrier Intensity Modulation
SNR	Signal-to-Noise Ratio

List of Symbols

Symbols	Definitions
$\Re[\cdot]$	The real part of a complex quantity
j	$j^2 = -1$
$\triangle f$	Effective noise bandwidth of a receiver
σ_R^2	The Rytov variance
C_n^2	The index of refraction structure parameter
σ_{si}^2	The scintillation index
$\Gamma(\cdot)$	The Gamma function
$K_\nu(\cdot)$	The modified Bessel function of the second kind of order ν
$E[\cdot]$	The statistical expectation operation
$\delta(\cdot)$	The Dirac delta function
$p!$	The factorial of a positive integer p
$\mathbb{Z}$	The set of all integers
$\mathcal{M}_R(\cdot)$	The moment generating function of a RV R
$\text{erfc}(x)$	The complementary error function
$Q(x)$	The Gaussian Q-function
$I_\nu(\cdot)$	The modified Bessel function of the first kind with order ν
$M_{u,v}(\cdot)$	The Whittaker function
$\log(\cdot)$	The log function with base 10
$\text{erf}(\cdot)$	The Gauss error function
$\binom{N}{n}$	The generalized binomial coefficient

$(\cdot)_i$	The Pochhammer symbol standing for a falling factorial
$\mathbb{R}$	The set of all real numbers
$\Pr[\cdot]$	The probability of an event
$\Im\{\cdot\}$	The imaginary part of a complex quantity
$\lvert\cdot\rvert$	The absolute value of the argument
$\lfloor\cdot\rceil$	The nearest integer to the argument
$x * y$	The convolution of x and y

Acknowledgements

I want to express my deepest gratitude to my supervisor Dr. Julian Cheng for his constant guidance and encouragement. I am deeply influenced by his work enthusiasm and scientific rigor.

I want to thank Dr. Hongchuan Yang from University of Victoria for serving as my external examiner. I would also like to thank Dr. Shawn Wang, Dr. Jonathan Holzman, and Dr. Jahangir Hossian for being my committee members. I really appreciate their valuable time. Besides, I would like to give special thanks to Dr. Bingcheng Zhu, Dr. Xuegui Song and Dr. Luanxia Yang for insightful discussions and valuable suggestions on my research work.

Here I would like to thank my fiance Wendi Zhang for accompanying me on my Ph.D. adventure. She helps me restart the journey after detour, and revive my strength after defeat.

I would like to thank my friends who helped me when I was in Kelowna and I miss the fun we had together.

Finally, I would like to thank my parents and grandparents for their unconditional love and support over the years. I would not have made it without them.

To My Parents

Chapter 1

Introduction

1.1 Background and Motivation

Free-space optical (FSO) communication system is a type of communication system that transfers information with a high frequency carrier at optical spectrum. The transmitter launches a narrow beam of light modulated by the signal. Then the light transmits through the atmosphere and is received and detected at the receiver. Such a system has several notable advantages:

- Potentially larger bandwidth than the radio frequency (RF) system
- Narrowness of the transmitted beam for power concentration and secure communication
- Reduced system complexity and easy to deploy

FSO systems have a long history. The first FSO system prototype is the "photophone" built by Alexander Bell and his assistant Charles Tainter on June 21, 1880. In this experiment, Mr. Tainter transmitted a wireless voice telephone message of a 213m distance from the roof of the Franklin School to the window of Bell's laboratory. The modulation of the transmitted light beam was accomplished by a mirror made to vibrate by a person's voice: the very thin mirror would alternate between concave and convex forms, thus focusing or dispersing the light from the light source. The brightness of the transmitted light beam was observed from the location of the receiver; therefore, it is varied in accordance with the audio-frequency variations acting upon the mirror on transmitter side. In 1960s, the invention of lasers boosted the development of FSO systems. However the technology lost its market for civilian uses when optical fiber networks were introduced and widely adopted, and the main applications for FSO system are for military purpose and deep space communication. In late 20th century, the main reason for the recession of FSO market are:

- Existing radio frequency (RF) systems can handle the demand of user at that time.

- The reliability of FSO system is determined by the atmospheric condition, and it can not be assured under extreme weather conditions.
- The pointing and tracking devices for FSO system add complexity to system design.

Now with the demand for larger bandwidth and rapid deployment, FSO finds its civilian applications. The development of optoelectronics device and extensive research on FSO systems also promotes the FSO technique as an add-on or alternative communication infrastructure to RF system. Many hybrid RF/FSO system are commercially available now. For instance, FSO system are being deployed for ultra low latency networks with high network capacity, and such networks are used in high frequency trading applications [1]. The company Facebook is applying free space optical technology to low orbit satellites and solar powered drones to connect people in developing countries to the internet [2]. The future of FSO systems is bright, while the challenges still remain:

- The atmospherical attenuation can affect the link significantly.
- The high directionality of the transmitted beam requires accurate acquisition and pointing.
- The atmospheric turbulence can degrade the system performance.

The attenuation of FSO channel is determined by the weather condition. At clear weather conditions, the attenuation is approximately 6.5 dB/km, and at a fog event, the attenuation can be 115 dB/km or even 173 dB/km [3]. Therefore the fog can usually cause outage of the FSO system and the link range of FSO is limited.

The scintillation of FSO channel is caused by thermally induced changes in the index of refraction of the air along the transmit path. The time scale of these fluctuations is of the order of milliseconds, approximately equal to the time that it takes a volume of air (having the same size as that of the beam) to move across the path. Therefore the time scale is related to the wind speed [3].

Pointing and alignment can also affect the performance of FSO systems. The narrow beam from transmitter has to be aligned with the receiver for proper detection; otherwise, the link can not be established. A typical FSO transceiver transmits one or more beams of light, each of which is $5 \sim 8$cm in diameter at the transmitter and typically spreads to roughly $1 \sim 5$m in diameter at a range of 1 km and it is important that both the transmitted

beam of light and the receive field of view cone encompass the transceiver at the opposite end of the link [3]. Because of the building sway and beam wander effects, the accurate pointing can not be easily achieved. Active pointing device is usually used for accurate alignment, which greatly increases the cost and complexity of the system. Therefore many FSO systems have relatively wider beam and operate with the initial pointing at first installation time (or requires manual monthly calibration).

The performance of FSO system depends on various system parameters including link range, atmospherical model, transmit power, pointing method, etc. Therefore understanding how these system parameters affect the overall performance of FSO system is critical in FSO system design. Our research will focus on analyzing the effects of different system parameters on the performance of FSO systems. It will include the performance of FSO systems over different fading channels, and the effect of pointing error and phase error on performance of FSO systems.

1.2 Literature Review

FSO communication systems gain much interest because of its capability for meeting the growing demand of high-data-rate connection and its rapid deployment[4]. Some terrestrial FSO products provide data rates on the order of Gbps, which is much greater than those of digital subscriber lines or coaxial cables [5]. Besides, the installation of an FSO system only requires days, making it flexible and effective for deployment. Recently, the applications of FSO communication systems include high data rate hybrid networks (also known as RF/FSO hybrid communication system) for high speed connection, ultra low latency networks for stock market trading [1], and fast deployed network for communication recovery.

The FSO systems can be categorized by two types: intensity modulation with direct detection (IM/DD) systems and coherent systems. In IM/DD system, the lens system and photodetector operate to detect the instantaneous power in the collected field when it arrives the receiver. In coherent systems, the collected field is optically mixed with a local generated field through a front end mirror before the photodetector. The on-off keying (OOK) modulation is widely used for IM/DD FSO systems, since optical communication systems with higher order modulation are complex to implement [6, 7]. In [8], the authors described several communication techniques to mitigate turbulence-induced intensity fluctuations for an IM/DD OOK system. In [9], the building sway problem was studied for an FSO

system with OOK modulation. In [10], the authors presented error rate performance bounds for an OOK FSO communication systems over K fading channels. In [11], the pointing error effect on a OOK FSO system was investigated and a statistical model for pointing error factor was derived. In [7], the author studied a multiple-input multiple-output (MIMO) FSO link over K turbulence channels, and IM/DD with OOK modulation is assumed. In [12], the authors analyzed the performance of an OOK FSO system with Hoyt distributed misalignments. In [13], the authors conducted experimental evaluation of error performance for IM/DD FSO communication links with different modulation schemes, which include OOK, pulse position modulation (PPM) and binary phase-shift keying (BPSK). In coherent FSO systems, the provision of phase information allows a variety of digital modulation formats in comparison to irradiance modulation with direct detection IM/DD. In such systems, the signal can be amplitude, frequency or phase modulated on the optical carrier. The received signals can be made shot-noise-limited through the use of a local oscillator. Such coherent FSO systems offer excellent background noise rejection capability [14], higher sensitivity, and improved spectral efficiency. While there has been a number of studies on IM/DD FSO systems [8], [10], there exists relatively fewer analysis of coherent FSO systems. In [15], Kiasaleh introduced an exact bit-error rate (BER) expression for FSO communication links with differential phase-shift keying (DPSK). Belmonte and Kahn analyzed the performance of M-ary phase-shift keying with lognormal turbulence [16]. In [17], Niu *et al.* analyzed a coherent FSO systems under K-distributed strong turbulence conditions. In [18], Sandalidis *et al.* analyzed a coherent FSO system in the presence of pointing errors.

The main challenge in FSO communication system design is that the deleterious effects in atmospherical channel can severely degrade the performance of such systems. The atmospheric attenuation can sometimes cause outage of an FSO system, which also considerably limits its link range. At clear weather conditions, the atmospheric attenuation is approximately 6.5 dB/km, while the attenuation can be 115 dB/km or even 173 dB/km at a fog event [3]. Therefore many FSO products operate at the link range less than 1km. Another adverse effect in atmospheric channel is scintillation, which is caused by thermally induced changes in the index of refraction of the air along the beam transmit path. As a result, the received irradiance at receiver will randomly fluctuate. Such fluctuation can dramatically degrade the performance of FSO systems [13, 19]. The atmospheric attenuation can be treated as a constant factor under the same weather condition, while the scintillation is considered as a random factor. Therefore we focus our study

on the scintillation effects rather than the attenuation. The scintillation effects can be characterized by many statistical models describing the distribution of channel states. The lognormal distribution is widely accepted to describe weak scintillation, while the negative exponential distribution is used to describe the limiting case of saturated scintillation. The probability density function (PDF) proposed for strong scintillation include the K distribution [20], [21], the lognormally modulated exponential distribution [22], and the generalized Gamma distribution [23], [24]. Furthermore, some universal PDFs, including the $I-K$ distribution [25], [26], the lognormal-Rician distribution [27], and the Gamma-Gamma distribution [28], have been proposed to model both weak and strong scintillation. Among these PDF models, the lognormal-Rician model has excellent agreement with experimental data for both weak and strong scintillation [29]. Despite the practical importance of the lognormal-Rician turbulence channel, there exists few performance study of FSO systems assuming this turbulence model. This is because the lognormal-Rician turbulence model is mathematically intractable. Therefore we propose to provide the engineering and scientific communities with a simple and accurate solution for evaluating the performance of FSO systems under the lognormal-Rician turbulence model.

In addition to the scintillation effects, pointing and alignment can also affect the performance of FSO systems. Because of the building sway and beam wander effects, the accurate pointing cannot be easily achieved. In terrestrial FSO communication systems, the transceivers are often positioned at the top of tall buildings to obtain a line of sight. The building sway, building vibration and thermal expansion of building can result in pointing errors that consist of two components: boresight and jitter. The boresight is the fixed displacement between beam center and center of the detector. Although typical terrestrial FSO systems are initially installed with near zero boresight error, the boresight is still considerable due to the thermal expansion of the building. In [30], the pointing errors are recorded over three days in a $TerraLink$ laser communication system. The radial displacement shows a cyclical pattern every 24 hours, which suggests the thermal expansion of the building plays an important role in pointing errors. The reported boresight can be as high as 0.3mrad [30]. In [31], the values of boresight in the range of $0.0039-0.0117$mrad are used. In [32], the author considered boresight up to 0.03mrad in a horizontal FSO link. The jitter is the random offset of the beam center at detector plane, which is mainly caused by building sway and building vibration. The typical value of jitter standard deviation in a terrestrial FSO system is below 0.3mrad [30]. In [31], the jitter standard deviations of $0.0033-0.0100$mrad are used. In [32], the

author considered jitter standard deviation up to 0.01mrad. In satellite-to-ground and intersatellite communications, the transmitter and receiver have high relative velocity, and there is mechanical noise due to satellite-based motion and gimbal friction [33]. Thus, it is difficult to realize perfect tracking, while jitter and boresight can also arise as residual pointing error. In [9], the author proposed a mathematical model to minimize the transmitter power and the beam divergence angle in an urban optical wireless communication system with pointing errors caused by building sway. In [34], a maximum-likelihood estimator was developed to estimate the boresight and jitter component of the pointing error. In this system model, a point detector and nonzero boresight component are assumed. In a follow-up work [32], the same authors further considered the effects of atmospheric turbulence for the lognormal and Gamma-Gamma fading channels, and they adopted a wave-optics based approach to evaluate the channel capacity. In [11], a statistical pointing error model was proposed by considering the laser beamwidth, jitter variance, and detector size. In this model, a closed-form PDF of the pointing error loss factor was derived by assuming that the pointing error has zero boresight. In [11], the size of detector area was taken into consideration. When the size of the detector area becomes negligibly small, this pointing error loss factor coincides with the one derived for the point detector in earlier works [9], [35]. In [36], the error rate performance of FSO links over K-distributed turbulence channels in the presence of pointing error is studied. The average bit-error rate (BER) is presented in closed-form using the Meijer G-function. In a related work [18], the authors studied the BER performance of a heterodyne differential phase shift keying optical wireless communication system in the presence of pointing error over the Gamma-Gamma turbulence channels. In [37], two optimization models were proposed to mitigate the pointing error effects with zero boresight by taking into account the transmitter power, wavelength, transmitter and receiver telescope gains. In [38], M-ary PPM was investigated with impairments from atmospheric turbulence and pointing error with zero boresight. In [39], asymptotic BER performance is analyzed for FSO communication systems using transmit laser selection over atmospheric turbulence channels with the same pointing error model developed in [11]. A statistical channel model was recently proposed for MIMO FSO communication systems over atmospheric fading channels with pointing errors [40]. Both outage probability and diversity order were studied, and it was found that the diversity order is determined by pointing error effects other than the number of transmitters or receivers. More recently, the pointing error model in [11] was generalized by modeling the radial displacement distance with a Hoyt

or Nakagami-q distribution [12], which allows the horizontal and elevation jitters to have nonidentical jitter standard deviations. The pointing error model developed in [11] is widely used in the literature [18, 36, 38, 39]. In this model, the boresight component of pointing error is assumed to be zero, and both horizontal and elevation displacements are assumed to follow an independent, identically distributed zero-mean Gaussian distribution [35]. As a result, the random radial displacement at the receiver is Rayleigh distributed. While most aforementioned literatures fucus on pointing errors with zero boresight, our proposed study will focus on the effect of nonzero boresight component on performance of terrestrial FSO systems.

Besides the scintillation and pointing error effects, the carrier phase error (CPE) can degrade the performance of an subcarrier intensity modulation (SIM) FSO system. Coherent modulation schemes are usually used for SIM FSO systems, which requires carrier phase recovery for the subcarrier signal [41]. In such system, the received optical intensity is first being converted to electrical signal, then the phase of the modulated signal is being locked/estimated by a phase locked loop (PLL), where there may exist certain errors on the estimated phase. In [42], the error rate performance of an SIM system with DPSK and M-ary phase-shift keying (MPSK) over the lognormal turbulence channels is analyzed. In [43–45], the authors studied BER performance of a BPSK SIM system over lognormal, negative exponential, and Gamma-Gamma fading channels. The BER performance of a BPSK SIM system over K-distributed turbulence channels was studied in [46]. In [47–49], the authors studied the error rate performance of SIM systems with various PSK modulations over different atmospheric turbulence channels. While the above mentioned literatures emphasize on the error rate performance of SIM systems over different atmospheric fading channels, there is few work studying the effect of carrier phase synchronization error on such systems. In fact, there exists certain errors in the carrier phase tracking for SIM systems using coherent modulation. Therefore, we propose to study the BER performance of CPE impaired SIM systems over atmospheric fading channels.

In order to combat scintillation, FSO designers often employ multi-branch reception (or transmitter) diversity technique [50]. Such technique can significantly reduce the probability of system outage caused by deep fading in the channel. Using multiple apertures can also increase the total transmit laser power while guarantee eye safety. Therefore the receiver can obtain higher power which allows the system to operate at higher signal-to-noise ratio or longer transmission distances. Aperture averaging can also be used for fading mitigation when the aperture size is much larger than

the correlation length [5]. However, it is not always feasible to make the aperture large enough, which justifies using spatial diversity at the receiver side [6]. There are several papers discussing the performance of FSO systems using spatial diversity. For examples, the author in [51] analyzed FSO systems with spatial diversity reception over independent and identically distributed (i.i.d.) lognormal fading channels. The system performance was studied under selection combinig (SC) and equal gain combining (EGC) receptions. In [52], the outage probability and the power gain of MIMO FSO systems are derived assuming i.i.d. lognormal fading channels. The performance of FSO channels using spatial diversity was investigated in [53]. The authors adopted i.i.d. lognormal fading channels and compared different reception techniques including aperture averaging, linear combining, and adaptive optics. They found that the maximum ratio combining (MRC) and EGC have similar performance in lognormal fading channels; however, they provided no analytical proof. In [54], the authors studied a MIMO FSO system with repetition Q-ary PPM. Both Rayleigh and lognormal fading models are considered for the system assuming independent fading. The BER for a spatial repetition code was analyzed in [7] for strong atmospheric turbulence. Closed-form expressions for the average BER of single-input multiple-output FSO systems over i.i.d. K-distributed fading channels was obtained. In [40], a generalized statistical model for MIMO FSO channels impaired by atmospheric and misalignment fading was developed. The derived model was then used to study the outage probability and diversity gain of FSO channels over i.i.d. lognormal fading channels. For FSO systems with spatial diversity, channel independence is often desired for optimum performance. The correlation length for such systems can be approximated by $\sqrt{\lambda L}$, where λ denotes the optical carrier's wavelength and L the link distance [6]. In order to guarantee channel independence, the detectors are preferred to be placed as far apart as possible [8]. However, in practice we may not always have sufficient spacing between optical apertures, and usually the receiver apertures are closely placed for better power concentration [51]. Besides, FSO links are highly directive that the channels between the transmitter and receiver are likely to be dependent. Therefore, the FSO systems with spatial diversity will likely experience correlated fading channels [8, 54–56]. As aforementioned, lognormal model is a common fading channel model for FSO systems with short link distance (several hundred meters) or under weak turbulence condition [57]. Lognormal is an important fading model because it fits empirical fading measurements well in many transmission scenarios of practical interest [58]. For example, the lognormal fading can characterize the shadowing effects in outdoor RF communications and

describe indoor radio propagation environments. The lognormal fading is also suitable for describing ultra-wideband channels [59]. The performance of an MIMO FSO system over correlated lognormal fading channels was analyzed in [8]. Assuming identically distributed lognormal channel model, the authors found that the diversity gain will be reduced by correlation when the spacing between receivers is not much greater than the fading correlation length. In order to reduce the diversity gain penalty caused by correlation, the authors further proposed a maximum-likelihood detection scheme for spatial diversity reception. In [6], the authors investigated the BER performance of FSO links with spatial diversity over lognormal atmospheric turbulence fading channels. An approximation for the sum of correlated lognormal random variables was used to study the EGC system over correlated lognormal channels with identical variance. In [55], the authors studied a cooperative diversity FSO system over Rayleigh and lognormal fading channels. They concluded that when the receivers in MIMO FSO systems suffer from correlation, relays can be a practical alternative to achieve full spatial diversity. Diversity analysis of communication systems can give us insights into how the parameters affect system performance over fading channels, and show which parameters dominate the system performance. By conducting diversity analysis, we can usually obtain two system performance metrics: diversity order and coding gain, which can be considered as simple criteria for system optimization [60]. The diversity order[1] will indicate how fast the BER decreases with increasing average signal-to-noise ratio (SNR) in high SNR region, and the coding gain denotes the amount of shift of the BER curve relative to the benchmark curve. There are many prior works conducting diversity analysis on FSO systems over various fading channels [7, 17, 39, 40, 61–63]. A modern FSO system may employ multiple transmitters and receivers at various locations (or multi-hop relays); therefore, the beams may experience different channel conditions. For example, the beams propagating on a horizontal path above a parking lot will experience different amount of fading than those above grass or other terrain. Therefore the terrestrial FSO communication systems employed in urban area may experience different amount of fading on different branches, due to the fact that the beam paths cross complex terrains. Although the beams may be close to each other, the thermal gradient and different wind level on the beam path may cause the beams to have nonidentical distribution. Other

[1]The diversity order used in this paper describes the rate of descending BER with increasing SNR in a loglog plot, which may have different definition with those used in traditional RF field.

examples include systems with closely located beam paths with different link distances, and systems involving relay nodes. Therefore the multiple channels of beams may have nonidentical distribution and be correlated with each other. However, there exists no prior works on diversity analysis of FSO systems over correlated lognormal fading channels with nonidentical distribution.

1.3 Thesis Organization and Contributions

In this thesis, we present the research work conducted on the following four topics:

- Performance of FSO systems over lognormal-Rician channels
- Effect of pointing errors on FSO systems over fading channels
- Effect of phase errors on FSO systems over lognormal channels
- Effect of correlation on FSO systems over lognormal channels

We discuss each topic with one chapter. The summary and contributions of each chapter are as follows.

In Chapter 1, we provide an introduction to FSO communication systems. The history of FSO is also discussed. The challenges in FSO systems are presented and related research works are reviewed.

Chapter 2 presents some background knowledge for the FSO systems studied in this thesis. Two types of FSO systems: Coherent and IM/DD systems, are discussed. We also present the performance factors of an FSO system and introduce atmospheric turbulence channel models including lognormal, Gamma-Gamma and lognormal-Rician fading models. The system model and receiver SNR statistics are also discussed, which will be used by the derivations in subsequent chapters.

In Chapter 3, we analyze the error rate performance of a coherent FSO system over lognormal-Rician turbulence channels. The PDF, cumulative distribution function (CDF) and mmoment generating function (MGF) of lognormal-Rician distributed irradiance are approximated using padé approximants (PA). We obtain highly accurate closed-form approximate BER for BPSK with MRC reception using an MGF approach, and we derive closed-form approximate BERs for DPSK with SC reception using a PDF approximated by PA. We then present an asymptotic error rate analysis to illustrate error rate performance under large SNR condition.

In Chapter 4, we propose a nonzero boresight pointing error model for an FSO system by taking into account of beamwidth, detector aperture, and jitter variance. A closed-form PDF has been derived for the nonzero boresight pointing error model. We derive closed-form composite PDF for the lognormal fading and highly accurate series based PDF for the Gamma-Gamma fading. Highly accurate convergent series BER expressions are obtained. Through the asymptotic BER analysis and numerical results, we observe that the boresight error causes an SNR penalty factor on error rate performance at high SNR. By examining the asymptotic BER curves, we find that the diversity order of the FSO system over the composite lognormal fading channel is solely determined by the pointing error parameter γ^2, and the boresight component does not affect the diversity order. While in the composite Gamma-Gamma fading channel, the diversity order is determined by either the Gamma-Gamma fading effect or the pointing error effect.

In Chapter 5, we study the effects of CPE on a SIM system. The BER performance of such system with M-ary phase-shift keying modulation is investigated under the lognormal turbulence channels. We use the Tikhonov model for CPE with the assumption that the SNR in receiver's PLL is proportional to the instantaneous receiver SNR. Using an auxiliary lognormal-Nakagami fading model, we obtain the CPE induced asymptotic noise reference losses of the FSO system over the lognormal channels.

In Chapter 6, we study a multiple-branch FSO systems over correlated lognormal fading channels. The diversity of FSO systems over composite fading channels is also analyzed, and we find that the diversity of the system is determined by the lowest diversity random variable (RV) in the product form. Based on this observation and the fact that lognormal channel does not have valid diversity order, we propose a lognormal-Nakagami model to facilitate asymptotic analysis on lognormal channels. Using this approach, we study different multi-branch FSO systems over correlated lognormal fading channels that may have nonidentical variance. We discover that the correlation among the lognormal channels can impose large SNR penalty to system BER performance, compared to that of a similar system with independent lognormal channels. This property is not shared with the other commonly used fading channels. In addition, we also derive a compact expression for the asymptotic relative diversity order (ARDO) between an L-branch combining system over correlated lognormal channels and a single-branch system. It is found that the ARDO is related to the number of diversity branches as well as entry-wise norm of the covariance matrix of the logarithm of the lognormal channel states. The derived ARDO can provide FSO system designers with a simple asymptotic performance metric

to allow asymptotic performance comparison between different FSO systems under various lognormal channel conditions. The MRC, EGC and SC combining techniques were also compared in the context of correlated lognormal channels. We found that the MRC and EGC have similar performance but SC suffers a $10\log(L)$dB loss, which suggests that EGC is desirable for multiple-branch FSO systems in terms of better performance and complexity tradeoff.

In Chapter 7, we summarize the works presented in this thesis, and discuss some future research topics that are closely related to the research work in previous chapters.

Chapter 2

Background

In this chapter, we first introduce the general FSO system model. Depending on the receiver structure, we discuss two categories of FSO systems: the IM/DD FSO system and the coherent FSO system. For IM/DD systems, the OOK modulation and SIM modulation are also discussed. Then we provide some basic knowledge on the atmospheric fading effects, and present three widely accepted atmospheric fading channel models. In the end, we discuss three system performance metrics including BER, outage probability and asymptotic BER, which are used for evaluating the performance of FSO systems in following chapters.

2.1 FSO Communication System Model

In an FSO communication system, a laser source first transmits a narrow beam of modulated light at the transmitter. Then the modulated light beam propagates through free space before being received by the receiver. Fig. 2.1 shows a simplified block diagram of such system, which employs two sets of transceivers for a full-duplex link. For communication purpose, the information can be modulated onto the amplitude, frequency, phase or intensity of the optical carrier. The optical carrier is then transmitted through the atmospheric channel. At the receiver, the incident optical field is collected by the lens system, and being converted to electrical signal by the

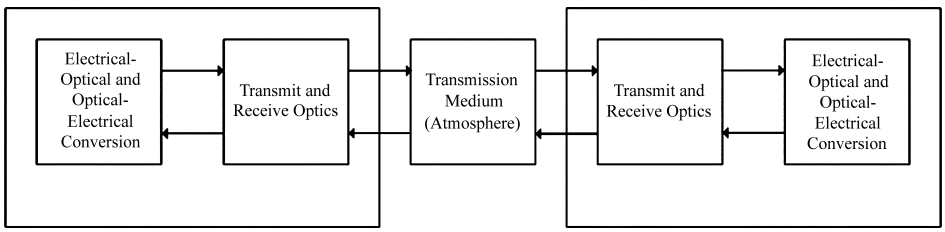

Figure 2.1: Block diagram of an FSO system.

photodetector. The electrical signal is further processed to recover information. Based on the receiver structure, the FSO communication systems can be categorized by two types: IM/DD systems and coherent systems. The receiver of an IM/DD FSO system often consists a power detector that responds only to the instantaneous power of the collected field. Such receiver is used when the signal is intensity modulated at the transmitter end, and it is often called a direct detection receiver. The structure of an intensity modulation transmitter with a direct detection receiver is acronymized as IM/DD. Another type of receiver is the heterodyning receiver used in coherent systems. In such a receiver, the received optical field is mixed with a locally generated field before the photodetector. Heterodyning receiver is used when the signal is amplitude, frequency or phase modulated on the optical carrier at the transmitter end, and it is often called a coherent receiver. The coherent receiver is more complex than the detection receiver, because the coherent receiver requires the local oscillator laser to be tuned to the same frequency and phase as the received carrier.

2.2 IM/DD FSO Systems

An IM/DD FSO system collects the transmitted optical field that is directly imaged through the receiver lens system onto the photodetector. The photodector is a power detecting device, which responds to the instantaneous intensity of the received optical field. At the transmitter, the information can be directly modulated or subcarrier-modulated on the intensity of the optical field. Assuming a turbulence free channel, the received instantaneous intensity can be expressed as

$$I(t) = I_r(1 + km(t)) \tag{2.1}$$

where I_r is the average received intensity, $m(t)$ is the modulating signal and k is a scaling factor. Since the transmitting intensity is a nonnegative quantity, $|km(t)| \leq 1$ is required.

In IM/DD FSO systems, the OOK modulation is widely used because of its simplicity. The modulating signal can be 1 for a logic "on" or -1 for a logic "off" with $k = 1$ [64]. At the nth symbol duration, we have

$$m(t) = \begin{cases} 1, & nT < t < (n+1)T \text{ "on"} \\ -1, & nT < t < (n+1)T \text{ "off"} \end{cases} \tag{2.2}$$

where T denotes the symbol duration.

Another modulation scheme for IM/DD systems is the subcarrier modulation. In such modulation scheme, the modulating signal can have the form

$$m(t) = \Re\left[\left(\sum_i a_i \exp(j(2\pi f_i + \theta_i))\right)\exp(j2\pi f_c)\right] \tag{2.3}$$

where $\Re[z]$ gives the real part of z, a_i, f_i and θ_i respectively denote the amplitude, frequency and phase of ith base band equivalent signal, and f_c is the carrier frequency.

In an IM/DD FSO system, the main noise source are background noise and circuit thermal noise, and we can express the receiver SNR as

$$\gamma = \frac{(RAkI)^2}{(qRN_b + N_c)2\Delta f} = C_s I^2 \tag{2.4}$$

where R denotes the photodetector responsivity, A is the detector area, q is the electronic charge, Δf denotes the noise equivalent bandwidth, N_b and N_c respectively denote the power spectrum density of background noise and circuit thermal noise, and $C_s = \frac{(RA)^2}{(qRN_b+N_c)2\Delta f}$ can be treated as a constant when the system parameters are set.

2.3 Coherent FSO Systems

A coherent FSO system mixes the received optical field with a local field generated by a local oscillator at the photodetector to downconvert the optical carrier to an intermediate frequency carrier. For simplicity, we discuss a coherent FSO system with BPSK modulation. At the photodector, the incident mixed optical field is being detected and a beat term containing both the amplitude and phase of optical carrier and local field is generated

$$i(t) = 2a_L a_s(t) cos((\omega_o - \omega_L)t + \theta_s(t) - \theta_L) \tag{2.5}$$

where $a_s(t)$, ω_o and $\theta_s(t)$ respectively denote the amplitude, frequency and phase of the received optical carrier, a_L, ω_L and θ_L respectively represent the amplitude, frequency and phase of the local field. After the filtering process, the received signal power can be expressed as

$$P_{signal} = E[(Ri(t))^2] = 2R^2 P_L P_s \tag{2.6}$$

where $E[\cdot]$ denotes the expectation, $P_L = a_L^2 A$ is the local field power term, $P_s = E[a_s^2(t)]A$ is the received optical field power term. Considering the

shot noise, background noise and circuit thermal noise, we can express the instantaneous SNR for coherent FSO systems as

$$\gamma = \frac{2R^2 P_L P_s}{2qR\Delta f P_L + 2qR\Delta f N_b + 2\Delta f N_c}. \tag{2.7}$$

In order to suppress the circuit thermal noise, we can use a strong local source with large P_L, and assuming negligible background noise, we can simplify the SNR in (2.7) as

$$\gamma \approx \frac{R}{q\Delta f} P_s = C_c I \tag{2.8}$$

where $C_c = \frac{RA}{q\Delta f}$ is a deterministic value for particular FSO system.

2.4 Atmospheric Turbulence Channel Models

The atmospheric channel can impose attenuation and scintillation effect on the light beam propagating through it.

The attenuation of atmospheric channels is determined by the weather condition. Under clear weather conditions, the attenuation is approximately 6.5 dB/km, and at a fog event, the attenuation can be 115 dB/km or even 173 dB/km [3]. Therefore the fog can usually cause outage of the FSO system and the link range of FSO is limited.

The scintillation effect of atmospheric channels is caused by thermally induced fluctuations in the index of refraction of the air along the transmit path. The time scale of these fluctuations is on the order of milliseconds, approximately equal to the time that takes a volume of air (having the same size as that of the beam) to move across the path. Therefore the time scale is related to the wind speed [3]. We can use scintillation index to describe the strength of turbulence induced fading, which is given as

$$\sigma_{si}^2 = \frac{\mathrm{Var}(I)}{(E[I])^2} = \frac{E(I^2)}{(E[I])^2} - 1. \tag{2.9}$$

The scintillation index is the normalized variance of the intensity and is used as a measure of scintillation. Another parameter related to the strength of the turbulence is Rytov variance, which approaches the scintillation index under weak turbulence conditions

$$\sigma_R^2 = 1.23 k^{7/6} C_n^2 z^{11/6} \tag{2.10}$$

where C_n^2 is the index of refraction structure parameter of atmosphere, $k = 2\pi/\lambda$ is the optical wavenumber with λ being the wavelength, and z denotes the link distance. Depending on the value of Rytov variance, we can approximately categorize the turbulence regime as follows [65]: the weak turbulence regime ($\sigma_R^2 < 0.3$), the moderate turbulence regime ($0.3 \leq \sigma_R^2 < 5$), and the strong turbulence regime ($\sigma_R^2 \geq 5$).

Under different levels of scintillation, there are different statistic models to describe the distribution of channel states. For weak turbulence conditions, the most widely accepted model is lognormal turbulence model. For moderate to strong turbulence conditions, Gamma-Gamma turbulence model is often used (describing a much wider irradiance fluctuations ranges with the K-distributed turbulence model being its special case).

2.4.1 Lognormal Fading Model

Lognormal model is often used for FSO systems with short link distance (several hundred meters) or under weak turbulence conditions [57]. Lognormal is an important fading model because it fits empirical fading measurements well in many transmission scenarios of practical interest [58]. A lognormal RV h has the PDF

$$f_h(h) = \frac{1}{2h\sqrt{2\pi\sigma_X^2}} \exp\left(-\frac{\left(\ln h + 2\sigma_X^2\right)^2}{8\sigma_X^2}\right) \tag{2.11}$$

where σ_X^2 is the log-amplitude variance given by [11]

$$\sigma_X^2 \approx \sigma_R^2/4 = 0.31 k^{7/6} C_n^2 z^{11/6}. \tag{2.12}$$

The parameters of the lognormal fading model can be measured directly for FSO systems [66].

2.4.2 Gamma-Gamma Fading Model

For medium to strong turbulence conditions, we can use the Gamma-Gamma turbulence model to characterize the atmospheric fading. A Gamma-Gamma distributed RV can be constructed by multiplying a Gamma RV with another Gamma RV, which denote, respectively, the fading process caused by small scale and large scale eddies. The PDF of a Gamma-Gamma RV h is given by

$$f_h(h) = \frac{2(\alpha\beta)^{(\alpha+\beta)/2}}{\Gamma(\alpha)\Gamma(\beta)} h^{\frac{\alpha+\beta}{2}-1} K_{\alpha-\beta}\left(2\sqrt{\alpha\beta h}\right) \tag{2.13}$$

where $\Gamma(\cdot)$ is the Gamma function, and $K_{\alpha-\beta}(\cdot)$ is the modified Bessel function of the second kind of order $\alpha - \beta$. The two shaping parameters α and β are directly related to the effective number of large scale cells and small scale cells of the scattering process respectively, and are related to the Rytov variance σ_R^2. Assuming plane wave propagation with negligible inner scale, the parameters α and β are, respectively, given by [28]

$$\alpha = \left[\exp\left(\frac{0.49\sigma_R^2}{(1 + 1.11\sigma_R^{12/5})^{7/6}} \right) - 1 \right]^{-1} \tag{2.14}$$

and

$$\beta = \left[\exp\left(\frac{0.51\sigma_R^2}{(1 + 0.69\sigma_R^{12/5})^{5/6}} \right) - 1 \right]^{-1}. \tag{2.15}$$

2.4.3 Lognormal-Rician Fading Model

Another important turbulence model is lognormal-Rician model [22, 62]. It fits the experimental data better than the Gamma-Gamma model under both weak and strong scintillation. The FSO communication inherently has a line-of-sight (LOS) link; therefore, a Rician model with shadowing is an appropriate channel model. The amplitude PDF of the optical wave at the receiver can be described as

$$p_Z(Z) = \int_0^\infty p(Z|S) p_S(S) dS \tag{2.16}$$

where $p(Z|S)$ represents the Rician PDF conditioned on a shadowing S, which is assumed to be lognormal distributed. Mathematically, it can be shown that

$$Z = RS \tag{2.17}$$

where R and S are, respectively, the Rician and lognormal RV. We let $R = |U_C + U_G|$ and $S = \exp(\chi)$, where U_C is a real deterministic quantity representing the LOS component, U_G is a circular complex Gaussian RV with zero mean, and χ is a real Gaussian RV. The channel gain is given by $h = Z^2$ [67], and it can be expressed as [22]

$$h = |U_C + U_G|^2 \exp(2\chi) \tag{2.18}$$

where $\exp(2\chi)$ is another lognormal RV, and $|U_C + U_G|^2$ is a noncentral chi-square RV with degree of freedom of two. Then the resulting PDF of

channel gain h is known as the lognormal-Rician [22]

$$f_h(h) = \int_0^\infty dz \frac{1+r}{z} \exp\left(-r - \frac{(1+r)h}{z}\right) h_0\left(2\sqrt{h}\sqrt{\frac{r(r+1)}{z}}\right) \times \frac{1}{\sqrt{2\pi}\sigma_z z} \exp\left[-\frac{1}{2}\left(\frac{\ln z + \frac{1}{2}\sigma_z^2}{\sigma_z}\right)^2\right] \tag{2.19}$$

where r is the coherence parameter defined by $r = |U_C|^2/\mathrm{E}[|\mathrm{U_G}|^2]$, σ_z^2 is the variance of the logarithm of the lognormal modulation factor $\exp(2\chi)$, and $I_0(\cdot)$ is the zero-order modified Bessel function of the first kind. The lognormal-Rician is a general scintillation model, and it includes several well-known PDFs as its special cases. For example, when the coherence parameter r approaches infinity, the lognormal-Rician distribution specializes to lognormal distribution, whose MGF does not exist on the domain R, with PDF [29]

$$f_h(h) = \frac{1}{\sqrt{2\pi}\sigma_z h} \exp\left[-\frac{1}{2}\left(\frac{\ln h + \frac{1}{2}\sigma_z^2}{\sigma_z}\right)^2\right]. \tag{2.20}$$

The lognormal-Rician model can also be used to describe strong turbulence when r approaches 0, and the resulting lognormally modulated exponential distribution has the PDF [22], [29]

$$f_h(h) = \frac{1}{\sqrt{2\pi}\sigma_z} \int_0^\infty dz \frac{1}{z^2} \exp\left[-\frac{h}{z} - \frac{1}{2\sigma_z^2}\left(\ln z + \frac{1}{2}\sigma_z^2\right)^2\right]. \tag{2.21}$$

2.5 Error Rate Performance Analysis

The error rate performance analysis is important for FSO system design. It can provide the designers with standard performance metrics of the system, which includes but not limit to the BER, outage probability and asymptotic error rate. For simplicity, we conduct the error rate performance analysis on an IM/DD FSO system with OOK modulation. Since the channel coherence time is on the order of msec and the data rate is assumed to be on the order of Gbps, we can therefore adopt a slow fading channel model. Assuming additive white gaussian noise (AWGN) for the noise source and unit detector responsitivity, we can express the received signal y at the detector as

$$y = hx + n \tag{2.22}$$

where x is the transmit intensity being either 0 or $2P_t$ where P_t is the average transmitted optical power, h is the channel state, n is zero-mean

AWGN with variance σ_n^2. We can express the instantaneous SNR of the system as

$$\gamma = \frac{2P_t^2 h^2}{\sigma_n^2} = \bar{\gamma} h^2 \tag{2.23}$$

where $\bar{\gamma} = \frac{2P_t^2}{\sigma_n^2}$ denotes the average SNR.

2.5.1 Bit Error Rate

Conditioned on the instantaneous SNR, the BER of IM/DD system with OOK modulation is

$$P_e(e|\gamma) = Q\left(\sqrt{\frac{\gamma}{2}}\right) = \frac{1}{2}\text{erfc}\left(\frac{P_t h}{\sqrt{2}\sigma_n}\right) \tag{2.24}$$

where $Q(\cdot)$ is the Gaussian Q-function and $\text{erfc}(\cdot)$ is the complementary error function that has definition $\text{erfc}(x) = \frac{2}{\sqrt{\pi}} \int_x^\infty \exp(-t^2)dt$. The average BER can be obtained as

$$P_e = \int_0^\infty P_e(e|\gamma) f_\gamma(\gamma) dh. \tag{2.25}$$

2.5.2 Outage Probability

We define the outage probability as the probability that the decoding error probability cannot be made arbitrarily small when the transmitter encodes the data at rate R. With channel state h, the outage probability is given as

$$P_{out} = \text{Prob}(\log_2(1 + |h|^2\bar{\gamma}) < R) \tag{2.26}$$

which can be calculated as

$$P_{out} = \int_0^{h_0} f_h(h) dh \tag{2.27}$$

where $h_0 = \sqrt{(2^R - 1)/\bar{\gamma}}$.

2.5.3 Asymptotic Error Rate

At asymptotically high average SNR, average symbol error probability of an uncoded system in fading channels can be accurately approximated as $P_e^\infty = (G_c\bar{\gamma})^{-G_d}$, where G_d is the diversity order indicating how fast the BER decreases with $\bar{\gamma}$ in high average SNR region, and G_c is the coding gain determining the shift of the BER curve in $\bar{\gamma}$ relative to the benchmark curve

$\bar{\gamma}^{-G_d}$. The asymptotic BER P_e^{∞} can reveal the behavior of BER in high average SNR region, which is helpful in conceptual understanding of performance limiting factors in communications over fading channels [60]. The diversity order and coding gain are determined from instantaneous SNR's PDF through its behavior near the origin. When $h \to 0$, the PDF of channel gain can be expanded into power series as [60]

$$f_h(h) = ah^t + g_t(h) \tag{2.28}$$

where $g_t(h)$ satisfies $\lim_{h\to 0} \frac{g_t(h)}{h^t} = 0$. Considering (2.23), the diversity order and coding gain are obtained as [60]

$$G_d = \frac{t+1}{2} \tag{2.29}$$

and

$$G_c = \left(\frac{2^{\frac{t-3}{2}} a \Gamma\left(\frac{t}{2}+1\right)}{\sqrt{\pi}\left(\frac{t+1}{2}\right)} \right)^{-\frac{2}{t+1}}. \tag{2.30}$$

2.6 Summary

In this chapter, we provided essential background knowledge for the rest of the thesis. We first introduced IM/DD and coherent FSO systems, which are adopted as system models in the following chapters. We also presented the atmospheric channel models including lognormal, Gamma-Gamma, lognormal-Rician models. In the end, we discussed the BER, outage probability and asymptotic error rate analysis for the performance study later conducted in this thesis.

Chapter 3

Performance Analysis of FSO Communications over Lognormal-Rician Fading Channels

In this chapter, we study a coherent FSO communication system over the lognormal-Rician turbulence channels. By using PA, we obtain accurate approximations of the PDF, CDF, and MGF of lognormal-Rician distribution. We use the MGF approach to derive a closed-form BER expression for BPSK and DPSK with MRC reception. Asymptotic error rate analysis is also presented to reveal the performance behavior of such systems in large SNR regimes.

3.1 Padé Approximants

The PA method was first introduced to obtain a rational approximation to the power series representation of MGFs in [68]. PA can be used to approximate infinite power series that are either not guaranteed to converge or converge slowly. The approximation is given in terms of a simple rational function of arbitrary numerator and denominator orders. This technique was successfully used in analyzing pre-detection EGC diversity systems in correlated Nakagami-m fading channels [69], and in studying the Weibull fading channels [70]. An accurate approximation of MGF of a RV can be efficiently obtianed using PA, and the process can be encapsulated as follows.

Starting with the definition of MGF of a RV X, $M_X(s) = E[e^{sX}]$, we seek power expansions of $M_X(s)$ around both $s \to 0$ and $s \to \infty$. A PA of

the MGF is then given by [68]

$$P_{(J,K)}^{[A/B]}(s) = \frac{\sum_{i=0}^{A} a_i s^i}{1 + \sum_{i=1}^{B} b_i s^i} \tag{3.1}$$

where the superscripts A and B are, respectively, the specified order for the numerator polynomial and the denominator polynomial in the rational function, and the subscripts J, K are respectively the number of coefficients as $s \to 0$ and $s \to \infty$. When $s \to 0$, we have

$$P_{(J,K)}^{[A/B]}(s) \approx \sum_{i=0}^{J} c_i s^i. \tag{3.2}$$

When $s \to \infty$, we have

$$P_{(J,K)}^{[A/B]}(s) \approx \sum_{i=1}^{K} d_i s^{-i}. \tag{3.3}$$

Typically, we require $A + B = J + K$ [68]. In order to obtain c_i, we can use

$$M_X(s) = \sum_{i=0}^{\infty} \frac{\mu_i}{i!} s^n, s \to 0 \tag{3.4}$$

where μ_i is the ith moment of X. In practice, moments of all orders may not be available or estimated with high accuracy. Therefore a truncated series with only a finite number of N moments is considered

$$M_X(s) = \sum_{i=0}^{N} \frac{\mu_i}{i!} s^i + g_i(s), s \to 0. \tag{3.5}$$

The coefficients d_i in (3.1) can be found by using

$$M_X(s) = \sum_{i=0}^{\infty} \frac{f_X^{(i)}(0)}{s^{i+1}}, s \to \infty \tag{3.6}$$

where the $f_X^{(i)}(0)$ denotes the ith order derivative of the PDF of X evaluated at origin. In practice, the information about the derivative of PDF at origin

can be limited, i.e. with only Mth order derivatives, the truncated series has the form

$$M_X(s) = \sum_{i=0}^{M} \frac{f_X^{(i)}(0)}{s^{i+1}} + o\left(\left(s^{-1}\right)^{i+1}\right), s \to \infty. \tag{3.7}$$

The truncated series in (3.5) and (3.7) respectively define the behavior of the MGF of X for small s and large s.

Matching the powers of s in the left and right hand side of (3.1) gives

$$a_j = \sum_{i=0}^{j} b_i c_{j-i}, \ 0 \le j \le J, \quad \begin{cases} a_j = 0, j > A \\ b_i = 0, i > B \end{cases} \tag{3.8}$$

$$a_{A-l} = \sum_{i=0}^{l} d_{i+1} b_{B-l+i}, \ 0 \le l \le K-1, \quad \begin{cases} a_j = 0, j > A \\ b_i = 0, i > B \end{cases} \tag{3.9}$$

where the values of c_i and d_i can be found in (3.5) and (3.7).

Intuitively, more power series coefficients provide more information at $s \to 0$, then the right tail of PDF is better approximated because the region $s \to 0$ corresponds to $x \to \infty$ in its PDF $f_X(x)$. Likewise, the region $s \to \infty$ corresponds to $x \to 0$, accurate approximation of the PDF $f_X(x)$ near its origin can be obtained by PA. By the theory of asymptotic analysis, we expect excellent estimation of error rates in large SNR regime.

3.2 Approximating PDF and CDF of Output SNR

Recall the discussion in Chapter 2, we can express the output SNR per symbol of a coherent FSO system as [15], [17]

$$\gamma = \frac{RA}{q\Delta f} I = CI \tag{3.10}$$

where $C = \frac{RA}{q\Delta f}$ is a multiplicative constant for a given FSO system. Of importance to the on-going investigation is the fact that the SNR in (3.10) is proportional to I and is independent of the local oscillator power. Without loss of generality we set the constant C to unity. The MGF of the single-branch output SNR, which is proportional to the instantaneous intensity I following lognormal-Rician distribution, can be approximated by PA with

$M_I(s) \approx P_{(J,K)}^{[A/B]}(s)$. The PDF of intensity I can be obtained using inverse Laplace transform

$$f_I(I) = \mathcal{L}^{-1}\left(P_{(J,K)}^{[A/B]}(s)\right). \tag{3.11}$$

To facilitate the inverse Laplace transform on MGF, we can first apply the residue inversion formula on the approximate MGF to obtain

$$M_I(s) \approx P_{(J,K)}^{[A/B]}(s) = \frac{\sum_{i=0}^{A} a_i s^i}{1 + \sum_{i=1}^{B} b_i s^i} = \sum_{k=1}^{B} \frac{\lambda_k}{s + p_k} \tag{3.12}$$

where p_k and λ_k are, respectively, the poles and the direct terms of the partial fraction expansion of $\frac{\sum_{i=0}^{A} a_i s^i}{1+\sum_{i=1}^{B} b_i s^i}$. Then we apply the inverse Laplace transform to obtain the PDF and CDF respectively as

$$f_I(I) = \sum_{k=1}^{B} \lambda_k \exp(-p_k I), \qquad p_k > 0 \tag{3.13}$$

and

$$F_I(I) = 1 - \sum_{k=1}^{B} \frac{\lambda_k}{p_k} \exp(-p_k I). \tag{3.14}$$

3.3 Error Rate Analysis

In this section, we use the approximate PDF, CDF and MGF of intensity I to study the error rate performance of a coherent FSO system with BPSK and DPSK modulation. In order to facilitate our analysis, we further normalize I by setting $E[I] = 1$.

3.3.1 BER for BPSK and DPSK with Spatial Diversity

The average BER over a turbulence channel can be expressed as $P_b = \int_0^\infty P_b(\gamma|I) f(I) dI$, where $P_b(\gamma|I)$ denotes the conditional bit error probability. For coherent BPSK, we have

$$P_b(\gamma|I) = Q(\sqrt{2\gamma}) = Q(\sqrt{2\bar{\gamma} I}). \tag{3.15}$$

For noncoherent DPSK, we have

$$P_b(\gamma|I) = \frac{1}{2}\exp(-\bar{\gamma}I). \tag{3.16}$$

Assuming an FSO link with L receivers, we denote the instantaneous SNR in the lth diversity branch by $\gamma_l, l = 1, 2, \cdots, L$. Since the noise terms in these branches are independent, the SNR at the output of the maximum ratio combiner is

$$\gamma_{MRC} = \sum_{l=1}^{L} \gamma_l = \bar{\gamma} \sum_{l=1}^{L} I_l \tag{3.17}$$

where I_l is the instantaneous received optical intensity in the lth branch. If the turbulence is independent for all L branches, the MGF of γ_{MRC} can be expressed using the approximated MGF of I_l as

$$M_{\gamma_{MRC}}(s) = \prod_{l=1}^{L} M_{I_l}(\bar{\gamma}s). \tag{3.18}$$

The BER for BPSK over i.i.d. turbulence with L branch MRC reception (we can write $M_{I_l} = M_I, l = 1, 2, \cdots, L$) is found to be

$$P_{e,BPSK} = \frac{1}{\pi}\int_0^{\frac{\pi}{2}} \left[M_I\left(-\frac{\bar{\gamma}}{\sin^2\theta}\right)\right]^L d\theta. \tag{3.19}$$

Substituting (3.12) into (3.19), we obtain

$$P_{e,BPSK} \approx \sum_{k=1}^{LB} \frac{\lambda_k}{2p_k}\left(1 - \sqrt{\frac{\bar{\gamma}}{\bar{\gamma} + p_k}}\right) \tag{3.20}$$

where p_k and λ_k are, respectively, the poles and the direct terms of the partial fraction expansion of the MGF of γ_{MRC} in (3.18).

The BER for DPSK over i.i.d. turbulence with L branch SC reception can be obtained as

$$P_{e,DPSK} = \int_0^{\infty} \frac{1}{2}\exp(-\bar{\gamma}I) L\left[F_I(I)\right]^{L-1} f_I(I) dI. \tag{3.21}$$

Substituting (3.13) and (3.14) into (3.21), we have the approximate BER as

$$P_{e,DPSK} \approx \frac{L}{2}\sum_{j=1}^{B}\left(\sum_{n_0+n_1+\cdots+n_B=L-1} \frac{(L-1)!\lambda_j \prod_{k=1}^{B}\left(-\frac{\lambda_k}{p_k}\right)^{n_k}}{\sum_{i=1}^{B}(p_i n_i) + \bar{\gamma} + p_j}\right) \tag{3.22}$$

where p_k and λ_k are, respectively, the poles and the direct terms of the partial fraction expansion of the MGF in (3.12).

3.3.2 Asymptotic Error Rate Analysis

The lognormal-Rician PDF shown in (2.19) has nonzero value at origin

$$f_I(0) = \lim_{I \to 0} f_I(I) = (1 + r) \exp(-r + \sigma_z^2) \tag{3.23}$$

and the first order derivative near origin is

$$f_I'(0) = \lim_{I \to 0^+} f_I'(I) = (r - 1)(1 + r)^2 \exp(-r + 3\sigma_z^2). \tag{3.24}$$

Therefore the Maclaurin series of $f_I(I)$ has the form $f_I(I) = f_I(0) + f_I'(0)I + g_1(I)$. Using (3.23) and (3.24), we can find the diversity order and coding gain in single branch transmission to be

$$\begin{array}{l} G_d = 1, \\ G_c = \frac{2k}{f(0)} \end{array} \tag{3.25}$$

where k is a constant determined by the type of digital modulation scheme (i.e. $k = 2$ for coherent BPSK, $k = 1$ for orthogonal coherent binary frequency shift keying). More generally, we approximate the PDF of output SNR γ_{MRC} with L branch MRC reception as

$$f_{\gamma_{MRC}}(x) = \frac{f_I(0)^L}{(L-1)!} x^{L-1} + g_{L-1}(x) \tag{3.26}$$

where $f_I(0)$ is given in (3.23). The diversity order and coding gain can be, respectively, obtained as

$$G_d = L \tag{3.27}$$

and

$$G_c = k \left[\frac{2^{L-1} [f_I(0)]^L \Gamma(L + 1/2)}{\sqrt{\pi} L!} \right]^{-\frac{1}{L}}. \tag{3.28}$$

Thus the asymptotic BER of coherent BPSK FSO with MRC reception becomes

$$P_{e,asym,BPSK} = \frac{2^{L-1} [f_I(0)]^L \Gamma(L + 1/2)}{\sqrt{\pi} L!} (2\bar{\gamma})^{-L}. \tag{3.29}$$

For noncoherent DPSK with SC reception, the PDF of the output SNR γ_{SC} with L branch SC reception over the lognormal-Rician fading has the form

$$f_{\gamma_{SC}}(x) = L f_I(0)^L x^{L-1} + g_{L-1}(x). \tag{3.30}$$

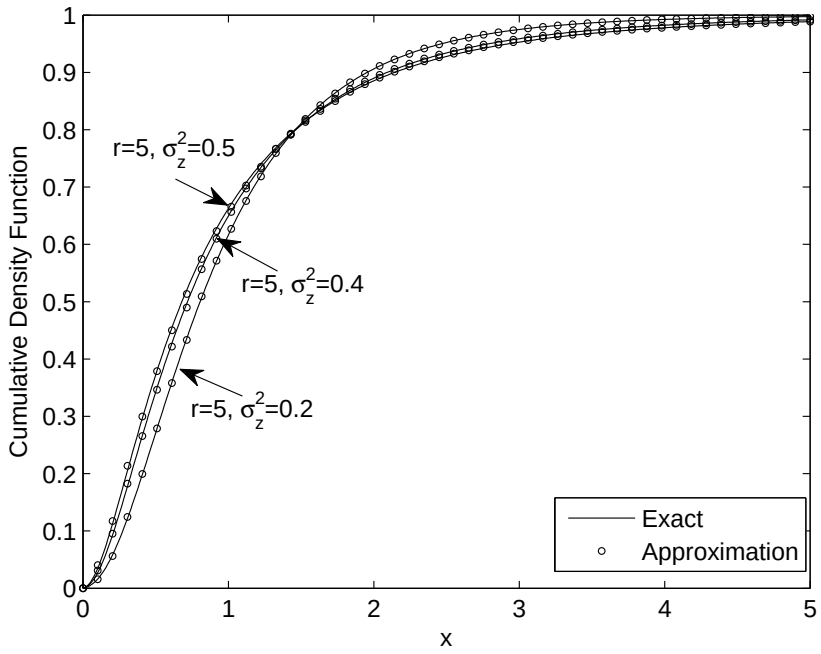

Figure 3.1: The exact and approximate CDF in different lognormal-Rician parameters.

From (3.30), the diversity order and coding gain can be respectively obtained as $G_d = L$ and

$$G_c = \left[\frac{L}{2}[f_I(0)]^L \Gamma(L)\right]^{-\frac{1}{L}}. \tag{3.31}$$

Thus, the corresponding asymptotic error rate at large SNR becomes

$$P_{e,asym,DPSK} = \frac{L}{2}[f_I(0)]^L \Gamma(L)(\bar{\gamma})^{-L}. \tag{3.32}$$

3.4 Numerical Results

In this section we present some numerical study of coherent FSO systems over the lognormal-Rician distributed turbulence. Considering that the higher order derivatives of PDF $f_I^{(i)}(0)$ can be difficult to obtain, we

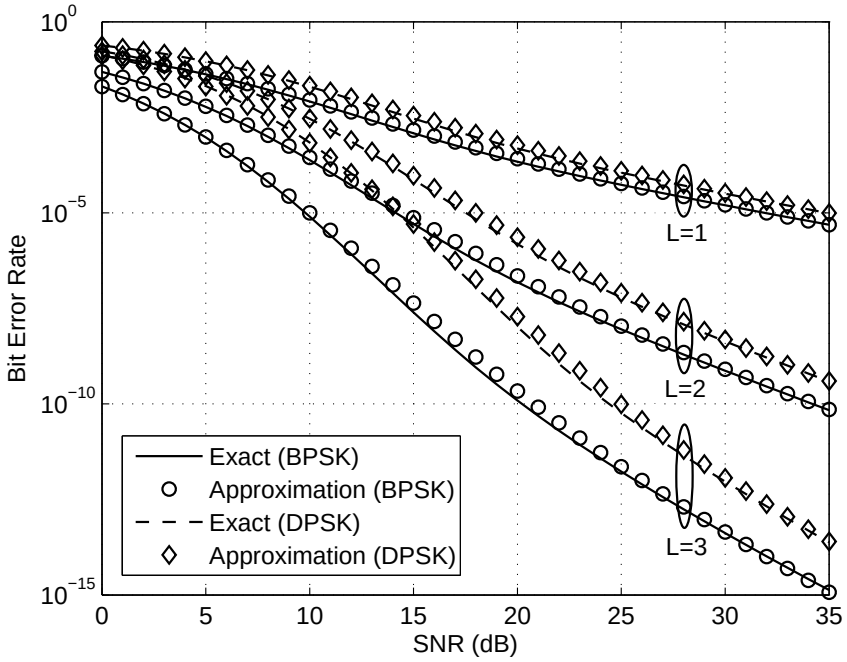

Figure 3.2: The exact and approximate BER of BPSK MRC and BER of DPSK SC ($L = 1, 2, 3$) in lognormal-Rician ($r = 5, \sigma_z^2 = 0.4$) turbulence.

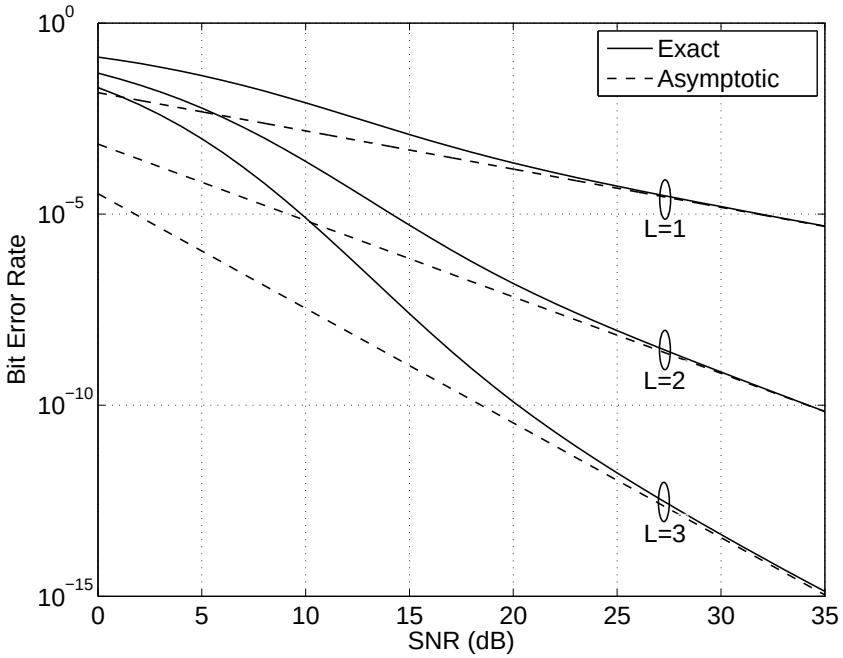

Figure 3.3: Asymptotic error analysis of BPSK over multi-branch MRC ($L = 1, 2, 3$) in lognormal-Rician ($r = 5, \sigma_z^2 = 0.4$) turbulence.

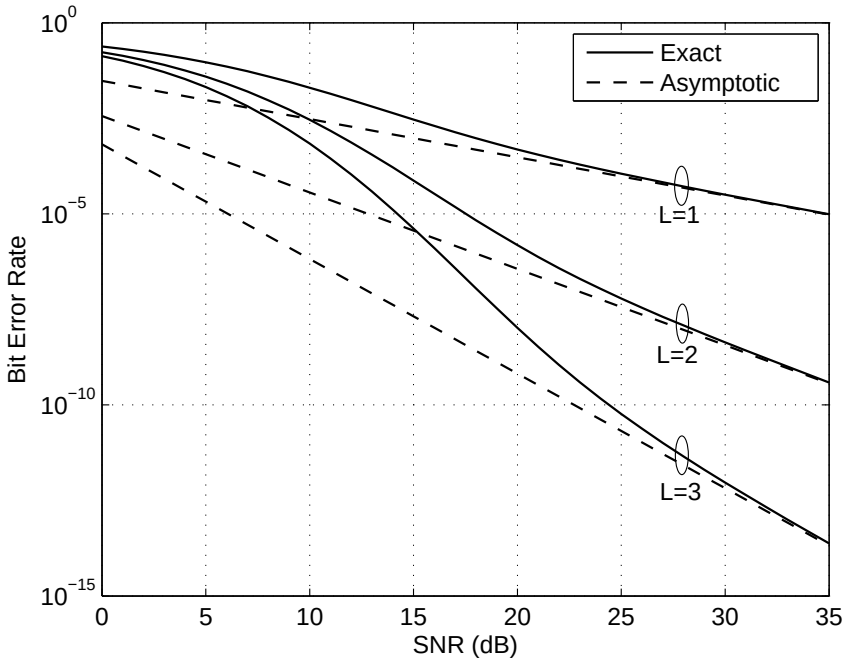

Figure 3.4: Asymptotic error analysis of DPSK over multi-branch SC ($L = 1, 2, 3$) in lognormal-Rician ($r = 5, \sigma_z^2 = 0.4$) turbulence.

choose $K = 1$ in (3.1). Moreover we find that 18 power series coefficients are sufficient to guarantee accuracy. We use the two-point ($s \to 0, s \to \infty$) subdiagonal (i.e., $A = B - 1$) PA with $A = 9, B = 10$, and $A + B - 1 = 18$ power series coefficients in (3.7), i.e. $P^{[9/10]}_{(18,1)}(s)$.

Figure 3.1 plots the exact CDF curve of the output SNR obtained from (2.19) and its approximation obtained from (3.14) under different lognormal-Rician parameter settings. Since the CDF of lognormal-Rician distribution can be sensitive to the parameter σ_z^2, we choose three distinct variance parameters $\sigma_z^2 = 0.2, 0.4, 0.5$ with coherence parameter $r = 5$. It can be seen from Fig. 3.1 that the approximate CDF is highly accurate.

In Fig. 3.2, we present the BER performance of an FSO system over the lognormal-Rician fading channels. The exact BER for BPSK and DPSK are respectively calculated using (3.19) and (3.21) via numerical integrations, while the approximate BER for BPSK and DPSK are respectively estimated using (3.20) and (3.22). We can observe that the approximation is accurate over a wide range of SNR values and it approaches the exact BER curve in large SNR region, which agrees with our expectation.

Figures. 3.3 and 3.4 plot the exact BERs for coherent FSO systems with BPSK MRC reception and with DPSK SC reception. Both figures validate the asymptotic error rates expressions developed in Section 3.3.2. It is interesting to observe that while the diversity order over a lognormal fading channel is undefined, the diversity order of a coherent FSO system in lognormal-Rician fading channel is well defined to be the number of diversity branches.

3.5 Summary

In this chapter, we analyzed the error rate performance of a coherent FSO system over the lognormal-Rician turbulence channels using a PA approach. We obtained closed-form BER expression for BPSK and DPSK FSO systems with MRC reception. Asymptotic error rate analysis is also presented. Our results suggested that PA is a powerful analytical tool for analyzing an optical communication system in a turbulence channel that is mathematically intractable. Our analysis further showed that the PA approach is particularly useful in obtaining highly accurate small error rate estimation.

Chapter 4

FSO Communication with Nonzero Boresight Pointing Error

In this chapter, we study the effect of pointing errors on the performance of FSO communication systems. A statistical model is investigated for pointing errors with nonzero boresight by taking into account the laser beamwidth, detector aperture size, and jitter variance. A novel closed-form PDF is derived for this new nonzero boresight pointing error model. Furthermore, we obtain closed-form PDF for the composite lognormal turbulence channels and finite series approximate PDF for the composite Gamma-Gamma turbulence channels, which are suitable for terrestrial FSO applications impaired by building sway. We conduct error rate analysis of OOK signaling with IM/DD over the lognormal and Gamma-Gamma fading channels. Asymptotic error rate analysis and outage probability of such a system are also presented based on the derived composite PDFs.

4.1 Nonzero Boresight Pointing Errors Model

Assuming AWGN for the thermal/shot noise and unit detector responsitivity, we can express the received signal y at the detector as

$$y = hx + n \tag{4.1}$$

where x is the transmit intensity being either 0 or $2P_t$ where P_t is the average transmitted optical power, h is the channel state, n is zero-mean AWGN with variance σ_n^2. The channel state h can be expressed as $h = h_l h_p h_a$, where h_l represents the path loss which is a constant at given weather condition and link distance, h_p is the pointing error loss factor, and h_a is the atmospheric fading loss factor. Note that pointing error loss factor h_p and atmospheric fading loss factor h_a are both RVs.

4.1.1 Pointing Errors

When a Gaussian beam propagates through distance z from the transmitter to a circular detector with aperture radius a, and the instantaneous radial displacement between the beam centroid and the detector center is r, the fraction of the collected power at receiver can be approximated as [11]

$$h_p(r;z) \approx A_0 \exp\left(-\frac{2r^2}{w_{z_{eq}}^2}\right) \tag{4.2}$$

where A_0 is the fraction of the collected power at $r = 0$, and $w_{z_{eq}}$ is the equivalent beamwidth. We have $A_0 = [\mathrm{erf}(v)]^2$ and $w_{z_{eq}}^2 = w_z^2 \frac{\sqrt{\pi}\mathrm{erf}(v)}{2v\exp(-v^2)}$, where $v = \sqrt{\pi/2}\frac{a}{\omega_z}$ is the ratio between aperture radius and beamwidth, and $\mathrm{erf}(x) = \frac{2}{\sqrt{\pi}}\int_0^x e^{-t^2}dt$ is the error function. The beamwidth w_z can be approximated by $w_z = \theta z$, where θ is the transmit divergence angle describing the increase in beam radius with distance from the transmitter. For example, at a range of 1 km, a 1 mrad divergence produces a beam radius of 1m at receiver. The approximation in (4.2) is accurate when $w_z/a > 6$, which is satisfied in typical terrestrial FSO communication systems.

At the receiver aperture plane, we can express the radial displacement vector as $\mathbf{r} = [r_x, r_y]^T$, where r_x and r_y, respectively, denote the displacements located along the horizontal and elevation axes at the detector plane. We consider a nonzero boresight error in addition to the random jitters, and model r_x and r_y as nonzero mean Gaussian distributed RVs, i.e., $r_x \sim \mathcal{N}(\mu_x, \sigma_x^2)$, $r_y \sim \mathcal{N}(\mu_y, \sigma_y^2)$. Then the radial displacement $r = |\mathbf{r}| = \sqrt{r_x^2 + r_y^2}$ follows the Beckmann distribution [71]

$$\begin{aligned} f_r(r) &= \frac{r}{2\pi\sigma_x\sigma_y} \\ &\times \int_0^{2\pi} \exp\left(-\frac{(r\cos\phi - \mu_x)^2}{2\sigma_x^2} - \frac{(r\sin\phi - \mu_y)^2}{2\sigma_y^2}\right) d\phi. \end{aligned} \tag{4.3}$$

The Beckmann distribution is also known as lognormal-Rician distribution [22, 62], which is used to describe the PDF of fading channels in general. It is a versatile model which applies to a variety of distributions. For examples, it can specialize to Rayleigh when $\mu_x = \mu_y = 0, \sigma_x = \sigma_y$; Rician with $\mu_x^2 + \mu_y^2 \neq 0, \sigma_x = \sigma_y$; Hoyt distribution when $\mu_x = \mu_y = 0, \sigma_x \neq \sigma_y$ [12]; and single-sided Gaussian when $\mu_x = \mu_y = \sigma_x = 0, \sigma_y \neq 0$ [72].

In satellite FSO communication systems, it is widely accepted that the jitter variance is the same for both horizontal and elevation axes [73], [74]. In

terrestrial FSO systems, however, the jitter is mainly caused by turbulence and building motion. Since the turbulence cells randomly appear on the beam path, and the building might be considered to sway in orthogonal and parallel directions to the beam path with equal probabilities, we can therefore assume $\sigma_x^2 = \sigma_y^2 = \sigma_s^2$ [11], [18],[40]. As a result, the PDF of radial displacement r in (4.3) becomes Rician

$$f_r(r) = \frac{r}{\sigma_s^2} \exp\left(\frac{-(r^2+s^2)}{2\sigma_s^2}\right) I_0\left(\frac{rs}{\sigma_s^2}\right) \tag{4.4}$$

where $s = \sqrt{\mu_x^2 + \mu_y^2}$ is the boresight displacement. From (4.2) and (4.4), we derive the PDF of nonzero boresight pointing error as

$$f_{h_p}(h_p) = \frac{\gamma^2 \exp\left(\frac{-s^2}{2\sigma_s^2}\right)}{A_0^{\gamma^2}} h_p^{\gamma^2-1} I_0\left(\frac{s}{\sigma_s^2}\sqrt{\frac{-w_{z_{eq}}^2 \ln\frac{h_p}{A_0}}{2}}\right), \quad 0 \le h_p \le A_0 \tag{4.5}$$

where $\gamma = w_{z_{eq}}/2\sigma_s$ is the ratio between the equivalent beamwidth and jitter standard deviation, which is a measure of the severity of the pointing error effect. If we consider zero boresight error with $s = 0$, our pointing error model in (4.5) specializes to the one in [11]. Our analytical result in (4.5) is accurate when $w_z/a > 6$. In Appendix A, we compare our derived PDF of h_p in (4.5) with the exact PDF, which is obtained numerically, without using (4.2) to show the accuracy of our analytical model. In Appendix B, we derive the moments of h_p as

$$E\left[h_p^n\right] = \frac{A_0^n \gamma^2}{n+\gamma^2} \exp\left(-\frac{n s^2}{(n+\gamma^2)2\sigma_s^2}\right). \tag{4.6}$$

4.1.2 Composite PDF with Generalized Pointing Error

The PDF of channel gain $h = h_l h_p h_a$ can be calculated as [11]

$$\begin{aligned} f_h(h) &= \int f_{h|h_a}(h|h_a) f_{h_a}(h_a) dh_a \\ &= \int \frac{1}{h_a h_l} f_{h_p}\left(\frac{h}{h_a h_l}\right) f_{h_a}(h_a) dh_a. \end{aligned} \tag{4.7}$$

In weak turbulence conditions, we use lognormal fading model to characterize the atmospheric turbulence fading. We substitute (2.11) into (4.7),

and after some mathematical manipulation, the composite PDF of lognormal fading with the pointing error model in (4.5) can be obtained as

$$f_{LN}(h) = \frac{\gamma^2 \exp(u_a)}{2(A_0 h_l)^{\gamma^2}} h^{\gamma^2-1} \text{erfc}\left(\frac{\ln \frac{h}{A_0 h_l} + u_b}{u_c}\right) \tag{4.8}$$

where we have $u_a = \frac{s^2}{\sigma_s^2} + 2\sigma_X^2\gamma^2 + 2\sigma_X^2\gamma^4$, $u_b = \frac{6s^2}{\omega_{z_{eq}}^2} + 2\sigma_X^2 + 4\sigma_X^2\gamma^2$, $u_c = \sqrt{8\left(\frac{4s^2\sigma_s^2}{\omega_{z_{eq}}^4} + \sigma_X^2\right)}$. It is worthy to note that our PDF in (4.8) can specialize to eq. (14) in [11] when we set the boresight to zero ($s = 0$).

Since h_l is a constant, while h_p and h_a are independent RVs, The nth moment of h can be obtained as $E[h^n] = h_l^n E[h_p^n]E[h_a^n]$. With the derived moments for h_p in (4.6) and the moments of the lognormal RV, we have

$$\begin{aligned} E[h^n] =& \frac{(A_0 h_l)^n \gamma^2}{n+\gamma^2} \\ & \times \exp\left(-2\sigma_X^2 n + 2\sigma_X^2 n^2 - \frac{n s^2}{(n+\gamma^2)2\sigma_s^2}\right). \end{aligned} \tag{4.9}$$

For medium to strong turbulence conditions, we model h_a as a Gamma-Gamma distributed RV. After some mathematical derivation shown in Appendix C, we obtain a finite series approximation of the composite PDF as

$$\begin{aligned} & f_{GG}(h) \approx \widetilde{f}_{GG}(h) = \\ & \sum_{j=0}^{J} \left\{ \frac{1}{j!} \left(\frac{\alpha\beta}{A_0 h_l}\right)^j \left(v_j(\alpha,\beta) h^{\beta-1+j} - v_j(\beta,\alpha) h^{\alpha-1+j}\right) \right\} \end{aligned} \tag{4.10a}$$

where

$$\begin{aligned} & v_j(\alpha,\beta) = \\ & \frac{\gamma^2 \pi \left(\frac{\alpha\beta}{A_0 h_l}\right)^\beta \exp\left(-\frac{s^2}{2\sigma_s^2} - \frac{s^2\gamma^2/\sigma_s^2}{2\beta - 2\gamma^2 + 2j}\right) \sin^{-1}((\alpha-\beta)\pi)}{\Gamma(\alpha)\Gamma(\beta)\Gamma(j-(\alpha-\beta)+1)| - (\beta-\gamma^2+j)|} \end{aligned} \tag{4.10b}$$

and $J = \lfloor \gamma^2 - \alpha \rfloor$. Therefore (4.10a) is an approximation[2] of the composite PDF of Gamma-Gamma fading with pointing error. Our composite PDF in (4.10a) is applicable under the condition $\gamma^2 > \alpha$. Using a rough

[2]This finite series approximation is accurate for strong turbulence conditions, but it can be inaccurate for weak turbulence conditions. A large boresight and jitter can also make the series inaccurate.

approximation, we can show that the condition $\gamma^2 > \alpha$ corresponds to $\frac{w_z^2}{4\sigma_s^2} > \max\{6, 2.31\sigma_R^{4/5}\}$. Now we present some examples where this condition holds: When $\sigma_R^2 = 5.0$ and the jitter angle is 0.3mrad, the transmit divergence is larger than 1.28mrad. When $\sigma_R^2 = 25.0$ and the transmit beam divergence is 2mrad, the jitter angle is less than 0.35mrad. In terrestrial FSO systems with link distance less than 5km, the system parameters have the following typical values: $5 \sim 20$cm for the receiver diameter, $2 \sim 10$mrad for the transmit divergence, and $0 \sim 0.3$mrad for the boresight and jitter angle [3, 30]. It can be shown that such systems generally operate under the condition $\gamma^2 > \alpha$. However, in applications with long link range or narrow beam divergence, our PDF in (4.10a) is not applicable since $\gamma^2 > \alpha$ may not hold in such applications. In the rest of this chapter, we assume $\gamma^2 > \alpha$ unless otherwise stated. In (4.10a), the parameters α, β are required to satisfy $(\alpha - \beta) \notin \mathbb{Z}$. When $(\alpha - \beta) \in \mathbb{Z}$, one can add a small value ε to α to satisfy the condition $(\alpha - \beta) \notin \mathbb{Z}$ [61]. The value of ε is empirically chosen, which should be small (i.e. 10^{-3}) that will not change the Gamma-Gamma distribution dramatically. For example, if we have $\alpha = 2.12, \beta = 1.12$, we can add 0.001 to α, and use $\alpha = 2.121$ in the Gamma-Gamma model.

Similar to the moments obtained for composite lognormal channel, using (4.6) and the moments for the Gamma-Gamma RV we can obtain the nth moment of h as

$$E[h^n] = \frac{(A_0 h_l)^n \gamma^2 \Gamma(\alpha + n)\Gamma(\beta + n)}{(n + \gamma^2)\Gamma(\alpha)\Gamma(\beta)(\alpha\beta)^n} \exp\left(-\frac{ns^2}{(n + \gamma^2)2\sigma_s^2}\right). \tag{4.11}$$

4.2 Error Rate Performance

4.2.1 Bit-Error Rate

We derive the average BER of lognormal fading with nonzero boresight pointing error as

$$P_{e,LN} = \frac{\gamma^2 \exp(u_a)}{4(A_0 h_l)^{\gamma^2}} \times \int_0^\infty h^{\gamma^2 - 1} \mathrm{erfc}\left(\frac{\ln \frac{h}{A_0 h_l} + u_b}{u_c}\right) \mathrm{erfc}\left(\frac{P_t}{\sqrt{2}\sigma_n} h\right) dh. \tag{4.12}$$

Using a change of variable rule, eq. (4.12) can be expressed as

$$\begin{aligned} P_{e,LN} &= \frac{\gamma^2 u_c}{4} \exp\left(u_a - \gamma^2 u_b\right) \\ &\times \int_{-\infty}^\infty \exp(\gamma^2 u_c x) \mathrm{erfc}(x) \mathrm{erfc}\left(\frac{P_t A_0 h_l}{\sqrt{2}\sigma_n \exp(u_b - u_c x)}\right) dx. \end{aligned} \tag{4.13}$$

By introducing an auxiliary parameter B and partitioning the integration interval in (4.13) into $[-\infty, B]$ and $[B, \infty]$, we can rewrite (4.13)

$$\begin{aligned} P_{e,LN} =& \frac{\gamma^2 u_c}{4} \exp\left(u_a - \gamma^2 u_b\right) \\ & \times \int_{-\infty}^{B} \exp\left(\gamma^2 u_c x\right) \mathrm{erfc}\left(x\right) \mathrm{erfc}\left(\frac{P_t A_0 h_l}{\sqrt{2}\sigma_n} \exp\left(u_c x - b\right)\right) dx + R_B \end{aligned} \tag{4.14}$$

where R_B is the approximation error given by

$$\begin{aligned} R_B =& \frac{\gamma^2 u_c}{4} \exp\left(u_a - \gamma^2 u_b\right) \\ & \times \int_{B}^{\infty} \exp(\gamma^2 u_c x) \mathrm{erfc}(x) \mathrm{erfc}\left(\frac{P_t A_0 h_l}{\sqrt{2}\sigma_n \exp(u_b - u_c x)}\right) dx. \end{aligned} \tag{4.15}$$

In Appendix D, it is shown that the approximation error R_B can be upper bounded by

$$R_B < \frac{\sqrt{\pi}\gamma^2 u_c}{8} \exp\left(u_a - \gamma^2 u_b + \frac{\gamma^4 u_c^2}{4}\right) \mathrm{erfc}\left(B - \frac{\gamma^2 u_c}{2}\right). \tag{4.16}$$

We quantify R_B under various system parameters and calculate the values of B for different R_B. The results are presented in Appendix D, showing that the approximation error R_B decreases rapidly with increasing B. We can always adjust the value of B to make R_B arbitrarily small. Therefore, eq. (4.14) can be accurately approximated as

$$\begin{aligned} P_{e,LN} \approx \widetilde{P}_{e,LN} =& \frac{\gamma^2 u_c}{4} \exp\left(u_a - \gamma^2 u_b\right) \\ & \times \int_{-\infty}^{B} \exp(\gamma^2 u_c x) \mathrm{erfc}(x) \mathrm{erfc}\left(\frac{P_t A_0 h_l}{\sqrt{2}\sigma_n \exp(u_b - u_c x)}\right) dx. \end{aligned} \tag{4.17}$$

Using a series expansion of the complementary error function, which is [75, eq. (06.27.06.0002.01)]

$$\mathrm{erfc}(z) = 1 - \frac{2}{\sqrt{\pi}} \sum_{k=0}^{\infty} \frac{(-1)^k z^{2k+1}}{k!(2k+1)} \tag{4.18}$$

and an integral identity [75, eq. (06.27.21.0011.01)]

$$\int e^{bz} \mathrm{erfc}(az) dz = \frac{1}{b} \left(e^{bz} \mathrm{erfc}(az) - e^{\frac{b^2}{4a^2}} \mathrm{erf}\left(\frac{b}{2a} - az\right) \right) \tag{4.19}$$

we derive an infinite series expression of the BER in (4.17) as

$$\begin{aligned}\widetilde{P}_{e,LN} =& \frac{\gamma^2 u_c}{4} \exp\left(u_a - \gamma^2 u_b\right) \\ &\times \left\{ \frac{1}{\gamma^2 u_c} \left[\exp(\gamma^2 u_c B)\mathrm{erfc}(B) + \exp\left(\frac{\gamma^4 u_c^2}{4}\right) \mathrm{erfc}\left(\frac{\gamma^2 u_c}{2} - B\right)\right] \right. \\ &\left. - \frac{2}{\sqrt{\pi}} \sum_{j=0}^{\infty} \left[\frac{(-1)^j}{j!(2j+1)} \left(\frac{P_t}{\sqrt{2}\sigma_n} A_0 h_l\right)^{2j+1} \frac{\exp(-u_b(2j+1))}{(2j+1+\gamma^2)u_c} S_j \right] \right\}\end{aligned} \tag{4.20}$$

where

$$\begin{aligned}S_j =& \exp((\gamma^2 + 2j + 1)u_c B)\mathrm{erfc}(B) \\ &+ \exp((\gamma^2 + 2j + 1)^2 u_c^2/4)\mathrm{erfc}((\gamma^2 + 2j + 1)u_c/2 - B).\end{aligned} \tag{4.21}$$

The infinite series in (4.20) can be rigorously shown to be convergent, and a detailed proof is presented in Appendix E.

For the Gamma-Gamma fading with nonzero boresight pointing error, we substitute (4.10a) into (2.25) to find its BER. Using an integral formula [75, eq. (06.27.21.0132.01)]

$$\int_0^{\infty} t^{\alpha-1}\mathrm{erfc}(t) = \frac{1}{\sqrt{\pi}\alpha}\Gamma\left(\frac{\alpha+1}{2}\right) \tag{4.22}$$

we can obtain the approximate BER in terms of a finite series as

$$\begin{aligned}P_{e,GG} \approx \widetilde{P}_{e,GG} =& \\ &\frac{1}{2\sqrt{\pi}} \sum_{j=0}^{J} \left\{ \frac{1}{j!}\left(\frac{2\alpha\beta}{A_0 h_l}\right)^j \left(\frac{2^\beta \Gamma\left(\frac{\beta+j+1}{2}\right)}{\beta+j} v_j(\alpha,\beta) \left(\frac{2P_t^2}{\sigma_n^2}\right)^{-\frac{\beta+j}{2}} \right.\right. \\ &\left.\left. - \frac{2^\alpha \Gamma\left(\frac{\alpha+j+1}{2}\right)}{\alpha+j} v_j(\beta,\alpha) \left(\frac{2P_t^2}{\sigma_n^2}\right)^{-\frac{\alpha+j}{2}} \right) \right\}.\end{aligned} \tag{4.23}$$

We comment (4.23) is obtained without additional approximations over those in (4.10a). The approximation error defined as $\varepsilon(P_e) = |P_e - \widetilde{P}_e|$ is discussed in Appendix F. When P_t is beyond the minimum required value in Table IV, we can guarantee the relative error $\frac{\varepsilon(P_{e,GG})}{P_{e,GG}}$ and $\frac{\varepsilon(P_{out,GG})}{P_{out,GG}}$ less

than 10^{-6}, where $P_{out,GG}$ denotes the outage probability of system in the composite Gamma-Gamma fading case and $\varepsilon(P_{out,GG})$ denotes the approximation error $|P_{out,GG} - \widetilde{P}_{out,GG}|$. With the setting $s/a = 1.0$ and $\sigma_s/a = 1.0$, the minimum required P_t is below -10 dBm, which can be satisfied for practical FSO systems.

4.2.2 Asymptotic Error Rate Analysis

We first derive the power series expansion of the PDF near its origin, then we obtain the diversity order and coding gain from (2.29) and (2.30). The asymptotic BER is obtained from $P_e^{\infty} = (G_c \cdot \overline{\mathrm{SNR}})^{-G_d}$. For the composite lognormal fading with pointing error, we obtain the PDF of the channel gain h near the origin $h \to 0$ as

$$f_{LN}(h) = \frac{\gamma^2}{(A_0 h_l)^{\gamma^2}} \exp(u_a)\, h^{\gamma^2-1} + g_{\gamma^2-1}(h). \tag{4.24}$$

From (4.24), we obtain the diversity order as $G_d = \frac{\gamma^2}{2} = \frac{w_{zeq}^2}{8\sigma_s^2}$. This indicates that the diversity order is determined by the ratio between equivalent beamwidth and jitter standard deviation. More specifically, the boresight component of pointing error does not affect the diversity order in lognormal fading channel. The coding gain can also be obtained from (4.24) as

$$G_c = \left[\frac{2^{\gamma^2-1}\Gamma\left(\frac{\gamma^2}{2} + \frac{1}{2}\right) \exp(u_a)}{\sqrt{\pi}(A_0 h_l)^{\gamma^2}} \right]^{-\frac{2}{\gamma^2}}. \tag{4.25}$$

With $\overline{\mathrm{SNR}} = \frac{2P_t^2}{\sigma_n^2}$, we can present the asymptotic BER as

$$P_{e,LN}^{\infty} = \frac{2^{\gamma^2-1}\Gamma\left(\frac{\gamma^2}{2} + \frac{1}{2}\right) \exp(u_a)}{\sqrt{\pi}(A_0 h_l)^{\gamma^2}} \left(\frac{2P_t^2}{\sigma_n^2}\right)^{-\frac{\gamma^2}{2}}. \tag{4.26}$$

For the Gamma-Gamma composite fading channels, we derive the power series expansion of PDF near the origin in Appendix C, and it is given by

$$f_{GG}(h) = v_0(\alpha, \beta) h^{\beta-1} + g_{\beta-1}(h) \tag{4.27}$$

where $v_0(\alpha, \beta)$ follows the definition in (4.10b) and we have assumed $\gamma^2 > \alpha$. From (4.27), we obtain the diversity order as $G_d = \beta/2$ and the coding gain

as

$$G_c = \left[\frac{2^{\beta-1}\Gamma\left(\frac{\beta}{2}+\frac{1}{2}\right)\exp\left(-\frac{s^2}{2\sigma_s^2}+\frac{-s^2\gamma^2/\sigma_s^2}{2\beta-2\gamma^2}\right)\left(\frac{\alpha\beta}{A_0 h_l}\right)^{\beta}}{\Gamma(\alpha)\Gamma(\beta)\sin((\alpha-\beta)\pi)\Gamma(-(\alpha-\beta)+1)|\gamma^2-\beta|\beta} \times \Gamma\left(\frac{\beta+1}{2}\right)\sqrt{\pi}\gamma^2 \right]^{-\frac{2}{\beta}}. \tag{4.28}$$

Thus, the asymptotic BER can be expressed as

$$P_{e,GG}^{\infty} = \frac{2^{\beta-1}\Gamma\left(\frac{\beta}{2}+\frac{1}{2}\right)\exp\left(-\frac{s^2}{2\sigma_s^2}+\frac{-s^2\gamma^2/\sigma_s^2}{2\beta-2\gamma^2}\right)\left(\frac{\alpha\beta}{A_0 h_l}\right)^{\beta}}{\Gamma(\alpha)\Gamma(\beta)\sin((\alpha-\beta)\pi)\Gamma(-(\alpha-\beta)+1)|\gamma^2-\beta|\beta} \times \Gamma\left(\frac{\beta+1}{2}\right)\sqrt{\pi}\gamma^2\left(\frac{2P_t^2}{\sigma_n^2}\right)^{-\frac{\beta}{2}}. \tag{4.29}$$

Note that the diversity order is $G_d = \beta/2$ when $\gamma^2 > \alpha$, which implies that the Gamma-Gamma fading effect is more dominant than the pointing error effect with respect to the BER performance at high average SNR region. However, when $\gamma^2 < \alpha$, the diversity order will depend on both γ^2 and the boresight s. An explicit expression of diversity order for nonzero boresight pointing case is difficult to obtain. For the special case with zero boresight, the diversity order is given as $\min\{\gamma^2/2, \beta/2\}$ [76].

To evaluate the performance loss caused by boresight error, we define an SNR penalty factor in dB as

$$\mathrm{SNR}_{boresight} = 10\log_{10}\left[\frac{\mathrm{SNR}_{P_e^{\infty},\mathrm{nonzeroboresight}}}{\mathrm{SNR}_{P_e^{\infty},\mathrm{zeroboresight}}}\right] \tag{4.30}$$

which represents the constant SNR loss caused by boresight error at certain error probability P_e^{∞} when SNR is asymptotically large. From (4.26) and (4.29), we obtain the SNR penalty factor for the composite lognormal and the composite Gamma-Gamma fading, respectively, as

$$\mathrm{SNR}_{boresight,LN} = \frac{80}{\ln 10}\left[\frac{s}{\omega_{z_{eq}}}\right]^2 \tag{4.31}$$

and

$$\mathrm{SNR}_{boresight,GG} = \frac{40}{\ln 10}\left[\frac{s}{\sqrt{\omega_{z_{eq}}^2 - 4\sigma_s^2\beta}}\right]^2 \tag{4.32}$$

where we have assumed $\gamma^2 > \alpha$, that is $w_{z_{eq}}^2 > 4\sigma_s^2\beta$ in (4.32). The results in (4.31) and (4.32) show that, for both composite lognormal and composite Gamma-Gamma cases, the boresight error imposes a constant SNR penalty on the error rate performance when SNR is large. As expected, larger beamwidth $\omega_{z_{eq}}$ can mitigate the adverse impact of the boresight error. However, we can not arbitrarily increase the beamwidth, because it will reduce the total received power. Moreover the maximum level of transmitted power is also limited by the heat dissipation and eye safety requirements at the transmitter, thus we can not increase the power too insensitively.

4.2.3 Outage Probability

For weak turbulence condition, substituting (4.8) into (2.27) and using the integral identity in (4.19) we obtain the outage probability as

$$P_{out,LN} = \frac{1}{2}\left[\left(\frac{h_0}{A_0 h_l}\right)^{\gamma^2} \exp(u_a)\operatorname{erfc}\left(\frac{\ln\frac{h_0}{A_0 h_l} + u_b}{u_c}\right) + \exp\left(u_a - u_b\gamma^2 + \frac{u_c^2\gamma^4}{4}\right)\operatorname{erfc}\left(\frac{u_c\gamma^2}{2} - \frac{\ln\frac{h_0}{A_0 h_l} + u_b}{u_c}\right)\right]. \tag{4.33}$$

For medium to strong turbulence conditions, by substituting (4.10a) into (2.27), we obtain the outage probability as

$$P_{out,GG} \approx \widetilde{P}_{out,GG} = \frac{\exp\left(-\frac{s^2}{2\sigma_s^2}\right)\gamma^2\pi}{\Gamma(\alpha)\Gamma(\beta)\sin((\alpha-\beta)\pi)} \times \sum_{j=0}^{J}\left(\frac{\alpha\beta}{A_0 h_l}\right)^j \left(\frac{\left(\frac{\alpha\beta}{A_0 h_l}\right)^{\beta}\exp\left(\frac{-s^2\gamma^2/\sigma_s^2}{2\beta-2\gamma^2+2j}\right)}{\Gamma(j-(\alpha-\beta)+1)j!|-(\beta-\gamma^2+j)|(\beta+j)}h_0^{\beta+j} - \frac{\left(\frac{\alpha\beta}{A_0 h_l}\right)^{\alpha}\exp\left(\frac{-s^2\gamma^2/\sigma_s^2}{2\alpha-2\gamma^2+2j}\right)}{\Gamma(j+(\alpha-\beta)+1)j!|-(\alpha-\gamma^2+j)|(\alpha+j)}h_0^{\alpha+j}\right). \tag{4.34}$$

It is worthy to mention that we can obtain the diversity order using the outage probability derived in (4.33) and (4.34), the derivation follows that in [40]. The results are $G_{d,LN} = \gamma^2/2$ and $G_{d,GG} = \beta/2$, which coincide with the ones obtained using the power series expansion approach.

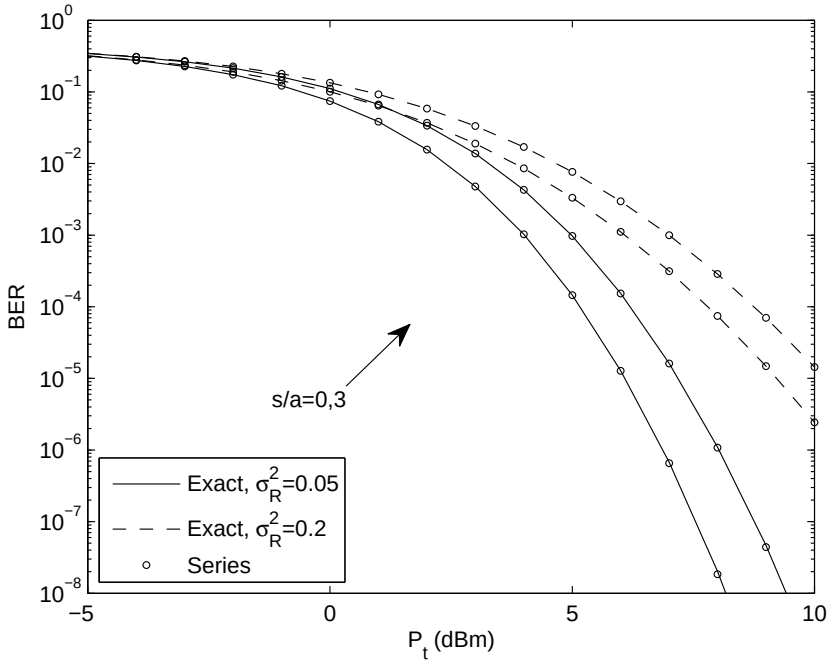

Figure 4.1: BER performance of IM/DD OOK over the lognormal fading with zero and nonzero boresight pointing errors.

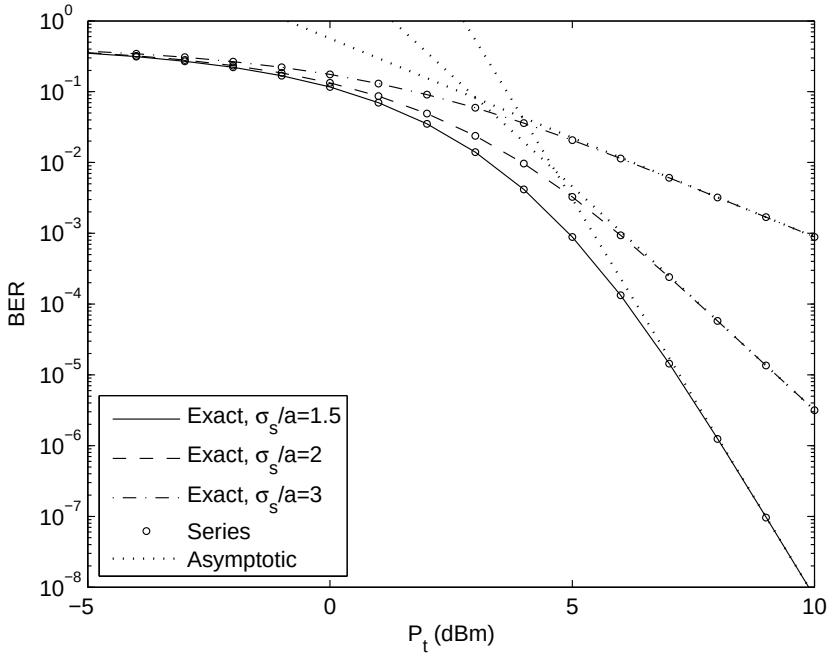

Figure 4.2: BER for the composite lognormal channel ($\sigma_R^2 = 0.01, s/a = 2$) with different jitter values.

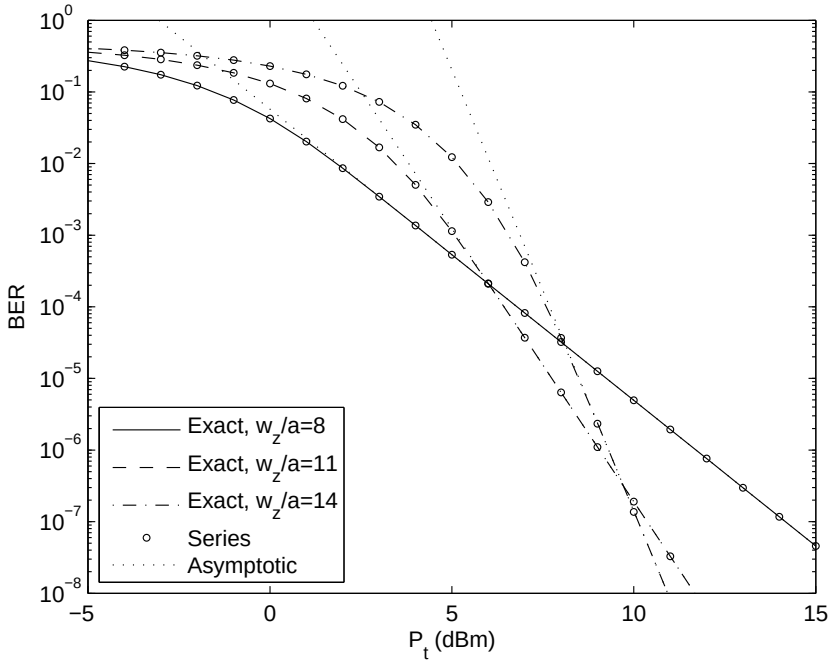

Figure 4.3: BER for the composite lognormal channel ($\sigma_R^2 = 0.01, s/a = 2, \sigma_s/a = 1.5$) with different beamwidth values.

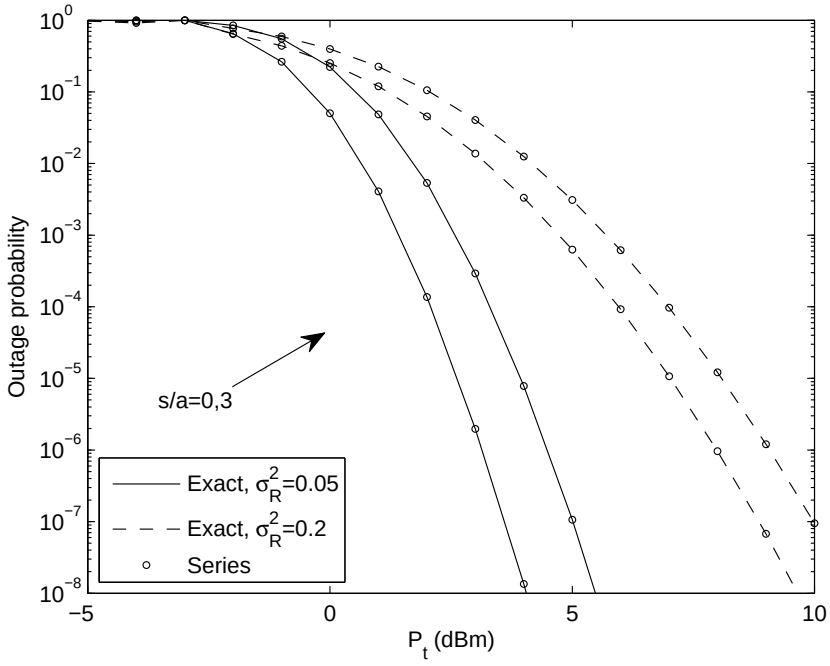

Figure 4.4: Outage probability of an FSO system over the lognormal fading with zero and nonzero boresight pointing errors.

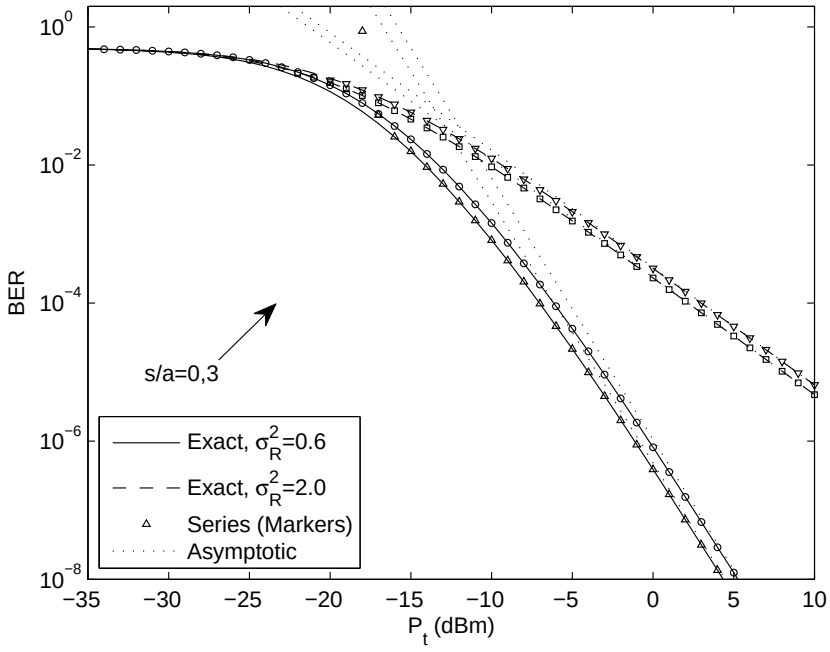

Figure 4.5: BER performance of IM/DD OOK over the Gamma-Gamma fading with zero and nonzero boresight pointing errors.

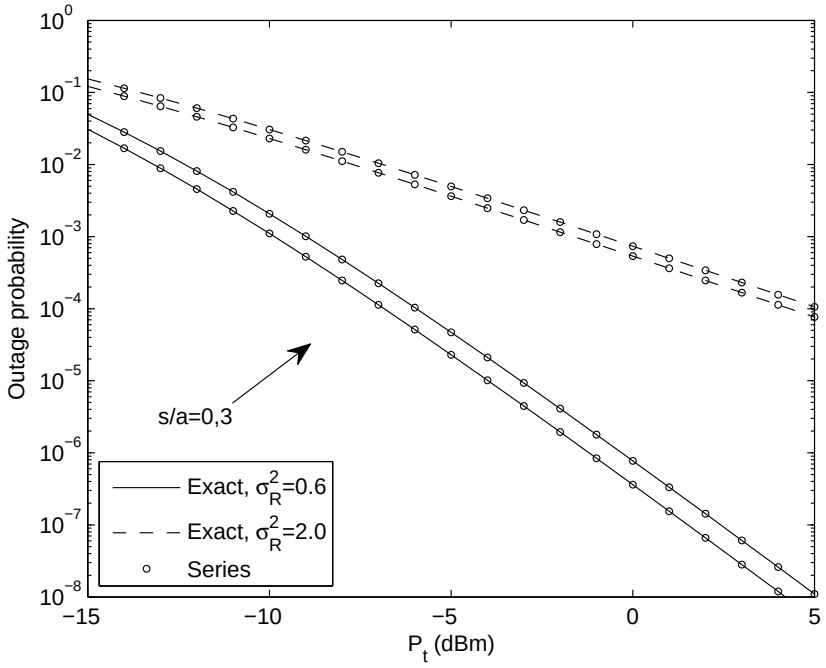

Figure 4.6: Outage probability of an FSO system over the Gamma-Gamma fading with zero and nonzero boresight pointing errors.

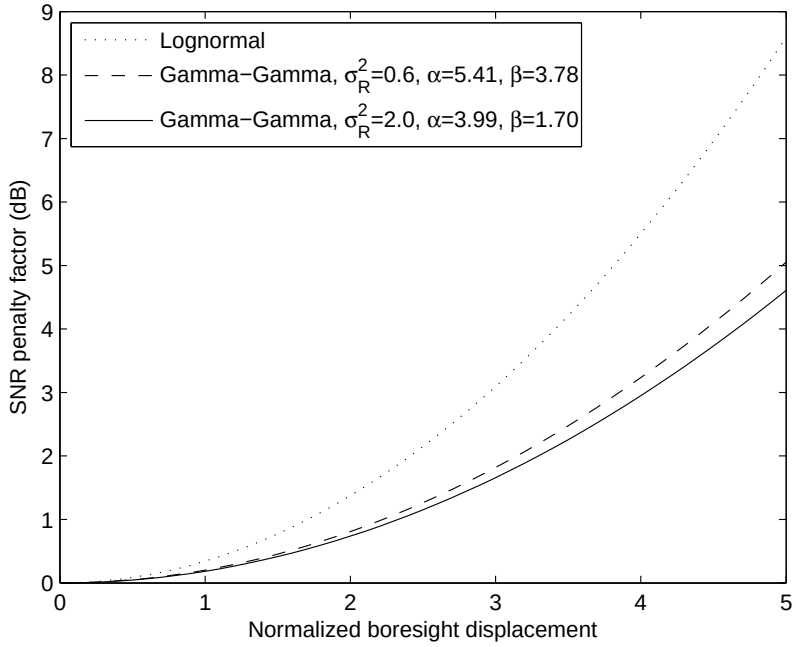

Figure 4.7: The SNR penalty factor induced by boresight error in different turbulence conditions.

Table 4.1: System Settings

Parameter	Value
Transmission rate	1 Gbps
Transmitted power (P_t)	10 dBm
Noise standard deviation (σ_n)	$\sigma_n = 10^{-7}$ A/Hz
Receiver Diameter ($2a$)	20 cm
Noise standard deviation (σ_n)	$\sigma_n = 10^{-7}$ A/Hz
Link distance	1 km
Transmit Divergence at $1/e$	1 mrad
Corresponding beam radius (ω_z) at 1 km	≈ 100 cm
Boresight angle	0.1 mrad
Corresponding boresight displacement (s) at 1 km	≈ 10 cm
Jitter angle	0.1 mrad
Corresponding jitter standard deviation (σ_s) at 1 km	≈ 10 cm

Table 4.2: Weather Conditions

Weather	Path loss (h_l)	Fading model	σ_R^2	Parameters
Light fog	0.008	Lognormal	0.05	$\sigma_X^2 = 0.0125$
			0.1	$\sigma_X^2 = 0.025$
			0.2	$\sigma_X^2 = 0.05$
Clear	0.9	Gamma-Gamma	0.6	$\alpha = 4.15, \beta = 3.78$
			2.0	$\alpha = 2.21, \beta = 1.70$
			5.0	$\alpha = 2.12, \beta = 1.24$

4.3 Numerical Results

In this section, we adopt the system settings shown in Table 4.2.3, which are used in many practical terrestrial FSO communication systems [3, 30, 77]. Under two typical weather conditions shown in Table 4.2.3 [11], we carry out the error rate performance of an FSO communication system. In order to investigate the degradation effects induced by the boresight error, we use two different values of normalized boresight displacement $s/a = 0, 3$.

In weak turbulence regime, we study the BER of an FSO link over the lognormal fading channel with nonzero boresight pointing errors. We calculate the exact BER from (4.12), the approximate BER from (4.20), and the asymptotic BER from (4.26). The BER curves are plotted in Fig. 4.1 against the transmitted optical power P_t. From Fig. 4.1, we can see how the boresight displacement s affects the BER performance of the system. We can infer from the result that for a Gaussian beam the energy collected at receiver aperture decreases with increasing boresight errors, and therefore the BER performance deteriorates with a large boresight displacement. However, if we assume a tophat beam profile, the boresight would not affect the collected power at the receiver as long as the boresight displacement s is smaller than the difference of distance between the beamwidth at receiver and the receiver aperture.

From the asymptotic BER curves in Fig. 4.2 and Fig. 4.3, we find that the diversity order is determined by the equivalent beamwidth as well as the jitter variance. A similar finding is reported in [40] for a MIMO FSO system with zero boresight. With larger beamwidth or smaller jitter variance, the diversity order of the system becomes larger.

The outage probability of an FSO system with code rate $R_0 = 0.5$ (bits per channel use) over the composite lognormal fading channel is presented in Fig. 4.4, where we use (4.33) to calculate outage probability. It can be seen that the outage probability of the system worsens with increasing boresight errors.

In medium to strong turbulence regimes, we study the BER of an FSO link over the Gamma-Gamma fading channel with nonzero boresight pointing errors. We calculate the exact BER from (2.25), the approximate BER from (4.23) (with $J = \lfloor \gamma^2 - \alpha \rfloor$), and the asymptotic BER from (4.29). The BER curves are plotted in Fig. 4.5 against the transmitted power P_t. It can be seen that our series solution developed in (4.23) can accurately approximate the exact BER when P_t is beyond a certain threshold (see Appendix F). However, for small values of P_t, the series approximation in (4.23) can be inaccurate. This is the limitation of the series approach for the Gamma-

Gamma channels with pointing errors, and the same limitation can also be seen from Fig. 2 of [12]. As expected, the BER performance worsens when the boresight displacement s becomes larger. Moreover, the boresight error causes a horizontal shift of the BER curve, resulting in an SNR penalty factor for the error rate performance. From the asymptotic curves in Fig. 4.5 we can find that the boresight displacement does not affect the diversity order of the system.

Assuming a code rate of $R_0 = 0.5$ (bits per channel use), we present the exact outage probability obtained from (2.27), and the approximate outage probability calculated using (4.34) in Fig. 4.6, and it can be seen that the approximate outage probability is accurate. (The threshold of P_t for accurate outage probability approximation is shown in Appendix F.)

In Fig. 4.7, we plot the SNR penalty factor versus the normalized boresight displacement s in both composite lognormal and composite Gamma-Gamma cases. The result indicates that the boresight displacement has larger penalty factor on SNR when the turbulence is weaker.

4.4 Summary

In this chapter, a nonzero boresight pointing error model was investigated by considering beamwidth, detector aperture, and jitter variance. Our derivation is based on the assumption that the boresight component of pointing error effects is not negligible. A closed-form PDF was derived for the nonzero boresight pointing error model. We derived closed-form composite PDF for the lognormal fading and highly accurate series based PDF for the Gamma-Gamma fading. Highly accurate convergent series BER expressions were obtained. Through the asymptotic BER analysis and numerical results, we observed that the boresight error causes an SNR penalty factor on error rate performance at high SNR. By examining the asymptotic BER curves, we found that the diversity order of the FSO system over the composite lognormal fading channel is solely determined by the pointing error parameter γ^2, which means that the boresight component does not affect the diversity order. While in the composite Gamma-Gamma fading channel, the diversity order is determined by either the Gamma-Gamma fading effect or the pointing error effect.

Chapter 5

Performance of Subcarrier M-ary PSK with Phase Recovery Error over Lognormal Fading Channels

In this chapter, we study the BER performance of subcarrier MPSK systems with CPE over lognormal turbulence channels. Since the traditional asymptotic analysis techniques cannot be applied directly on FSO communication systems over the lognormal channels, we introduce an auxiliary RV approach to analyze the asymptotic performance of such systems. We derive exact asymptotic noise reference loss expressions for subcarrier MPSK systems with CPE over the lognormal channels. Our analysis quantifies the performance degradation introduced by the CPE.

5.1 System Model

For a subcarrier FSO system, the instantaneous receiver SNR is defined as the ratio of the time-averaged AC photocurrent power to the total noise variance, and it can be expressed as [48]

$$\gamma = \frac{(PR\xi)^2}{\sigma_n^2} I^2 = \overline{\gamma} I^2 \tag{5.1}$$

where P is the average transmitter power, R is the photodetector responsivity, ξ is the modulation index, σ_n^2 is the noise variance, I is the turbulence induced channel gain, and $\overline{\gamma}$ is the average SNR assuming normalized mean of channel gain. The SNR γ defined in (5.1) is SNR per symbol. For an M-ary modulation scheme, we have $\gamma = \gamma_b \log_2 M$ and $\overline{\gamma} = \overline{\gamma}_b \log_2 M$ with γ_b and $\overline{\gamma}_b$ denoting the instantaneous SNR per bit and the electrical SNR per bit, respectively.

5.1.1 Phase Error

In this chapter, the CPE is assumed to be derived from the pilot tone using a PLL in the presence of AWGN and fading. Thus, the CPE follows a Tikhonov distribution conditioned on the channel gain [78, 79]. The PLL SNR ρ can be expressed as $\rho = P_c/(N_0 B_L)$ where P_c is the power allocated to the carrier phase recovery pilot, N_0 is the noise spectral density, and B_L is the loop bandwidth. We further assume that a fixed fraction (ς) of the available total power P_t is allocated to the pilot (i.e., $P_c = \varsigma P_t$) and the remaining fraction is for data detection. Therefore, we have $(1-\varsigma)P_t = E_b/T_b$ where E_b is the energy per bit and T_b is the bit interval. In a fading environment, it is straightforward to obtain [78]

$$\rho = \frac{\varsigma}{1-\varsigma}\frac{1}{B_L T_b}\frac{I^2 E_b}{N_0} = \frac{\varsigma}{1-\varsigma}\frac{1}{B_L T_b}\gamma_b. \tag{5.2}$$

From (5.2), we observe that the PLL SNR ρ is proportional to the instantaneous receiver SNR γ_b, i.e., $\rho = C\gamma_b$ where C is a constant defined as $C = \varsigma/[(1-\varsigma)B_L T_b]$ with typical value around 10 [78, 80]. The PDF of the CPE conditioned on the fading is given by [79]

$$f_\Theta(\theta|\rho) = \frac{\exp(\rho\cos\theta)}{2\pi I_0(\rho)}, \quad -\pi \le \theta \le \pi. \tag{5.3}$$

Substituting $\rho = C\gamma_b$ into (5.3), we obtain

$$f_\Theta(\theta|\gamma_b) = \frac{\exp(C\gamma_b\cos\theta)}{2\pi I_0(C\gamma_b)}. \tag{5.4}$$

With a specific fading model, we can average the conditional PDF of the CPE over the PDF of SNR per bit γ_b and obtain the PDF of Θ as

$$f_\Theta(\theta) = \int_0^\infty \frac{\exp(C\gamma_b\cos\theta)}{2\pi I_0(C\gamma_b)} f_{\gamma_b}(\gamma_b)\, d\gamma_b \tag{5.5}$$

where $f_{\gamma_b}(\gamma_b)$ is the PDF of the instantaneous SNR per bit γ_b. It is important to note that the condition $\rho \gg 1$ holds in practice; therefore, the variance of the CPE σ_θ^2 can be approximated by $\sigma_\theta^2 \approx 1/\rho$ [78, 81, 82]. We will make this assumption in our analysis.

5.2 Asymptotic Noise Reference Loss Analysis

5.2.1 Subcarrier MPSK System

For nonideal coherent detection of MPSK and assuming Gray mapping, we can express the conditional BER as [83]

$$P_{b,\mathrm{MPSK}}(\theta,\gamma_b)=\frac{1}{2\log_2 M}\sum_{n=0}^{M/2-1}\mathrm{erfc}\left(\sqrt{\log_2 M\gamma_b}\sin\left(\frac{(2n+1)\pi}{M}+\theta\right)\right) \tag{5.6}$$

where θ denotes the CPE. The average BER of a subcarrier MPSK system over turbulence channels can be obtained as

$$P_{b,\mathrm{MPSK}}=\int_0^\infty\int_{-\pi}^{\pi}P_{b,\mathrm{MPSK}}(\theta,\gamma_b)f_\Theta(\theta|\gamma_b)f_{\gamma_b}(\gamma_b)d\theta d\gamma_b. \tag{5.7}$$

We can use (5.7) to calculate the average BER of a subcarrier MPSK system. The performance gap between systems with phase error and that without phase error can also be obtained using (5.7). We define the noisy reference loss SNR_L as the amount of additional SNR (compared with the ideal coherent detection) required to achieve a specific BER in the presence of CPE [78]. In this chapter, we obtain the asymptotic noisy reference loss, SNR_L^∞, when the SNR is asymptotically large. This asymptotic measurement can give insights of the system performance.

In a lognormal turbulence environment, the receiver SNR γ_b is another lognormal RV having PDF

$$f_{\gamma_b,\mathrm{LN}}(\gamma_b)=\frac{1}{2\sqrt{2\pi}\sigma\gamma_b}\exp\left(-\frac{(\ln\gamma_b-\ln\overline{\gamma}_b+\sigma^2)^2}{8\sigma^2}\right) \tag{5.8}$$

where $\ln\gamma_b$ is a Gaussian RV with mean $\sigma^2-\ln\overline{\gamma}_b$ and variance $4\sigma^2$. Using (5.7) and (5.8), we can evaluate the BER of subcarrier MPSK systems in the lognormal turbulence channels. However, it is well-known that the asymptotic BER analysis cannot be performed on a lognormal channel directly because the diversity order of such a channel is undefined. In order to investigate the asymptotic noisy reference loss of subcarrier BPSK in the lognormal channels, we introduce the lognormal-Nakagami fading as an auxiliary channel model where the receiver SNR follows a lognormal-Gamma distribution. Since the lognormal-Gamma distribution approaches a lognormal distribution as the channel parameter m approaches infinity, the results

obtained for the lognormal-Nakagami channels will reveal the performance characteristics of the lognormal channels when $m \to \infty$.

In a lognormal-Nakagami fading environment, the receiver SNR γ_b follows a lognormal-Gamma distribution with PDF

$$\begin{aligned} f_{\gamma_b,\mathrm{LG}}(\gamma_b) =& \frac{1}{2\sqrt{2\pi}\sigma\Omega} \int_0^\infty \frac{m^m \gamma_b^{m-1}}{\Omega^m \Gamma(m)} \exp\left(-\frac{m\gamma_b}{\Omega}\right) \\ & \times \exp\left(-\frac{(\ln\Omega - \ln\overline{\gamma}_b + \sigma^2)^2}{8\sigma^2}\right) d\Omega \end{aligned} \tag{5.9}$$

where m is the Nakagami-m fading parameter and Ω is the second moment of a Nakagami-m RV. When $m \to \infty$, we can show that

$$\lim_{m\to\infty} f_{\gamma_b,\mathrm{LG}}(\gamma_b) = \frac{1}{2\sqrt{2\pi}\sigma\gamma_b} \exp\left(-\frac{(\ln\gamma_b - \ln\overline{\gamma}_b + \sigma^2)^2}{8\sigma^2}\right) \tag{5.10}$$

which is the lognormal PDF given in (5.8).

Substituting $u = \Omega/\overline{\gamma}_b$ into (5.9), we rewrite the lognormal-Gamma PDF as

$$\begin{aligned} f_{\gamma_b,\mathrm{LG}}(\gamma_b) =& \frac{m^m \gamma_b^{m-1} \overline{\gamma}_b^{-m}}{2\sqrt{2\pi}\sigma\Gamma(m)} \int_0^\infty \frac{1}{u^{m+1}} \exp\left(-\frac{m\gamma_b}{u\overline{\gamma}_b}\right) \\ & \times \exp\left(-\frac{(\ln u + \sigma^2)^2}{8\sigma^2}\right) du. \end{aligned} \tag{5.11}$$

When $\overline{\gamma}_b$ approaches ∞, we obtain from (5.7) and (5.11) the asymptotic BER of subcarrier MPSK in the lognormal-Nakagami channels as

$$\begin{aligned} P_{b,\mathrm{MPSK}}^{\infty} =& \int_0^\infty \int_{-\pi}^{\pi} P_{b,\mathrm{MPSK}}(\theta,\gamma_b) f_\Theta(\theta|\gamma_b) f_{\gamma_b}(\gamma_b) d\theta d\gamma_b \\ =& \frac{g_c G(m)}{4\pi \log_2 M} \overline{\gamma}_b^{-m} \end{aligned} \tag{5.12}$$

where

$$g_c = \frac{m^m}{2\sqrt{2\pi}\sigma\Gamma(m)} \int_0^\infty \frac{1}{u^{m+1}} \exp\left(-\frac{(\ln u + \sigma^2)^2}{8\sigma^2}\right) du \tag{5.13}$$

and $G(x)$ is defined as

$$\begin{aligned} G(x) =& \int_0^\infty \int_{-\pi}^{\pi} \frac{\exp\left(C\gamma_b \cos\theta\right) {\gamma_b}^{x-1}}{I_0(C\gamma_b)} \\ & \times \sum_{n=0}^{M/2-1} \mathrm{erfc}\left(\sqrt{\log_2 M \gamma_b} \sin\left(\frac{(2n+1)\pi}{M} + \theta\right)\right) d\theta d\gamma_b. \end{aligned} \tag{5.14}$$

For the systems without phase error, we can express the conditional BER as

$$P_{b,\,\mathrm{MPSK}}(\gamma) = \frac{1}{\log_2 M} \sum_{k=1}^{M-1} d_k P_k(\gamma) \tag{5.15}$$

where

$$d_k = 2\left|\frac{k}{M} - \left\lfloor \frac{k}{M} \right\rceil\right| + 2\sum_{i=2}^{\log_2 M}\left|\frac{k}{2^i} - \left\lfloor \frac{k}{2^i} \right\rceil\right| \tag{5.16}$$

and

$$P_k(\gamma) = \frac{1}{2\pi}\left[\int_0^{m_k\pi} \exp\left(-\frac{A_k \log_2 M\gamma_b}{\sin^2\phi}\right) d\phi - \int_0^{n_k\pi} \exp\left(-\frac{B_k \log_2 M\gamma_b}{\sin^2\phi}\right) d\phi\right] \tag{5.17}$$

where we have

$$\begin{aligned} m_k &= (M-2k+1)/M, \\ n_k &= (M-2k-1)/M, \\ A_k &= \sin^2\left((2k-1)\pi/M\right), \\ B_k &= \sin^2\left((2k+1)\pi/M\right). \end{aligned} \tag{5.18}$$

The asymptotic BER can be obtained as

$$P^{\infty}_{b,\,\mathrm{MPSK}} = \frac{1}{2\pi \log_2 M} \sum_{k=1}^{M-1} d_k \left(P^{\infty}_k(m_k, A_k) - P^{\infty}_k(n_k, B_k)\right) \tag{5.19}$$

where

$$\begin{aligned} P^{\infty}_k(m_k, A_k) &= \int_0^{m_k\pi}\int_0^{\infty} \exp\left(-\frac{A_k \log_2 M\gamma_b}{\sin^2\phi}\right) \frac{g_c \gamma^{m-1}}{\overline{\gamma}^m} d\gamma d\phi \\ &= \frac{g_c \Gamma(m)\, g\left(m_k, \sin^2\phi, m\right)}{(\log_2 M A_k)^m} \overline{\gamma}^{-m} \end{aligned} \tag{5.20}$$

and where

$$g(\eta, u(\phi), v) \triangleq \int_0^{\eta\pi} (u(\phi))^v \, d\phi. \tag{5.21}$$

Using (5.12) and (5.19), we obtain the asymptotic noisy reference over the LG channel as

$$SNR^{\infty}_{L,M,LG}(m) = \frac{1}{m}10\log\left(\frac{g_c G_3(m)}{2\sum_{k=1}^{M-1} d_k\left(P_k^{\infty}(m_k,A_k) - P_k^{\infty}(n_k,B_k)\right)}\right). \tag{5.22}$$

After some mathematical manipulation and keeping only the dominant terms, we can rewrite (5.22) as

$$\begin{aligned}
&SNR^{\infty}_{L,M,LG}(m)\\
&\approx \frac{1}{m}10\log\left(\frac{g_c G_3(m)}{2d_1\left(P_1^{\infty}(m_1,A_1) - P_1^{\infty}(n_1,B_1)\right)}\right)\\
&= \frac{1}{m}10\log\left(\frac{g_c G_3(m)}{2g_c\Gamma(m)\int_0^{\frac{M-1}{M}\pi}\left(\frac{\sin\theta}{\sqrt{\log_2 M}\sin\left(\frac{\pi}{M}\right)}\right)^{2m}d\theta}\right)\\
&= \frac{1}{m}10\log\left(\frac{\sum_{n=0}^{M/2-1}\int_{-\frac{\pi}{2}}^{\frac{\pi}{2}}\frac{\sqrt{2\pi C}\Gamma(m)}{\left(\frac{(2n+1)\pi}{M}+\theta\right)\left(C-C\cos\theta+\log_2 M\sin^2\left(\frac{(2n+1)\pi}{M}+\theta\right)\right)^m}d\theta}{2\Gamma(m)\int_0^{\frac{M-1}{M}\pi}\left(\frac{\sin\theta}{\sqrt{\log_2 M}\sin\left(\frac{\pi}{M}\right)}\right)^{2m}d\theta}\right).
\end{aligned} \tag{5.23}$$

In order to approach the lognormal fading channel, we let $m \to \infty$ in (5.23), and the asymptotic noisy reference over the lognormal channel can be obtained as

$$SNR^{\infty}_{L,M,\mathrm{LN}} = 10\log\left(\frac{q_{max}}{\frac{1}{\log_2 M\sin^2\frac{\pi}{M}}}\right) \tag{5.24}$$

where we have

$$\begin{aligned}
q_{max} =& \max\left\{\frac{1}{\left(C - C\cos\theta + \log_2 M\sin^2\left(\frac{(2n+1)\pi}{M}+\theta\right)\right)}\right\},\\
& n = 0,1,\cdots,\frac{M}{2}-1; \theta\in(-\frac{\pi}{2},\frac{\pi}{2}).
\end{aligned} \tag{5.25}$$

Therefore for the BPSK case, we can obtain the asymptotic noisy reference loss from (5.24) as

$$\mathrm{SNR}^{\infty}_{L,2,\mathrm{LN}} = 10\log\left(\frac{1}{1}\right) = 0\,\mathrm{dB}. \tag{5.26}$$

From (5.26), we can find that the CPE introduced asymptotic noisy reference loss is 0 dB for subcarrier BPSK system over the lognormal channels.

For QPSK system, we can obtain the asymptotic noisy reference loss from (5.24) as

$$\mathrm{SNR}^{\infty}_{L,4,\mathrm{LN}} = 10\log(qmax) = 10\log\left(\frac{1}{C+1+\sin(2\hat{\theta})-C\cos\hat{\theta}}\right) \quad (5.27)$$

where

$$\hat{\theta} = \sin^{-1}\left(\frac{C-\sqrt{C^2+32}}{8}\right). \quad (5.28)$$

Using (5.24), we can obtain the asymptotic noisy reference loss for arbitrary M and C. For $M = 8, C = 15$, we have

$$SNR^{\infty}_{L,8,\mathrm{LN}} = 10\log\frac{3.0859}{\frac{1}{3\sin(\frac{\pi}{8})}} = 1.3218\,\mathrm{dB}. \quad (5.29)$$

For $M = 8, C = 10$, we have

$$SNR^{\infty}_{L,8,\mathrm{LN}} = 10\log\frac{3.5056}{\frac{1}{3\sin(\frac{\pi}{8})}} = 1.8756\,\mathrm{dB}. \quad (5.30)$$

For $M = 16, C = 15$, we have

$$SNR^{\infty}_{L,16,\mathrm{LN}} = 10\log\frac{9.9801}{\frac{1}{4\sin(\frac{\pi}{16})}} = 1.8167\,\mathrm{dB}. \quad (5.31)$$

For $M = 16, C = 10$, we have

$$SNR^{\infty}_{L,16,\mathrm{LN}} = 10\log\frac{11.7014}{\frac{1}{4\sin(\frac{\pi}{16})}} = 2.5077\,\mathrm{dB}. \quad (5.32)$$

From the above results, we can see that the noisy reference loss increases with higher modulation order and smaller PLL SNR coefficient C values.

5.3 Numerical Results

In this section, for simplicity, we will present the noisy reference loss of a BPSK ($M = 2$) and a QPSK ($M = 4$) subcarrier FSO systems.

Figure. 5.1 presents the asymptotic noisy reference loss of subcarrier BPSK system over the lognormal-Nakagami channels. From (5.26), we expect the asymptotic noisy reference loss to be 0 dB, which can be observed

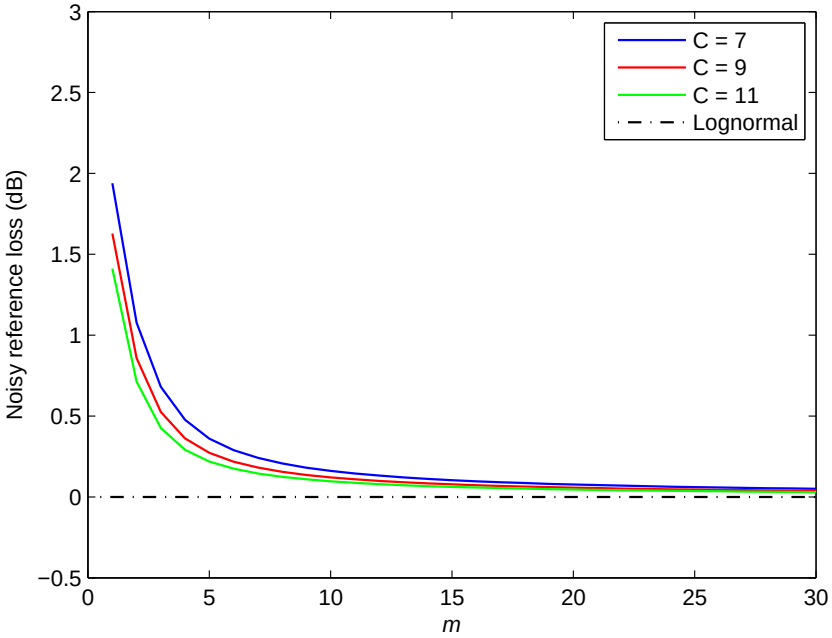

Figure 5.1: Asymptotic noisy reference loss of subcarrier BPSK system over the lognormal-Nakagami channel with different PLL parameter C values.

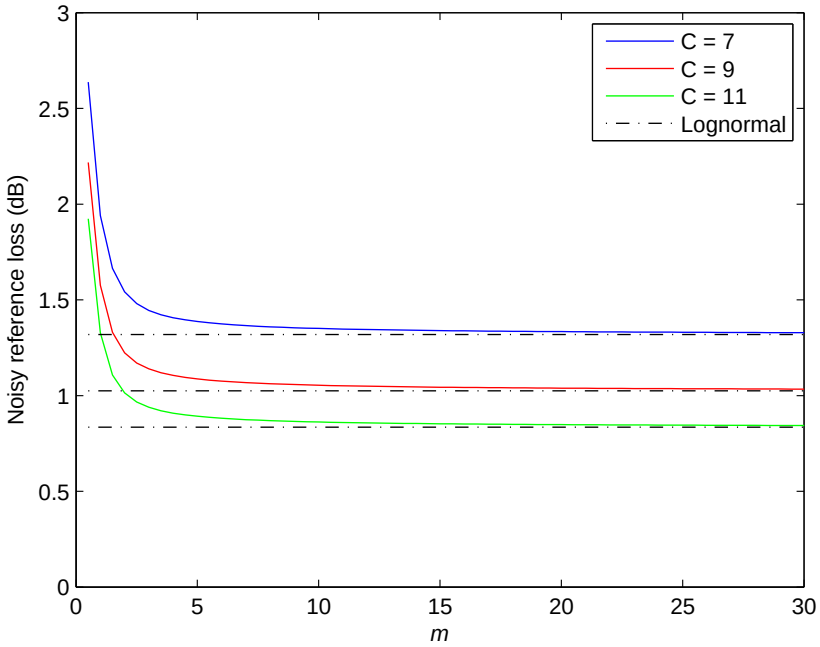

Figure 5.2: Asymptotic noisy reference loss of subcarrier QPSK system over the lognormal-Nakagami channel and the lognormal channels with different PLL parameter C values.

from Fig. 5.1. The noisy reference loss tends to approach 0 dB with increasing channel parameter m.

In Fig. 5.2, we present the asymptotic noisy reference loss of subcarrier QPSK system over the lognormal-Nakagami channels with different PLL parameter C values. We observe from Fig. 5.2 that the asymptotic noisy reference losses for the lognormal-Nakagami channel approach the ones obtained in (5.27) with increasing channel parameter m, which validate our asymptotic noisy reference loss results for lognormal channels.

5.4 Summary

In this chapter, we studied the BER performance of subcarrier MPSK systems with CPE over lognormal fading channels. We quantified the CPE induced asymptotic noise reference loss over the lognormal channels. Our results showed that the CPE induced performance degradation for a subcarrier BPSK system over the lognormal channel is negligible. The CPE induced performance degradation increases with higher modulation order and smaller PLL SNR coefficient C values.

Chapter 6

Asymptotic Performance Analysis of FSO Communication over Correlated Lognormal Fading Channels

In this chapter, we analyze the performance of a multi-branch FSO system over correlated lognormal fading channels. We propose a lognormal-Nakagami model to facilitate asymptotic analysis on lognormal channels. Using such an approach, we study different multi-branch FSO systems over correlated lognormal fading channels that may have nonidentical variance. We discover that the correlation among the lognormal channels can impose large asymptotic SNR penalty to system BER performance. We also derive a compact expression for the ARDO between an L-branch combining system over correlated lognormal channels and a single-branch system. For MRC, EGC and SC receptions, we obtain the coding gain differences on such systems.

6.1 System Model

In this chapter, we consider an L-branch OOK FSO system with IM/DD. Assuming AWGN for the thermal/shot noise [7, 36, 40] and unit detector responsitivity, we can express the received signal y_l at the lth detector as

$$y_l = h_l I + n_l, l = 1, 2, \cdots, L \tag{6.1}$$

where I is the transmit intensity being either 0 or $2P_t$, where P_t is the average transmitted optical power, h_l is the lth channel gain, n_l is zero-mean AWGN with variance σ_n^2. Therefore we denote the average SNR at a

single receiver as $\bar{\gamma} = \frac{2P_t^2}{\sigma_n^2}$, and the instantaneous SNR at the lth receiver can be written as

$$\gamma_l = \bar{\gamma} h_l^2. \tag{6.2}$$

Assuming weak turbulence, we can model the lth channel gain h_l as

$$h_l = \exp(V_l) \tag{6.3}$$

where $V_l, l = 1, 2, \cdots, L$ are Gaussian distributed RVs with mean μ_l and variance σ_l^2. Therefore the channel gain h_l follows the lognormal distribution with PDF

$$f_{h_l}(h_l) = \frac{1}{h_l \sigma_l \sqrt{2\pi}} \exp\left(-\frac{(\ln h_l - \mu_l)^2}{2\sigma_l^2}\right) \tag{6.4}$$

and the instantaneous SNR has the PDF

$$f_{\gamma_l}(\gamma_l) = \frac{1}{2\sigma_l \gamma_l \sqrt{2\pi}} \exp\left(-\frac{(\ln \gamma_l + 2\mu_l - \ln \overline{\gamma_l})^2}{8\sigma_l^2}\right). \tag{6.5}$$

For normalized received intensity, we have $\mu_l = -\frac{\sigma_l^2}{2}$. The parameters of the lognormal fading model can be measured directly for FSO systems [66]. For an L-branch FSO system, we use the covariance matrix to model the correlation between receive apertures, which is given by

$$\Sigma = \begin{bmatrix} \sigma_{1,1}^2 & \sigma_{1,2}^2 & \cdots & \sigma_{1,L}^2 \\ \sigma_{2,1}^2 & \sigma_{2,2}^2 & \cdots & \sigma_{2,L}^2 \\ \vdots & \vdots & \ddots & \vdots \\ \sigma_{L,1}^2 & \sigma_{L,2}^2 & \cdots & \sigma_{L,L}^2 \end{bmatrix} \tag{6.6}$$

where $\sigma_{i,j}^2 = E[(V_i - \mu_i)(V_j - \mu_j)]$. When every branch has identical variance σ^2, we have $\Sigma = \sigma^2 R$ where R is the correlation matrix of RVs $V_l, l = 1, 2, \cdots, L$.

In order to perform diversity analysis on systems over lognormal fading channels, we have to obtain a Taylor series expansion of the lognormal PDF near its origin [60]. Since lognormal PDF does not have a Taylor series expansion at the origin, it is infeasible to perform the conventional asymptotic analysis directly on the lognormal channel. Therefore, we introduce the lognormal-Nakagami fading as an auxiliary channel model where the receiver instantaneous SNR follows a lognormal-Gamma (LG) distribution. Note that such model is an auxiliary channel model rather than a experimentally validated model, and the reason for choosing lognormal-Nakagami is that the Nakagami component is easy for us to manipulate,

i.e., it will approach a Dirac delta function when $m \to \infty$. Moreover, we will have the diversity of system over lognormal-Nakagami fading tend to ∞ when $m \to \infty$, which corresponds to lognormal channel's behavior. The lognormal-Nakagami random variable z for the channel state can be constructed by multiplying a lognormal RV x by a Nakagami-m RV y. Unlike the lognormal PDF, the lognormal-Gamma PDF indeed has a Taylor series expansion at the origin; therefore, one can perform asymptotic analysis on such a channel. It will be shown in Section 6.2 that the diversity order of the lognormal-Nakagami channel is just the Nakagami fading parameter m. As m approaches ∞, the lognormal-Gamma PDF approaches that of a lognormal [84, 85]. The lognormal RV x follows the PDF shown in (6.4). The Nakagami RV y's PDF is

$$f_{Naka}(y) = \frac{2m^m}{\Gamma(m)\Omega^m} y^{2m-1} \exp\left(-\frac{m}{\Omega} y^2\right) \tag{6.7}$$

where m is the shape parameter, Ω is the spread parameter and $\Gamma(\cdot)$ is the Gamma function. For normalization purpose, we often have $\Omega = 1$. For the lognormal-Nakagami channels with channel gain $h = z$, the received instantaneous SNR γ follows a lognormal-Gamma distribution with PDF

$$\begin{aligned} f_{LG}(\gamma) = \int_0^\infty & \frac{m^m \gamma^{m-1}}{\Omega^m \Gamma(m)} \exp\left(-\frac{m\gamma}{\Omega}\right) \\ & \times \frac{1}{2\sigma\Omega\sqrt{2\pi}} \exp\left(-\frac{(\ln\Omega + 2\mu - \ln\overline{\gamma})^2}{8\sigma^2}\right) d\Omega. \end{aligned} \tag{6.8}$$

When $m \to \infty$, we can show that

$$\lim_{m\to\infty} \frac{m^m \gamma^{m-1}}{\Omega^m \Gamma(m)} \exp\left(-\frac{m\gamma}{\Omega}\right) = \delta\left(\frac{\gamma}{\Omega} - 1\right) \tag{6.9}$$

where $\delta(\cdot)$ is the Dirac delta function. Applying (6.9) to (6.8), we obtain

$$\lim_{m\to\infty} f_{LG}(\gamma) = \frac{1}{2\sigma\gamma\sqrt{2\pi}} \exp\left(-\frac{(\ln\gamma + 2\mu - \ln\overline{\gamma})^2}{8\sigma^2}\right) \tag{6.10}$$

which corresponds the lognormal PDF given in (6.5). In the remainder of this chapter, we will use this lognormal-Nakagami composite model to study the asymptotic performance of multiple-branch FSO systems over the correlated lognormal channels.

6.2 Diversity Analysis of FSO Systems

In this section, we will present useful results on the diversity of FSO systems over fading channels. These results will facilitate the analysis in Section 6.3.

Lemma 6.1. *For a channel state h having asymptotic PDF*[3] $f_{H,asym}(h) = ah^t + g_t(h)$*, if the received instantaneous SNR has the form $\gamma = Ch^k$, where C is a constant and k is a positive number, the asymptotic PDF of the instantaneous SNR can be obtained as $f_{\gamma,asym}(\gamma) = \frac{a}{kC^{\frac{t+1}{k}}}\gamma^{\frac{t+1}{k}-1} + g_{\frac{t+1}{k}-1}(\gamma)$.*

Proof. This result can be easily obtained by using a change of variable rule $h = \left(\frac{\gamma}{C}\right)^{\frac{1}{k}}$ in $f_{H,\text{asym}}(h) = ah^t + g_t(h)$. □

Lemma 6.1 will be frequently used in this chapter to convert the asymptotic PDF of channel state to that of received instantaneous SNR and vice versa.

Proposition 6.2. *For an L-branch system with independent received instantaneous SNRs $\gamma_i, i = 1, 2, \cdots, L$, the MRC combiner output instantaneous SNR $\gamma = \gamma_1 + \gamma_2 + \cdots + \gamma_L$ has the diversity order of $G_{d,1} + G_{d,2} + \cdots + G_{d,L}$, where $G_{d,i}$ is the diversity order on the ith branch.*

Proof. We first discuss the two-branch case ($L = 2$) and the multi-branch case can be proved iteratively by using the result of the two-branch case. For two received SNRs γ_1, γ_2 having PDFs $f_1(\gamma_1)$, $f_2(\gamma_2)$ and asymptotic PDFs

$$\begin{aligned} f_{1,\text{asym}}(\gamma_1) =& a_1\gamma_1^{t_1} + g_{t_1}(\gamma_1), \\ f_{2,\text{asym}}(\gamma_2) =& a_2\gamma_2^{t_2} + g_{t_2}(\gamma_2) \end{aligned} \tag{6.11}$$

the MRC output instantaneous SNR $\gamma = \gamma_1 + \gamma_2$ has the PDF

$$f_{\gamma,\text{MRC}}(\gamma) = \int_0^\gamma f_1(\gamma - a) f_2(a) da. \tag{6.12}$$

When $\gamma \to 0$, we have $a \to 0$ and $(\gamma - a) \to 0$; therefore, we can obtain the asymptotic PDF of γ using the asymptotic PDFs of γ_1 and γ_2 via convolution as

$$f_{\gamma,\text{asym}}(\gamma) = \int_0^\gamma f_{1,asym}(\gamma - a) f_{2,asym}(a) da. \tag{6.13}$$

[3]Hereafter we use the term asymptotic PDF to denote the PDF near origin.

Substituting (6.11) into (6.13) and using Newton's generalised binomial theorem, we can obtain the asymptotic PDF of γ as

$$f_{\gamma,\text{asym}} = a_1 a_2 \left(\sum_{k=0}^{\infty} (-1)^k \frac{\binom{t_1}{k}'}{t_2 + k + 1} \right) \gamma^{t_1+t_2+1} + g_{t_1+t_2+1}(\gamma) \tag{6.14}$$

where $\binom{r}{k}' = \frac{r(r-1)\cdots(r-k+1)}{k!}$. Therefore we have

$$G_d = (t_1 + t_2 + 1) + 1 = (t_1 + 1) + (t_2 + 1) = G_{d,1} + G_{d,2}. \tag{6.15}$$

For the L-branch case, we can construct $\gamma = ((\cdots(\gamma_1 + \gamma_2) + \gamma_3) + \gamma_4) + \cdots + \gamma_{L-1}) + \gamma_L)$ and use the two-branch result iteratively to obtain $G_d = \sum_{i=1}^{L} G_{d,i}$. □

Proposition 6.3. *When the received instantaneous SNR can be expressed as $\gamma = x \cdot y$, where x and y are independent random variables, the diversity order of the system is defined by the one with lower diversity order:* $\min\{G_{d,x}, G_{d,y}\}$*, where $G_{d,x}$ and $G_{d,y}$ are the diversity orders of system having instantaneous SNR x and y respectively.*

Proof. We first define the asymptotic PDFs of x and y as

$$\begin{aligned} f_{X,\text{asym}}(x) =& a_1 x^{t_1} + g_{t_1}(x), \\ f_{Y,\text{asym}}(y) =& a_2 y^{t_2} + g_{t_2}(y). \end{aligned} \tag{6.16}$$

For the $t_1 > t_2$ case, we can use the product distribution rule to obtain the PDF of received instantaneous SNR as

$$f_\gamma(\gamma) = \int_0^\infty f_X(x) f_Y\left(\frac{\gamma}{x}\right) \frac{1}{x} dx \tag{6.17}$$

where we have used the fact that the SNR is always a positive quantity. Partitioning the interval $[0, \infty]$ into $[0, \varepsilon]$ and $[\varepsilon, \infty]$, where ε is an arbitrarily small positive quantity, we can rewrite the PDF of γ as a sum of two parts:

$$f_\gamma(\gamma) = \int_0^\varepsilon f_X(x) f_Y\left(\frac{\gamma}{x}\right) \frac{1}{x} dx + \int_\varepsilon^\infty f_X(x) f_Y\left(\frac{\gamma}{x}\right) \frac{1}{x} dx \tag{6.18}$$

When $\gamma \to 0$, we have

$$f_{\gamma,\text{asym}}(\gamma) = \int_0^\varepsilon f_{X,\text{asym}}(x) f_{Y,\text{asym}}\left(\frac{\gamma}{x}\right) \frac{1}{x} dx + \int_\varepsilon^\infty f_X(x) f_{Y,\text{asym}}\left(\frac{\gamma}{x}\right) \frac{1}{x} dx. \tag{6.19}$$

Substituting (6.16) in (6.19), we can get

$$f_{\gamma,\text{asym}}(\gamma) = \left(\frac{a_1 a_2}{t_1 - t_2} \varepsilon^{t_1 - t_2} + a_2 \int_{\varepsilon}^{\infty} \frac{1}{x^{t_2+1}} f_X(x) dx \right) \gamma^{t_2} + g_{t_2}(\gamma). \quad (6.20)$$

Let $\varepsilon \to 0$, we can rewrite (6.20) as

$$f_{\gamma,\text{asym}}(\gamma) = a_2 M_{\log(X)}(-t_2 - 1)\gamma^{t_2} + g_{t_2}(\gamma) \quad (6.21)$$

where $M_X(t)$ is the moment-generating function (MGF) of RV x. From (6.20), we have $G_\gamma = t_2 + 1 = \min\{G_{d,1}, G_{d,2}\}$. For the case $t_1 < t_2$, we can use an equivalent product distribution rule

$$f_\gamma(\gamma) = \int_0^{\infty} f_X\left(\frac{\gamma}{y}\right) f_Y(y) \frac{1}{y} dy \quad (6.22)$$

and follow the derivation in the $t_1 > t_2$ case to obtain

$$f_{\gamma,\text{asym}}(\gamma) = a_1 M_{\log(Y)}(-t_1 - 1)\gamma^{t_1} + g_{t_1}(\gamma) \quad (6.23)$$

which shows that $G_\gamma = t_1 + 1 = \min\{G_{d,1}, G_{d,2}\}$. Therefore, the proof of Proposition 6.3 is complete. □

Corollary 6.4. *When the received instantaneous SNR can be expressed as a product of multiple independent RVs, the diversity order of the system is defined by the one with the lowest diversity order.*

Proof. We can obtain this corollary by using the derivation for the two RVs case (Proposition 6.3) iteratively. □

Proposition 6.3 and Corollary 6.4 facilitate the diversity analysis of systems with composite fading channel or with channel state that can be decomposed to multiplication of independent random variables. Based on extended Rytov theory, many atmospheric fading models that can be described by the modulation process having the channel gain of the form $h = XY$, and the received instantaneous SNR will have the same form [5]. The RV X is assumed to arise from large-scale turbulent eddy effects and Y from statistically independent small-scale eddy effects. Such product form can be considered as one random process modulating another: the mean of one distribution (fading) is modulated by another distribution (shadowing). These composite channels include, but are not limited to, lognormal-Nakagami, K, lognormal-Rician, Gamma-Gamma and $\mathcal{M}$ fading channels in FSO systems. We also find that in these atmospheric fading models, the diversity order is

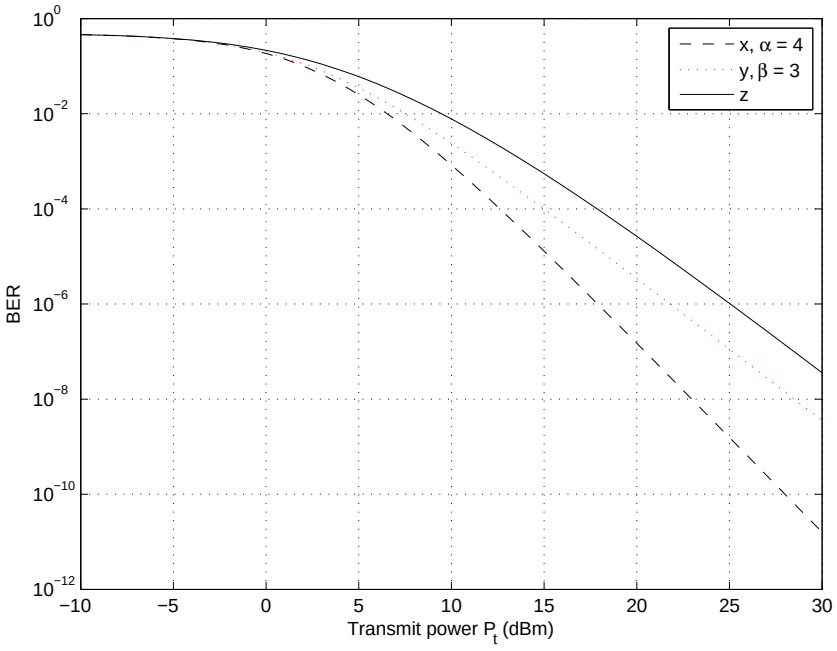

Figure 6.1: The BER of an IM/DD OOK system over the Gamma-Gamma fading channel with parameters $\alpha = 4, \beta = 3$.

usually determined by small scale effects (fading). Moreover, this proposition can be used on FSO systems with composite fading and pointing error channels [86], as well as Rayleigh, Rice, Nakagami fading with lognormal shadowing channels in radio frequency systems.

Here we assume that the thermal noise is the dominant noise source, and it is modeled by a zero mean Gaussian distribution. In the rest of this chapter, unless otherwise stated, we set its variance as $\sigma_n^2 = 10^{-6}$. We now use the Gamma-Gamma distribution and the lognormal-Nakagami distribution to exemplify Proposition 6.3.

The Gamma-Gamma RV z can be expressed as the multiplication of two Gamma RVs, namely, $z = x \cdot y$. In Fig. 6.1, we have $\alpha = 4, \beta = 3$ and the BER of IM/DD OOK systems with three channel states corresponding to RVs x, y, z are shown. In Fig. 6.2, we have $\alpha = 4, \beta = 1.3$. It can be seen that the diversity order of the system having channel state z is the same as that of the system having channel state y, which is $G_d = G_y = \min\{G_{d,x}, G_{d,y}\}$.

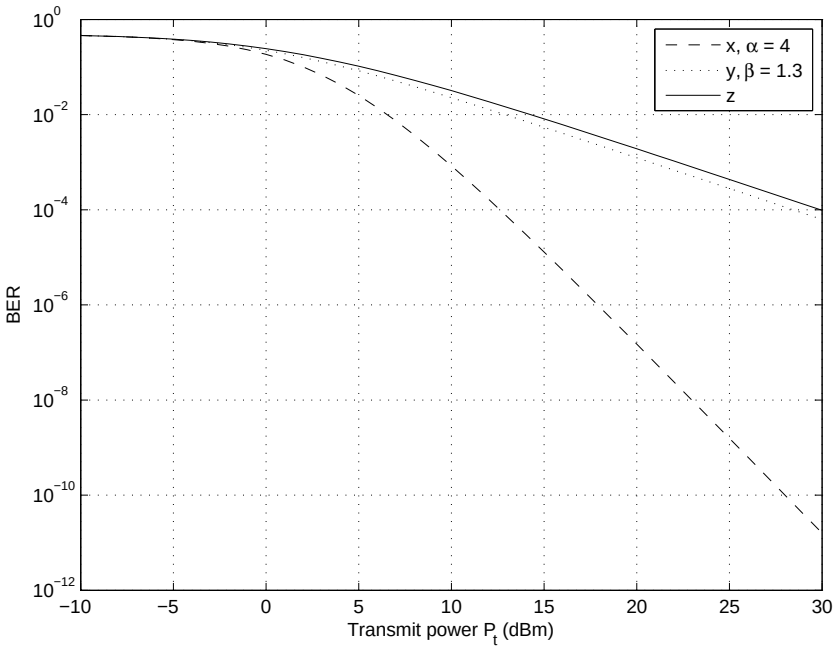

Figure 6.2: The BER of an IM/DD OOK system over the Gamma-Gamma fading channel with parameters $\alpha = 4, \beta = 1.3$.

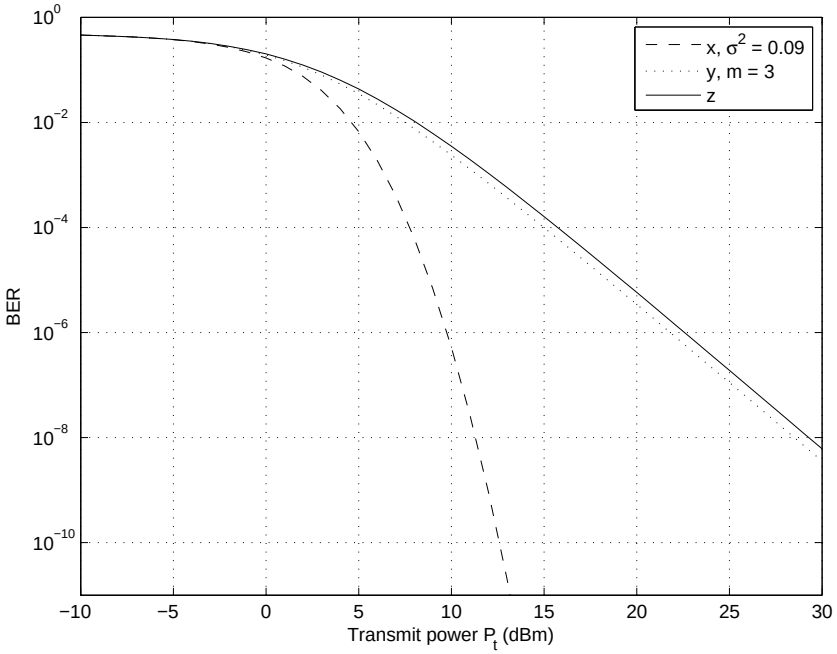

Figure 6.3: The BER of an IM/DD OOK system over the lognormal-Nakagami fading channel with parameters $\sigma^2 = 0.09, m = 3$.

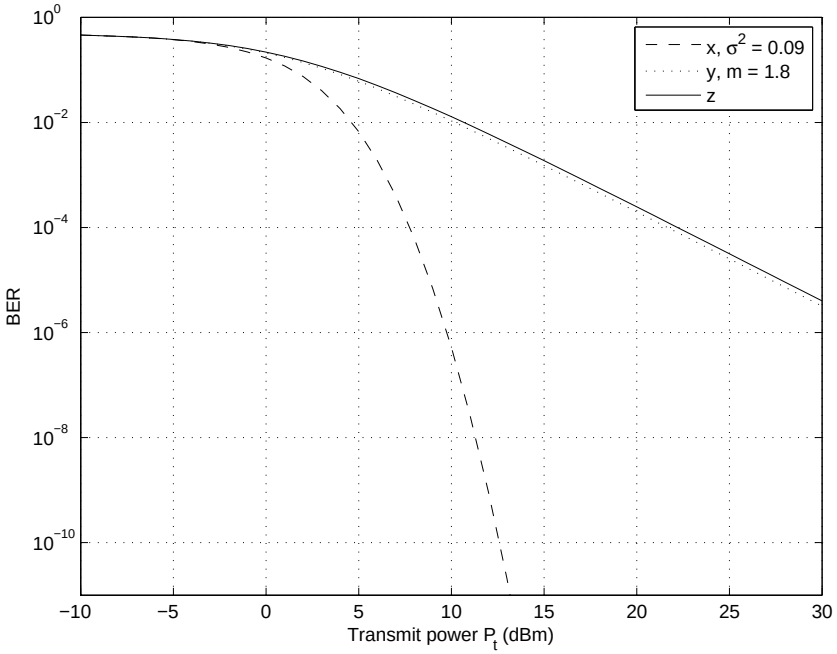

Figure 6.4: The BER of an IM/DD OOK system over the lognormal-Nakagami fading channel with parameters $\sigma^2 = 0.09, m = 1.8$.

In the lognormal-Nakagami case, we have $z = x \cdot y$, where x follows the lognormal distribution and y follows the Nakagami-m distribution. The BER of the IM/DD OOK systems having channel states x, y, z are shown in Fig. 6.3 with $\sigma^2 = 0.09, m = 3$ and Fig. 6.4 with $\sigma^2 = 0.09, m = 1.8$. It can be seen that the diversity order of the system is determined by the m parameter, which is $G_d = G_{d,y} = \min\{G_{d,x}, G_{d,y}\}$.

Therefore, we can observe that the diversity order of the system is $\min\{G_{d,x}, G_{d,y}\}$, which is predicted by Proposition 6.3.

6.3 FSO Systems over Correlated Lognormal Fading Channels

In order to investigate the performance characteristics of correlated lognormal channels, we use the lognormal-Nakagami fading model introduced in Section 6.1. First we consider a dual-branch system, then we generalize it to the multiple-branch case.

6.3.1 Dual-branch System

For a dual-branch system, we model the two channel states h_1 and h_2 as

$$\begin{aligned} h_1 &= x_1 \cdot y_1, \\ h_2 &= x_2 \cdot y_2 \end{aligned} \tag{6.24}$$

where y_1 and y_2 are i.i.d. Nakagami-m RVs; x_1 and x_2 are correlated lognormal RVs with PDF

$$f_{logn,logn}(x_1, x_2) = \frac{1}{2\pi\sigma_1\sigma_2\sqrt{1-\rho^2}x_1x_2} \times \exp\left(-\frac{1}{2(1-\rho^2)}\left(\begin{array}{l}\frac{(\ln x_1-\mu_1)^2}{\sigma_1^2}+ \\ \frac{(\ln x_2-\mu_2)^2}{\sigma_2^2}- \\ \frac{2\rho(\ln x_1-\mu_1)(\ln x_2-\mu_2)}{\sigma_1\sigma_2}\end{array}\right)\right) \tag{6.25}$$

where ρ is the correlation coefficient between x_1 and x_2. Based on the derivation in Appendix G.1.1, we can obtain the asymptotic PDF of the instantaneous SNR γ at the output of MRC as

$$f_{\gamma,\text{asym}}(\gamma) = \frac{m^{2m}}{\Gamma(m)^2} S_{1,1} \gamma^{2m-1} \exp\left(\tfrac{m}{2}(m+1)(\sigma_1^2+\sigma_2^2) + m^2\rho\sigma_1\sigma_2\right) \tag{6.26}$$

where $S_{p,q} = \left(\sum_{i=0}^{pm-1} (-1)^i \frac{\binom{pm-1}{i}}{qm+i} \right), p, q = 1, 2, \cdots$. The diversity order can be obtained from (6.26) as

$$G_d = 2m. \tag{6.27}$$

The coding gain is obtained as

$$G_c = 2 \left[\begin{array}{l} \frac{2^{2m-2}\Gamma\left(2m+\frac{1}{2}\right)m^{2m}}{\sqrt{\pi}m\Gamma(m)^2} \left(\sum\limits_{i=0}^{m-1} (-1)^i \frac{\binom{m-1}{i}}{m+i} \right) \\ \times \exp\left(\frac{m}{2}(m+1)(\sigma_1^2+\sigma_2^2) + m^2\rho\sigma_1\sigma_2\right) \end{array} \right]^{-\frac{1}{2m}} \tag{6.28}$$

where $\binom{n}{k} = \frac{n!}{(n-k)!k!}$.

It is clear from (6.27) and (6.28) that the diversity order is determined only by the parameter m in Nakagami distribution, while the coding gain is affected by the correlation ρ. Therefore, the relative coding gain can be obtained as

$$\frac{G_{c,\text{correlated}}}{G_{c,\text{independent}}} = \exp\left(-\frac{m}{2}\rho\sigma_1\sigma_2\right) = -2.17m\rho\sigma_1\sigma_2 \quad \text{dB}. \tag{6.29}$$

From (6.29), we conclude that the SNR penalty (w.r.t. the independent branches) induced by correlation trends to be infinity when $m \to \infty$.

6.3.2 Multiple-Branch System

Lemma 6.5. *The asymptotic PDF of L-branch MRC, EGC and SC system over the correlated lognormal-Nakagami channels can be expressed as*

$$f_{\gamma,asym}(\gamma) = \frac{m^{Lm}c}{\Gamma(m)^L}\gamma^{Lm-1}\exp\left(\frac{1}{2}m\left(\left(\sum_{i=1}^{L}\sigma_i^2\right) + m||\Sigma||_1\right)\right) \tag{6.30}$$

where $||\Sigma||_1$ *denotes the entry-wise norm of the covariance matrix* Σ *in* (6.6), *which is defined as* $||\Sigma||_1 = \sum\limits_{i=1}^{L}\sum\limits_{j=1}^{L}|\sigma_{i,j}^2|$, *and we have*

$$\begin{cases} c = \prod\limits_{i=1}^{L-1} S_{1,i} & MRC, \\ c = 2^{L-1}L^{Lm}\prod\limits_{i=1}^{L-1} S_{2,2i} & EGC, \\ c = Lm^{1-L} & SC. \end{cases} \tag{6.31}$$

Proof. See Appendix A. □

From (6.30), we can obtain the SNR penalty induced by correlation on multi-branch systems as

$$\frac{G_{c,\text{correlated}}}{G_{c,\text{independent}}} = \exp\left(-\frac{m}{4}\left(||\Sigma||_1 - \text{tr}(\Sigma)\right)\right) = -1.09m\left(||\Sigma||_1 - \text{tr}(\Sigma)\right) \tag{6.32}$$

where $\text{tr}(A)$ denotes the trace of an square matrix A. It can be seen from (6.32) that the SNR penalty induced by correlation is also infinity when $m \to \infty$ for the multi-branch systems over the correlated lognormal fading channels. In [6], the authors also reached a similar conclusion based only on numerical observations.

In order to compare the asymptotic performance of different FSO systems over different lognormal fading channels, we define the asymptotic relative diversity order as

$$ARDO \triangleq \lim_{\bar{\gamma}\to\infty} \frac{\log(P_{e,1}(\bar{\gamma}))}{\log(P_{e,L}(\bar{\gamma}))}. \tag{6.33}$$

Proposition 6.6. *The asymptotic relative diversity order between L-branch MRC system with covariance matrix Σ of the logarithm of lognormal channel states and single-branch system with lognormal fading variance of σ^2 is $L^2\sigma^2$ divided by the entry-wise norm of the covariance matrix of L-branch system, which is $ARDO = \frac{L^2\sigma^2}{||\Sigma||_1}$. When every branch of L-branch system has identical variance of that of single-branch system, we have $ARDO = \frac{L^2}{||R||_1}$ where R is the correlation matrix of the logarithm of lognormal channel states in an L-branch system.*

Proof. See Appendix H. □

Note that when each branch of the L-branch system has identical variance of that of single channel system, we have $1 \leq ARDO \leq L$. The left equality sign can be achieved when the channels are fully correlated (all-ones correlation matrix), and the right equality sign can be achieved when the channels are uncorrelated (identity correlation matrix). It is worthy to note that the ARDO between different systems can be obtained using the ARDO derived from Proposition 6.6.

In Fig. 6.5 and Fig. 6.6, we use a dual-branch system to exemplify Proposition 6.6. Fig. 6.5 presents the RDO between a dual-branch system having identical lognormal fading ($\sigma_1^2 = \sigma_2^2 = 0.49$) and a single-branch system ($\sigma^2 = 0.49$). The the ARDO calculated by $ARDO = \frac{L^2}{||R||_1}$ is also

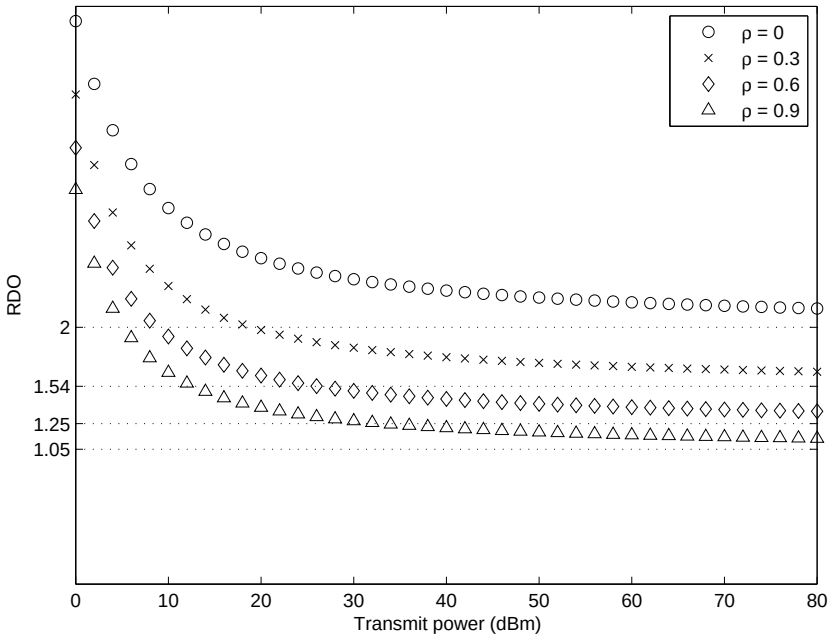

Figure 6.5: The RDO between a dual-branch system in the lognormal fading channels with $\sigma_1^2 = \sigma_2^2 = 0.49$ and a single-branch system with $\sigma^2 = 0.49$.

shown in Fig. 6.5 as the dot lines. In Fig. 6.6, the RDO is presented for a dual-branch system having nonidentical lognormal fading ($\sigma_1^2 = 0.49, \sigma_2^2 = 0.64$) and a single-branch system ($\sigma^2 = 0.49$). In Fig. 6.7, we present the RDO between a three-branch system and a single-branch system ($\sigma^2 = 0.49$). For simplicity, we set the covariance matrix of the three-branch system as

$$\Sigma = \sigma^2 \begin{bmatrix} 1 & \rho & \rho^2 \\ \rho & 1 & \rho \\ \rho^2 & \rho & 1 \end{bmatrix}. \tag{6.34}$$

Due to the computational limitations in mathematical softwares, some RDOs can not be calculated when the transmit power is large. From the obtained results, we can see that the RDO tends to approach the ARDO given in Proposition 6.6.

Proposition 6.7. *The coding gain difference between the L-branch MRC and EGC systems over correlated lognormal channels tends to be* $0dB$*, that*

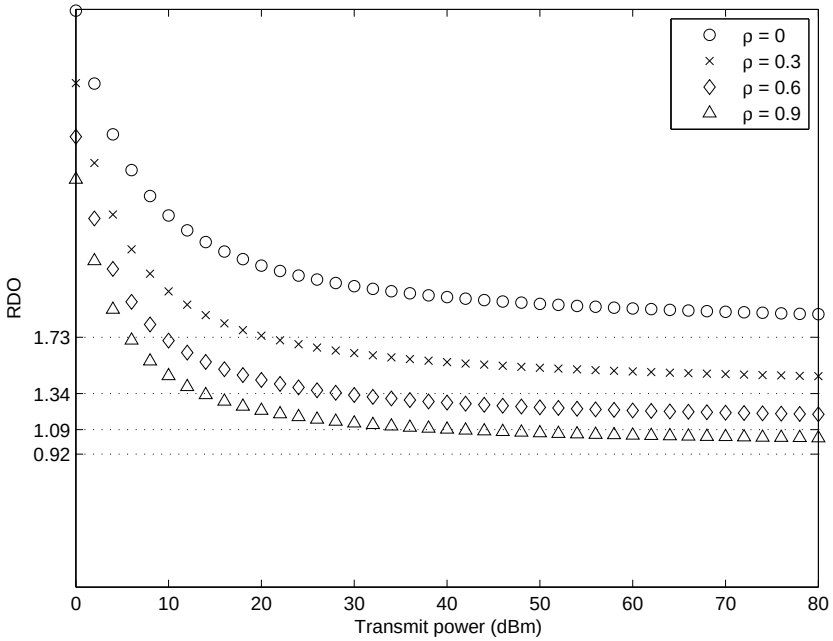

Figure 6.6: The RDO between a dual-branch system in the lognormal fading channels with $\sigma_1^2 = 0.49, \sigma_2^2 = 0.64$ and a single-branch system with $\sigma^2 = 0.49$.

is $\lim_{\bar{\gamma}\to\infty} \frac{G_{c,EGC}}{G_{c,MRC}} = 0dB$*,while the asymptotic BER difference is* $3.01(L-1)dB$*, that is* $\lim_{\bar{\gamma}\to\infty} \frac{P_{e,EGC,asym}}{P_{e,MRC,asym}} = 2^{L-1}$*. The coding gain difference between the MRC and SC systems is* $\lim_{\bar{\gamma}\to\infty} \frac{G_{c,SC}}{G_{c,MRC}} = \frac{1}{L} = -10\log(L)dB$.

Proof. This proposition can be obtained by comparing the results in Lemma 6.5. First we have $P_e = (G_c\bar{\gamma})^{-G_d}$, and from (6.30) we can obtain that

$$G_d = Lm,$$

$$G_c = 2\left(\frac{2^{Lm-1}\Gamma\left(Lm+\frac{1}{2}\right)m^{Lm}c}{\sqrt{\pi}Lm\Gamma(m)^L}\exp\left(\frac{1}{2}m\left(\left(\sum_{i=1}^{L}\sigma_i^2\right)+m||\Sigma||_1\right)\right)\right)^{-\frac{1}{Lm}}. \tag{6.35}$$

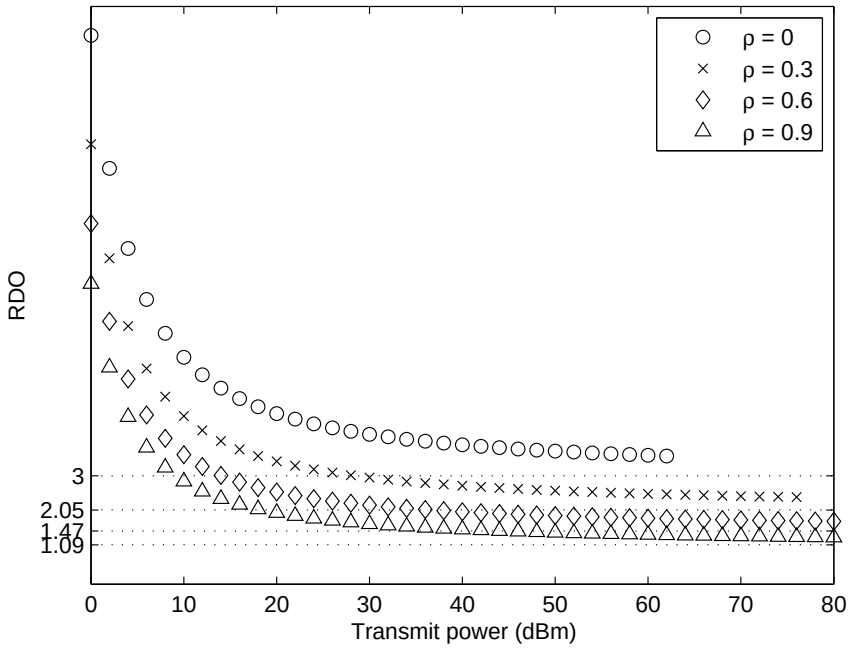

Figure 6.7: The RDO between a three-branch system in the lognormal fading channels and a single-branch system with $\sigma^2 = 0.49$.

Therefore we have

$$\begin{aligned} G_{d,\mathrm{MRC}} &= G_{d,\mathrm{EGC}} = G_{d,\mathrm{SC}}, \\ \frac{G_{c,\mathrm{EGC}}}{G_{c,\mathrm{MRC}}} &= \left(\frac{c_{\mathrm{EGC}}}{c_{\mathrm{MRC}}}\right)^{-\frac{1}{Lm}}, \\ \frac{G_{c,\mathrm{SC}}}{G_{c,\mathrm{MRC}}} &= \left(\frac{c_{\mathrm{SC}}}{c_{\mathrm{MRC}}}\right)^{-\frac{1}{Lm}}. \end{aligned} \tag{6.36}$$

Recall that $S_{p,q} = \sum_{i=0}^{pm-1}(-1)^i \frac{\binom{pm-1}{i}}{qm+i}$, which can be shown to have the following equivalent form:

$$S_{p,q} = \int_0^1 (1-a)^{pm-1} a^{qm-1} da. \tag{6.37}$$

For $m \to \infty$, we have

$$\begin{aligned}\lim_{m\to\infty} S_{p,q}{}^{\frac{1}{m}} =& ||(1-a)^p a^q||_\infty \\ =& \max\{(1-a)^p a^q, a \in [0,1]\} \\ =& \frac{p^p q^q}{(p+q)^{p+q}}.\end{aligned} \tag{6.38}$$

Therefore for a sufficiently large value of m, we have

$$S_{p,q} \approx \left(\frac{p^p q^q}{(p+q)^{p+q}}\right)^m. \tag{6.39}$$

When $m \to \infty$, we can use (6.39), (6.31) and (6.36) to obtain

$$\begin{aligned}\lim_{m\to\infty} \frac{G_{c,\mathrm{EGC}}}{G_{c,\mathrm{MRC}}} &= \lim_{m\to\infty} \left(2^{L-1}\right)^{-\frac{1}{Lm}} = 1, \\ \lim_{m\to\infty} \frac{G_{c,\mathrm{SC}}}{G_{c,\mathrm{MRC}}} &= \lim_{m\to\infty} \left(L^{Lm}\right)^{-\frac{1}{Lm}} = L^{-1}.\end{aligned} \tag{6.40}$$

While the coding gain difference of MRC and EGC tends to be $0dB$, the BER difference in large average SNR region is a constant and it is given by

$$\begin{aligned}\lim_{\bar{\gamma}\to\infty} \frac{P_{e,\mathrm{EGC}}}{P_{e,\mathrm{MRC}}} &= \left(\frac{G_{c,\mathrm{EGC}}}{G_{c,\mathrm{MRC}}}\right)^{-Lm} \\ &= \left(\frac{c_{\mathrm{EGC}}}{c_{\mathrm{MRC}}}\right)^{-Lm} \\ &= 2^{L-1}.\end{aligned} \tag{6.41}$$

With the results in (6.40) and (6.41), we have completed the proof. □

For a dual-branch system, the asymptotic BER difference between MRC and EGC is $3.01dB$, which represents the vertical distance between the BER plots of MRC and EGC systems. The coding gain difference between MRC and SC is $3.01dB$, which represents the horizontal distance between the BER plots of MRC and SC systems. These results suggest that the MRC and EGC has similar diversity performance while SC suffers certain SNR loss. Similar results have also been observed in the numerical results section of [6, 52]. In Tables I and II, we present the results on the SNR and BER offset among the MRC, EGC and SC systems. It can be seen that the results tend to match those stated in Proposition 6.7.

Table 6.1: SNR and BER offset between MRC, EGC and SC system over lognormal fading channels ($\sigma_1^2 = \sigma_2^2 = 4$).

Transmit Power (dB)	0	50	100	150	200
SNR offset: EGC/MRC (dB)	-0.76	-0.22	-0.12	-0.08	-0.06
SNR offset: SC/MRC (dB)	-0.56	-2.06	-2.38	-2.56	-2.67
BER offset: EGC/MRC (dB)	-0.34	-1.23	-1.36	-1.41	-1.43
BER offset: SC/MRC (dB)	-0.23	-10.76	-26.25	-42.58	-59.22

Table 6.2: SNR and BER offset between MRC, EGC and SC system over lognormal fading channels ($\sigma_1^2 = \sigma_2^2 = 0.64$).

Transmit Power (dB)	0	20	40	60	80
SNR offset: EGC/MRC (dB)	-0.17	-0.07	-0.04	-0.03	-0.02
SNR offset: SC/MRC (dB)	-1.90	-2.57	-2.72	-2.80	-2.83
BER offset: EGC/MRC (dB)	-0.51	-1.15	-1.29	-1.36	-1.39
BER offset: SC/MRC (dB)	-3.47	-38.10	-79.33	-121.54	-164.12

6.4 Summary

In this chapter, we studied a multiple-branch FSO system over correlated lognormal fading channels. The diversity of FSO systems over composite fading channels was also analyzed, and we found that the diversity of the system is determined by the lowest diversity RV in the product form. For multiple-branch FSO systems, we found that the correlation of lognormal channels can cause large SNR penalty. We also showed that the ARDO between L-branch FSO system and a single-branch FSO system over the lognormal fading channel is $L^2\sigma^2$ divided by the entry-wise norm of the covariance matrix Σ. The derived ARDO can provide FSO system designers with a simple asymptotic performance metric to allow asymptotic performance comparison between different FSO systems under various lognormal channel conditions. The MRC, EGC and SC combining techniques were also compared in the context of correlated lognormal channels. We found that the MRC and EGC have similar performance but SC suffers a $10\log(L)$dB loss, which suggests that EGC is desirable for multiple-branch FSO systems in terms of better performance and complexity tradeoff.

Chapter 7

Conclusions

In this chapter, we summarize the results obtained in this thesis. Also, we present several potential future research topics which are related to our accomplished work.

7.1 Summary of Results

In this thesis, we conducted analytical performance evaluation of FSO systems over atmospheric fading channels. The obtained results can provide the FSO system designers with insights into the performance of such systems, which include the system performance over different atmospheric fading channels, the effects of adverse factors on system performance, and the effects of spatial diversity and correlation on system performance. First, we investigated the FSO systems over lognormal, Gamma-Gamma and lognormal-Rician fading channels. Then we studied the pointing error effects and phase error effects, which may cause performance degradation in practical FSO systems. In the end, we analyzed an FSO system with multiple branch reception over correlated lognormal fading channels. Here we summarize the results obtained in each chapters as follows.

In Chapter 3, we analyzed the error rate performance of a coherent FSO system over the lognormal-Rician turbulence channels using a PA approach. Closed-form BER expressions for BPSK and DPSK FSO systems with MRC reception were obtained. We also presented the asymptotic error rate analysis. We proved that PA is a powerful analytical tool for analyzing optical communication systems in lognormal-Rician channel that is analytically intractable. Our analysis further showed that the PA approach is particularly useful in obtaining highly accurate small error rate estimation.

In Chapter 4, we proposed a nonzero boresight pointing error model by considering beamwidth, detector aperture, and jitter variance. We assume that the boresight component of pointing error effects is not negligible, and the sway on x-axis and y-axis are Gaussian distributed. We derived closed-form PDF for the nonzero boresight pointing error model. Based on such a pointing error model, we derived closed-form composite PDF for the lognor-

mal fading and accurate series based PDF for the Gamma-Gamma fading. Highly accurate convergent series BER expressions were obtained. Through the asymptotic BER analysis and numerical results, we observed that the boresight error causes an SNR penalty factor on error rate performance at high SNR. By examining the asymptotic BER curves, we found that the diversity order of the FSO system over the composite lognormal fading channel is solely determined by the pointing error parameter γ^2, which means that the boresight component does not affect the diversity order. While in the composite Gamma-Gamma fading channel, the diversity order is determined by either the Gamma-Gamma fading effect or the pointing error effect, depending on which is stronger.

In Chapter 5, we studied the BER performance of a subcarrier MPSK system with CPE over lognormal fading channels. The CPE induced asymptotic noise reference loss over the lognormal channels was quantified. In the derivation, we proposed to use an auxiliary RV method to approach the lognormal channel with a lognormal-Nakagami channel. Our results showed that the CPE induced performance degradation for a subcarrier BPSK system over the lognormal channel is negligible. We also found that the CPE induced performance degradation increases with higher modulation order and lower PLL SNR coefficient C.

In Chapter 6, we studied an FSO system with spatial diversity reception over correlated lognormal fading channels. The diversity of such system over composite fading channels was also analyzed, and we found that the diversity is determined by the lowest diversity RV in the product form. We also found that the correlation of lognormal channels can cause large SNR penalty for multiple-branch FSO systems. We obtained that the ARDO between L-branch FSO system and a single-branch FSO system over the lognormal fading channel is $L^2\sigma^2$ divided by the entry-wise norm of the covariance matrix Σ. The derived ARDO can provide FSO system designers with a simple asymptotic performance metric to allow asymptotic performance comparison between different FSO systems under various lognormal channel conditions. The MRC, EGC and SC combining techniques were also compared in the context of correlated lognormal channels. We observed that the MRC and EGC have similar performance but SC suffers a $10\log(L)$dB loss, which suggests that EGC is desirable for multiple-branch FSO systems due to its near optimal performance and moderate complexity.

7.2 Future Work

7.2.1 FSO system with pointing errors

In Chapter 4, we proposed a nonzero boresight pointing error model by assuming Gaussian distribution on x-axis and y-axis sway. In practical FSO systems, the displacement between beam center and receiver center may follow other distributions, such as uniform distribution, arcsin distribution and truncated normal distribution. Therefore it is useful to investigate the effects of pointing errors with different distributions on the system performance. On the other hand, in the thesis we only obtain the diversity order for FSO systems with nonzero boresight pointing errors over the Gamma-Gamma fading channels when $\gamma^2 > \alpha$, which implies that the Gamma-Gamma fading effect is more dominant than the pointing error effect with respect to the BER performance at high average SNR region. However, when $\gamma^2 < \alpha$, the diversity order will depend on both γ^2 and the boresight s. An explicit expression of diversity order for nonzero boresight pointing case has not been obtained yet. It is interesting to investigate the case of $\gamma^2 < \alpha$ for such a system model.

7.2.2 FSO Networks over Correlated Lognormal Fading Channels

In Chapter 6, we conducted the asymptotic performance analysis on FSO systems over lognormal fading channels. The diversity of FSO systems over composite fading channels was also analyzed, and we found that the diversity of the system is determined by the lowest diversity RV in the product form. Such a result can be used to analyze the diversity of system under various fading channels. The ARDO obtained for multiple branch FSO systems can be used as a performance metric for multihop FSO networks, which will greatly simplify the asymptotic analysis on these systems.

Bibliography

[1] Lightpointe, http://www.lightpointe.com/. → pages 2, 3

[2] Facebook, https://www.internet.org/. → pages 2

[3] S. Bloom, E. Korevaar, J. Schuster, and H. Willebrand, "Understanding the performance of free-space optics," *J. Opt. Netw.*, vol. 2, pp. 178–200, June 2003. → pages 2, 3, 4, 16, 37, 51

[4] L. C. Andrews, R. L. Phillips, and C. Y. Hopen, *Laser Beam Scintillation With Applications*. SPIE Press, 2001. → pages 3

[5] L. C. Andrews and R. L. Phillips, *Laser Beam Propagation Through Random Media*. SPIE Press, 2005. → pages 3, 8, 68

[6] S. M. Navidpour, M. Uysal, and M. Kavehrad, "BER performance of free-space optical transmission with spatial diversity," *IEEE Trans. Wireless Commun.*, vol. 6, pp. 2813–2819, Aug. 2007. → pages 3, 8, 9, 75, 79

[7] T. A. Tsiftsis, H. G. Sandalidis, G. K. Karagiannidis, and M. Uysal, "Optical wireless links with spatial diversity over strong atmospheric turbulence channels," *IEEE Trans. Wireless Commun.*, vol. 8, pp. 951–957, Feb. 2009. → pages 3, 4, 8, 9, 63

[8] X. Zhu and J. M. Kahn, "Free-space optical communication through atmospheric turbulence channels," *IEEE Trans. Commun.*, vol. 50, pp. 1293–1300, Aug. 2002. → pages 3, 4, 8, 9

[9] S. Arnon, "Optimization of urban optical wireless communication systems," *IEEE Trans. Wireless Commun.*, vol. 2, pp. 626–629, July 2003. → pages 3, 6

[10] M. Uysal, S. M. Navidpour, and J. Li, "Error rate performance of coded free-space optical links over strong turbulence channels," *IEEE Commun. Lett.*, vol. 8, pp. 635–637, Oct. 2004. → pages 4

[11] A. A. Farid and S. Hranilovic, "Outage capacity optimization for free-space optical links with pointing errors," *IEEE/OSA J. Lightwave Technol.*, vol. 25, pp. 1702–1710, July 2007. → pages 4, 6, 7, 17, 34, 35, 36, 51, 94

[12] W. Gappmair, S. Hranilovic, and E. Leitgeb, "Ook performance for terrestrial fso links in turbulent atmosphere with pointing errors modeled by hoyt distributions," *IEEE Commun. Lett.*, vol. 15, pp. 875–877, Aug. 2011. → pages 4, 7, 34, 52, 100

[13] S. Rajbhandari, Z. Ghassemlooy, P. A. Haigh, T. Kanesan, and X. Tang, "Experimental error performance of modulation schemes under a controlled laboratory turbulence fso channel," *IEEE/OSA J. Lightwave Technol.*, vol. 33, pp. 244–250, Jan. 2015. → pages 4

[14] M. Z. Win, C. C. Chen, and R. A. Scholtz, "Optical phase-locked loop for an amplitude modulated communications link using solid-state lasers," *IEEE J. Sel. Areas Commun.*, vol. 13, pp. 569–576, Apr. 1995. → pages 4

[15] K. Kiasaleh, "Performance of coherent dpsk free-space optical communication systems in k-distributed turbulence," *IEEE Trans. Commun.*, vol. 54, pp. 604–607, Apr. 2006. → pages 4, 24

[16] A. Belmonte and J. Khan, "Performance of synchronous optical receiversusing atmospheric compensation techniques," *Opt. Express*, vol. 16, pp. 14 151–14 162, Sep. 2008. → pages 4

[17] M. Niu, J. Cheng, and J. F. Holzman, "Error rate analysis of m-ary coherent free-space optical communication systems with k-distributed turbulence," *IEEE Trans. Commun.*, vol. 59, pp. 664–668, Mar. 2011. → pages 4, 9, 24

[18] H. G. Sandalidis, T. A. Tsiftsis, and G. K. Karagiannidis, "Optical wireless communications with heterodyne detection over turbulence channels with pointing errors," *IEEE/OSA J. Lightwave Technol.*, vol. 27, pp. 4440–4445, Oct. 2009. → pages 4, 6, 7, 35

[19] W. Gappmair, "Further results on the capacity of free-space optical channels in turbulent atmosphere," *IET Communications*, vol. 5, pp. 1262–1267, June 2011. → pages 4

[20] E. Jakeman and P. N. Pusey, "Significance of k distributions in scattering experiments," *Phys. Rev. Lett.*, vol. 40, pp. 546–550, Feb. 1978. → pages 5

[21] E. Jakeman, "On the statistics of k-distributed noise," *Journal of Physics A: Mathematical and General*, vol. 13, p. 31, Jan. 1980. → pages 5

[22] J. H. Churnside and R. J. Hill, "Probability density of irradiance scintillations for strong path-integrated refractive turbulence," *J. Opt. Soc. Am. A*, vol. 4, pp. 727–733, Apr. 1987. → pages 5, 18, 19, 34

[23] T. E. Ewart, "A model of the intensity probability distribution for wave propagation in random media," *J. Acoust. Soc. Am.*, vol. 86, pp. 1490–1498, Oct. 1989. → pages 5

[24] T. E. Ewart and D. B. Percival, "Forward scattered waves in random media—the probability distribution of intensity," *J. Acoust. Soc. Am.*, vol. 80, pp. 1745–1753, Dec. 1986. → pages 5

[25] L. C. Andrews and R. L. Phillips, "I-k distribution as a universal propagation model of laser beams in atmospheric turbulence," *J. Opt. Soc. Am. A*, vol. 2, pp. 160–163, Feb. 1985. → pages 5

[26] ——, "Mathematical genesis of the i-k distribution for random optical fields," *J. Opt. Soc. Am. A*, vol. 3, pp. 1912–1919, Nov. 1986. → pages 5

[27] J. H. Churnside and S. F. Clifford, "Log-normal rician probability-density function of optical scintillations in the turbulent atmosphere," *J. Opt. Soc. Am. A*, vol. 4, pp. 1923–1930, Oct. 1987. → pages 5

[28] M. A. Alhabash, L. C. Andrews, and R. L. Phillips, "Mathematical model for the irradiance probability density function of a laser beam propagating through turbulent media," *Optical Engineering*, vol. 40, pp. 1554–1562, Feb. 2001. → pages 5, 18

[29] J. H. Churnside and R. G. Frehlich, "Experimental evaluation of log-normally modulated rician and ik models of optical scintillation in the atmosphere," *J. Opt. Soc. Am. A*, vol. 6, pp. 1760–1766, Nov. 1989. → pages 5, 19

[30] I. I. Kim, R. Stieger, J. A. Koontz, C. Moursund, M. Barclay, P. Adhikari, J. Schuster, E. Korevaar, R. Ruigrok, and C. DeCusatis, "Wireless optical transmission of fast ethernet, fddi, atm, and escon protocol data using the terralink laser communication system," *Optical Engineering*, vol. 37, pp. 3143–3155, June 1998. → pages 5, 37, 51

[31] D. K. Borah and D. G. Voelz, "Estimation of laser beam pointing parameters in the presence of atmospheric turbulence," *Applied Optics*, vol. 46, pp. 6010–6018, Aug. 2007. → pages 5

[32] ——, "Pointing error effects on free-space optical communication links in the presence of atmospheric turbulence," *IEEE/OSA J. Lightwave Technol.*, vol. 27, pp. 3965 –3973, Sept. 2009. → pages 5, 6

[33] C. C. Chen and C. S. Gardner, "Impact of random pointing and tracking errors on the design of coherent and incoherent optical intersatellite communication links," *IEEE Trans. Commun.*, vol. 37, pp. 252–260, Mar. 1989. → pages 6

[34] D. K. Borah, D. Voelz, and S. Basu, "Maximum-likelihood estimation of a laser system pointing parameters by use of return photon counts," *Appl. Opt.*, vol. 45, pp. 2504–2509, Apr. 2006. → pages 6

[35] S. Arnon, "Effects of atmospheric turbulence and building sway on optical wireless-communication systems," *Opt. Lett.*, vol. 28, pp. 129–131, Jan. 2003. → pages 6, 7

[36] H. G. Sandalidis, T. A. Tsiftsis, G. K. Karagiannidis, and M. Uysal, "BER performance of FSO links over strong atmospheric turbulence channels with pointing errors," *IEEE Commun. Lett.*, vol. 12, pp. 44–46, Jan. 2008. → pages 6, 7, 63

[37] X. Liu, "Free-space optics optimization models for building sway and atmospheric interference using variable wavelength," *IEEE Trans. Commun.*, vol. 57, pp. 492–498, Feb. 2009. → pages 6

[38] W. Gappmair, S. Hranilovic, and E. Leitgeb, "Performance of ppm on terrestrial fso links with turbulence and pointing errors," *IEEE Commun. Lett.*, vol. 14, pp. 468–470, May 2010. → pages 6, 7

[39] A. García-Zambrana, B. Castillo-Vázquez, and C. Castillo-Vázquez, "Asymptotic error-rate analysis of fso links using transmit laser selection over gamma-gamma atmospheric turbulence channels with point-

ing errors," *Opt. Express*, vol. 20, pp. 2096–2109, Jan. 2012. → pages 6, 7, 9

[40] A. A. Farid and S. Hranilovic, "Diversity gain and outage probability for mimo free-space optical links with misalignment," *IEEE Trans. Commun.*, vol. 60, pp. 479–487, Feb. 2012. → pages 6, 8, 9, 35, 42, 51, 63

[41] J. Li, J. Q. Liu, and D. P. Tayler, "Optical communication using subcarrier psk intensity modulation through atmospheric turbulence channels," *IEEE Trans. Commun.*, vol. 55, pp. 1598–1606, Aug. 2007. → pages 7

[42] W. Huang, J. Takayanagi, T. Sakanaka, and M. Nakagawa, "Atmospheric optical communication system using subcarrier psk modulation," *IEICE Trans. Commun.*, vol. E76-B, pp. 1169–1177, Sept. 1993. → pages 7

[43] W. O. Popoola, Z. Ghassemlooy, J. I. H. Allen, E. Leitgeb, and S. Gao, "Free-space optical communication employing subcarrier modulation and spatial diversity in atmospheric turbulence channel," *IET Optoelectron.*, vol. 2, pp. 16–23, Feb. 2008. → pages 7

[44] W. O. Popoola, Z. Ghassemlooy, and V. Ahmadi, "Performance of subcarrier modulated free-space optical communication link in negative exponential atmospheric turbulence environment," *Int. J. Auton. Adapt. Commun. Syst.*, vol. 1, pp. 342–355, Jan. 2008. → pages

[45] W. O. Popoola and Z. Ghassemlooy, "Bpsk subcarrier intensity modulated free-space optical communications in atmospheric turbulence," *IEEE/OSA J. Lightwave Technol.*, vol. 27, pp. 967–973, Apr. 2009. → pages 7

[46] H. Samimi and P. Azmi, "Subcarrier intensity modulated free-space optical communications in K-distributed turbulence channels,," *IEEE/OSA J. Opt. Commun. Netw.*, vol. 2, pp. 625–632, Aug. 2010. → pages 7

[47] X. Song, M. Niu, and J. Cheng, "Error rate of subcarrier intensity modulations for wireless optical communications," *IEEE Commun. Lett.*, vol. 16, pp. 540–543, Apr. 2012. → pages 7

[48] X. Song and J. Cheng, "Optical communication using subcarrier intensity modulation in strong atmospheric turbulence," *IEEE/OSA J. Lightwave Technol.*, vol. 30, pp. 3484–3493, Nov. 2012. → pages 53

[49] ——, "Subcarrier intensity modulated optical wireless communications using noncoherent and differentially coherent modulations," *IEEE/OSA J. Lightwave Technol.*, vol. 31, pp. 1906–1913, June 2013. → pages 7

[50] I. I. Kim, H. Hakakha, P. Adhikari, E. J. Korevaar, and A. K. Majumdar, "Scintillation reduction using multiple transmitters," *Proc. SPIE*, vol. 2990, pp. 102–113, Apr. 1997. → pages 7

[51] M. M. Ibrahim and A. M. Ibrahim, "Performance analysis of optical receivers with space diversity reception," *Proc. IEEE*, vol. 143, pp. 369–372, Dec. 1996. → pages 8

[52] E. J. Shin and V. W. S. Chan, "Optical communication over the turbulent atmospheric channel using spatial diversity," in *Global Telecommunications Conference, 2002. GLOBECOM '02. IEEE*, vol. 3, Nov. 2002, pp. 2055–2060. → pages 8, 79

[53] M. Razavi and J. H. Shapiro, "Wireless optical communications via diversity reception and optical preamplification," *IEEE Trans. Wireless Commun.*, vol. 4, pp. 975–983, May 2005. → pages 8

[54] S. G. Wilson, M. Brandt-Pearce, Q. Cao, and J. H. Leveque, "Free-space optical mimo transmission with q-ary PPM," *IEEE Trans. Commun.*, vol. 53, pp. 1402–1412, Aug. 2005. → pages 8

[55] C. Abou Rjeily and A. Slim, "Cooperative diversity for free-space optical communications: Transceiver design and performance analysis," *IEEE Trans. Commun.*, vol. 59, pp. 658–663, Mar. 2011. → pages 9

[56] S. Haddad and O. Leveque, "Diversity analysis of free-space optical networks with multihop transmissions," in *2014 IEEE International Conference on Communications (ICC)*, June 2014, pp. 3406–3411. → pages 8

[57] E. J. Lee and V. W. S. Chan, "Part 1: optical communication over the clear turbulent atmospheric channel using diversity," *IEEE J. Sel. Areas Commun.*, vol. 22, no. 9, pp. 1896–1906, Nov. 2004. → pages 8, 17

[58] F. Lotse, J. E. Berg, and R. Bownds, "Indoor propagation measurements at 900 mhz," in *Vehicular Technology Conference, 1992, IEEE 42nd*, vol. 2, May 1992, pp. 629–632. → pages 8, 17

[59] A. F. Molisch, J. R. Foerster, and M. Pendergrass, "Channel models for ultrawideband personal area networks," *IEEE Wireless Commun.*, vol. 10, no. 6, pp. 14–21, Dec. 2003. → pages 9

[60] Z. Wang and G. B. Giannakis, "A simple and general parameterization quantifying performance in fading channels," *IEEE Trans. Commun.*, vol. 51, pp. 1389–1398, Aug. 2003. → pages 9, 21, 64

[61] E. Bayaki, R. Schober, and R. Mallik, "Performance analysis of mimo free-space optical systems in gamma-gamma fading," *IEEE Trans. Commun.*, vol. 57, pp. 3415–3424, Nov. 2009. → pages 9, 37

[62] F. Yang and J. Cheng, "Coherent free-space optical communications in lognormal-rician turbulence," *IEEE Commun. Lett.*, vol. 16, pp. 1872–1875, Nov. 2012. → pages 18, 34

[63] X. Song, J. Cheng, and N. C. Beaulieu, "Asymptotic analysis of different multibranch diversity receivers with arbitrarily correlated rician channels," *IEEE Trans. Wireless Commun.*, vol. 13, pp. 5676–5689, Oct. 2014. → pages 9

[64] H. Henniger and O. Wilfert, "An introduction to free-space optical communications," *Radioengineering*, vol. 19, pp. 203–212, June 2010. → pages 14

[65] N. Perlot, *Characterization of Signal Fluctuations in Optical Communications with Intensity Modulation and Direct Detection Through the Turbulent Atmospheric Channel*, ser. Berichte aus der Kommunikationstechnik. Shaker Verlag GmbH, 2005. → pages 17

[66] S. Karp, *Optical Channels: Fibers, Clouds, Water, and the Atmosphere*, ser. Applications of communications theory. Plenum Press, 1988. → pages 17, 64

[67] J. W. Strohbehn, T. Wang, and J. P. Speck, "On the probability distribution of line-of-sight fluctuations of optical signals," *Radio Science*, vol. 10, pp. 59–70, Jan. 1975. → pages 18

[68] H. Amindavar and J. A. Ritcey, "Pade approximations of probability density functions," *IEEE Trans. Aerosp. Electron. Syst.*, vol. 30, pp. 416–424, Apr. 1994. → pages 22, 23

[69] G. K. Karagiannidis, "Moments-based approach to the performance analysis of equal gain diversity in nakagami-m fading," *IEEE Trans. Commun.*, vol. 52, pp. 685–690, May 2004. → pages 22

[70] M. H. Ismail and M. M. Matalgah, "On the use of pade approximation for performance evaluation of maximal ratio combining diversity over weibull fading channels," *EURASIP J. Wirel. Commun. Netw.*, vol. 2006, pp. 6:1–6:7, June 2006. → pages 22

[71] P. Beckmann and A. Spizzichino, *The scattering of electromagnetic waves from rough surfaces*, A. Beckmann, P. & Spizzichino, Ed. MA: Artech House, 1987. → pages 34

[72] M. K. Simon and M.-S. Alouini, *Digital Communication over Fading Channels*. Wiley, 2005. → pages 34

[73] G. Lukesh, S. Chandler, and D. Voelz, "Estimation of laser system pointing performance by use of statistics of return photons," *Appl. Opt.*, vol. 39, pp. 1359–1371, Mar. 2000. → pages 34

[74] V. S. Rao, Gudimetla, and J. F. Riker, "Moment-matching method for extracting beam jitter and boresight in experiments with satellites of small physical cross section," *Appl. Opt.*, vol. 46, pp. 5608–5616, Aug. 2007. → pages 34

[75] Wolfram, http://functions.wolfram.com/. → pages 38, 39, 98, 99

[76] X. Song, F. Yang, and J. Cheng, "Subcarrier intensity modulated optical wireless communications in atmospheric turbulence with pointing errors," *IEEE/OSA J. Opt. Commun. Netw.*, vol. 5, pp. 349–358, Apr. 2013. → pages 41

[77] I. I. Kim, B. McArthur, and E. J. Korevaar, "Comparison of laser beam propagation at 785 nm and 1550 nm in fog and haze for optical wireless communications," E. J. Korevaar, Ed., vol. 4214, no. 1. SPIE, 2001, pp. 26–37. → pages 51

[78] M. K. Simon and M. S. Alouini, "Simplified noisy reference loss evaluation for digital communication in the presence of slow fading and

carrier phase error," *IEEE Trans. Veh. Technol.*, vol. 50, pp. 480–486, Mar. 2001. → pages 54, 55

[79] W. J. Weber, "Performance of phase-locked loops in the presence of fading communication channels," *IEEE Trans. Commun.*, vol. 24, pp. 487–499, May 1976. → pages 54

[80] T. Eng and L. B. Milstein, "Partially coherent ds-ss performance in frequency selective multipath fading," *IEEE Trans. Commun.*, vol. 45, pp. 110–118, Jan. 1997. → pages 54

[81] C. M. Lo and W. H. Lam, "Error probability of binary phase shift keying in nakagami-m fading channel with phase noise," vol. 36, pp. 1773–1774, Oct. 2000. → pages 54

[82] M. A. Smadi and V. K. Prabhu, "Performance analysis of generalized-faded coherent psk channels with equal-gain combining and carrier phase error," vol. 5, pp. 509–513, Mar. 2006. → pages 54

[83] Y. Jang, D. Yoon, and S.-K. Lee, "Generalized ber expression of MPSK in the presence of phase error," *IEEE Commun. Lett.*, vol. 17, pp. 2213–2216, Dec. 2013. → pages 55

[84] X. Song, F. Yang, J. Cheng, and M. S. Alouini, "Asymptotic ser performance comparison of MPSK and MDPSK in wireless fading channels," *IEEE Wireless Commun. Lett.*, vol. 4, pp. 18–21, Feb. 2015. → pages 65

[85] X. Song, F. Yang, J. Cheng, N. Al-Dhahir, and Z. Xu, "Subcarrier phase-shift keying systems with phase errors in lognormal turbulence channels," *IEEE/OSA J. Lightwave Technol.*, vol. 33, pp. 1896–1904, May 2015. → pages 65

[86] F. Yang, J. Cheng, and T. A. Tsiftsis, "Free-space optical communication with nonzero boresight pointing errors," *IEEE Trans. Commun.*, vol. 62, pp. 713–725, Feb. 2014. → pages 69

[87] A. Jeffrey and D. Zwillinger, *Table of Integrals, Series, and Products.* Elsevier Science, 2000. → pages 96, 97, 99, 101

[88] J. M. Wozencraft and I. M. Jacobs, *Principles of Communication Engineering.* Waveland Press, Incorporated, 1990. → pages 103

Appendices

Appendix A

Analytical and Numerical Results of $f_{h_p}(h_p)$

When a Gaussian beam propagates through distance z from the transmitter to a circular detector with aperture radius a, the fraction of the collected power at receiver is [11]

$$h_p(r;z) = G(r) \triangleq \int_{-a}^{a} \int_{-\sqrt{a^2-x'^2}}^{\sqrt{a^2-x'^2}} \frac{2}{\pi w_z^2} \exp\left(-2\frac{(x'-r)^2+y'^2}{w_z^2}\right) dy'dx' \tag{A.0.1}$$

where r is the instantaneous radial displacement between the beam centroid and the detector center. We use the approximation given in (4.2) to derive the analytical PDF of h_p in (4.5), and the approximation in (4.2) has normalized mean-squared error less than 10^{-3} when $w_z/a > 6$. Using (A.0.1), we obtain the exact PDF of h_p as

$$f_{h_p}(h_p) = f_r(G^{-1}(h_p)) \cdot \frac{dG^{-1}(h_p)}{dh_p}. \tag{A.0.2}$$

Since there is no explicit expression of $G^{-1}(h_p)$, we calculate it numerically.

In Fig. A.1, we compare the analytical PDF of h_p in (4.5) as well as the exact PDF of h_p without using (4.2) under various system settings. It is shown that our analytical model in (4.5) is accurate even with large boresight ($s/a = 5$) and large jitter ($\sigma_s/a = 3$).

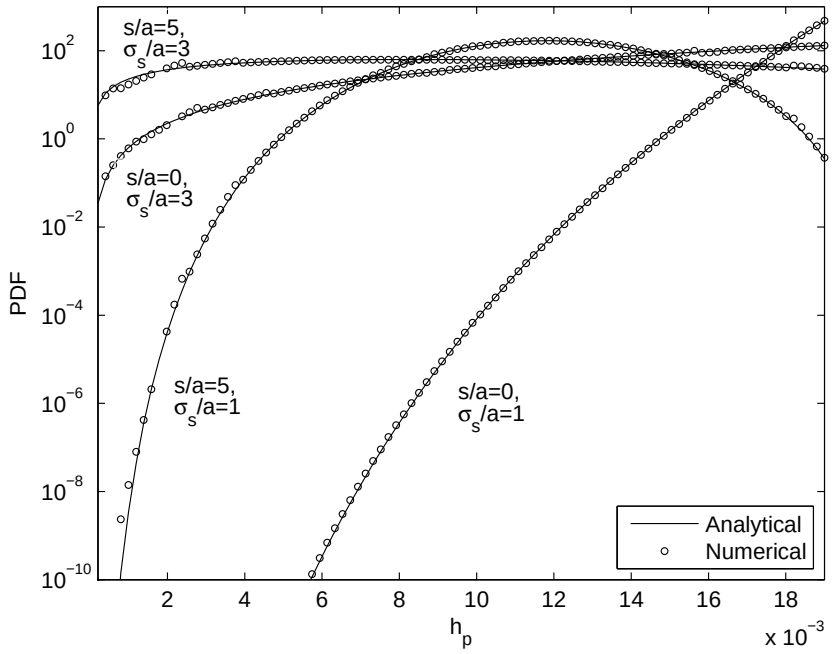

Figure A.1: Comparison of the analytical PDF in (4.5) and the exact PDF of h_p under various system settings ($w_z/a = 10$).

Appendix B

Derivation of the moments of h_p

The moments of the generalized pointing error h_p are given by

$$E\left[h_p^n\right] = \int_0^{A_0} h_p^n f_{h_p}(h_p) dh_p. \tag{B.0.1}$$

Substituting (4.5) into (B.0.1), we obtain

$$E\left[h_p^n\right] = \int_0^{A_0} \frac{\gamma^2 \exp\left(-\frac{s^2}{2\sigma_s^2}\right)}{A_0^{\gamma^2}} h_p^{n+\gamma^2-1} I_0\left(\frac{s\nu}{\sigma_s^2}\right) dh_p \tag{B.0.2}$$

where $\nu = \sqrt{\frac{-\omega_{zeq}^2 \ln \frac{h_p}{A_0}}{2}}$. Using a series representation of $I_0(\cdot)$ [87, Eq.(8.445)], we have

$$\begin{aligned} &E\left[h_p^n\right] \\ &= \frac{\gamma^2 \exp\left(-\frac{s^2}{2\sigma_s^2}\right)}{A_0^{\gamma^2}} \int_0^{A_0} h_p^{n+\gamma^2-1} \sum_{m=0}^{\infty} \frac{1}{(m!)^2} \left(\frac{s\nu}{2\sigma_s^2}\right)^{2m} dh_p. \end{aligned} \tag{B.0.3}$$

Since each term of the series is non-negative and the infinite series uniformly converges to $I_0\left(\frac{s\nu}{\sigma_s^2}\right)$, we can swap the integral and infinite summation and

write (B.0.3) as

$$\begin{aligned}
&E\left[h_p^n\right] \\
&= \frac{\gamma^2 \exp\left(-\frac{s^2}{2\sigma_s^2}\right)}{A_0^{\gamma^2}} \\
&\quad \times \sum_{m=0}^{\infty} \frac{1}{(m!)^2} \int_0^{A_0} h_p^{n+\gamma^2-1} \left(\frac{s^2}{4\sigma_s^4} \cdot \frac{-\omega_{z_{eq}}^2 \ln \frac{h_p}{A_0}}{2} \right)^m dh_p \\
&= \frac{\gamma^2 \exp\left(-\frac{s^2}{2\sigma_s^2}\right)}{A_0^{\gamma^2}} \\
&\quad \times \sum_{m=0}^{\infty} \left[\frac{\left(\frac{-\omega_{z_{eq}}^2 s^2}{8\sigma_s^4} \right)^m}{(m!)^2} A_0^{n+\gamma^2} \int_0^1 x^{n+\gamma^2-1} (\ln x)^m dx \right].
\end{aligned} \tag{B.0.4}$$

Applying an integral identity [87, Eq.(4.294.10)] to (B.0.4), we have

$$\begin{aligned}
&E\left[h_p^n\right] \\
&= \gamma^2 \exp\left(-\frac{s^2}{2\sigma_s^2}\right) A_0^n \sum_{m=0}^{\infty} \left[\frac{\left(\frac{\gamma^2 s^2}{2\sigma_s^2(n+\gamma^2)} \right)^m}{m!} \frac{1}{(n+\gamma^2)} \right] \\
&= \frac{A_0^n \gamma^2}{n+\gamma^2} \exp\left(-\frac{n s^2}{(n+\gamma^2) 2\sigma_s^2}\right).
\end{aligned} \tag{B.0.5}$$

Appendix C

Gamma-Gamma Composite PDF

C.1 Composite PDF Approximation

We substitute (2.13) into (4.7) and write the composite PDF of the Gamma-Gamma fading with nonzero boresight pointing error as

$$f_{GG}(h) = \frac{2\gamma^2 \exp(-s^2/2\sigma_s^2)(\alpha\beta)^{(\alpha+\beta)/2}}{(A_0 h_l)^{\gamma^2}\Gamma(\alpha)\Gamma(\beta)} h^{\gamma^2-1} \times \int_{h/(A_0 h_l)}^{\infty} h_a^{\frac{\alpha+\beta}{2}-\gamma^2-1} I_0\left(\frac{s}{\sigma_s^2}\sqrt{-\frac{w_{z_{eq}}^2}{2}\ln\left(\frac{h}{h_a A_0 h_l}\right)}\right) K_{\alpha-\beta}(2\sqrt{\alpha\beta h_a}) dh_a. \tag{C.1.1}$$

Applying a change of variable rule $x = \sqrt{-\frac{w_{z_{eq}}^2}{2}\ln\left(\frac{h}{h_a A_0 h_l}\right)}$, eq. (C.1.1) can be expressed as

$$\begin{aligned} f_{GG}(h) =& \frac{8\gamma^2 \exp(-s^2/2\sigma_s^2)(\alpha\beta)^{(\alpha+\beta)/2}}{(A_0 h_l)^{\frac{\alpha+\beta}{2}}\Gamma(\alpha)\Gamma(\beta) w_{z_{eq}}^2} \\ & \times \int_0^{\infty} x \exp\left(\frac{2x^2}{w_{z_{eq}}^2}\left(\frac{\alpha+\beta}{2}-\gamma^2\right)\right) I_0\left(\frac{s}{\sigma_s^2}x\right) W(h) dx \end{aligned} \tag{C.1.2}$$

where $W(h) = h^{\frac{\alpha+\beta}{2}-1} K_{\alpha-\beta}\left(2\sqrt{\frac{\alpha\beta h}{A_0 h_l}}\exp\left(\frac{x^2}{w_{z_{eq}}^2}\right)\right)$. Using a series expansion of the modified Bessel function of the second kind [75, eq. (3.4.6.2.1)]

$$K_v(x) = \frac{\pi}{2\sin(\pi v)}\sum_{p=0}^{\infty}\left[\frac{(x/2)^{2p-v}}{\Gamma(p-v+1)p!} - \frac{(x/2)^{2p+v}}{\Gamma(p+v+1)p!}\right] \tag{C.1.3}$$

where it requires $v \notin \mathbb{Z}$ and $|x| < \infty$, we can express $W(h)$ as

$$W(h) = \frac{\pi}{2\sin(\pi(\alpha-\beta))}\sum_{j=0}^{\infty}\left(\frac{\left(\frac{\alpha\beta}{A_0 h_l}\exp\left(\frac{2x^2}{w_{z_{eq}}^2}\right)\right)^{j-\frac{\alpha-\beta}{2}}}{\Gamma(j-(\alpha-\beta)+1)j!}h^{j+\beta-1} - \frac{\left(\frac{\alpha\beta}{A_0 h_l}\exp\left(\frac{2x^2}{w_{z_{eq}}^2}\right)\right)^{j+\frac{\alpha-\beta}{2}}}{\Gamma(j+(\alpha-\beta)+1)j!}h^{j+\alpha-1}\right). \tag{C.1.4}$$

Substituting (C.1.4) into (C.1.2), and, after some manipulation, we have

$$\begin{aligned} f_{GG}(h) = {} & \frac{4\pi\gamma^2\exp(-s^2/2\sigma_s^2)(\alpha\beta)^{(\alpha+\beta)/2}}{(A_0 h_l)^{(\alpha+\beta)/2}\Gamma(\alpha)\Gamma(\beta)\sin((\alpha-\beta)\pi)w_{z_{eq}}^2}h^{(\alpha+\beta)/2-1} \\ & \times\sum_{j=0}^{\infty}\left\{\frac{1}{\Gamma(j-(\alpha-\beta)+1)j!}\left(\frac{\alpha\beta h}{A_0 h_l}\right)^{j-(\alpha-\beta)/2}G\left(\frac{\beta-\gamma^2+j}{w_{z_{eq}}^2},\frac{s}{\sigma_s^2}\right)\right. \\ & \left. -\frac{1}{\Gamma(j+(\alpha-\beta)+1)j!}\left(\frac{\alpha\beta h}{A_0 h_l}\right)^{j+(\alpha-\beta)/2}G\left(\frac{\alpha-\gamma^2+j}{w_{z_{eq}}^2},\frac{s}{\sigma_s^2}\right)\right\} \end{aligned} \tag{C.1.5}$$

where $G(a,b) = \int_0^\infty x\exp(2ax^2)I_0(bx)dx$. In the following derivation, we use an integral identity [87, eq. (6.643.2)]

$$\begin{aligned} & \int_0^\infty x^{u-\frac{1}{2}}e^{-\alpha x}I_{2v}(2\beta\sqrt{x})dx \\ & = \frac{\Gamma\left(u+v+\frac{1}{2}\right)}{\Gamma(2v+1)}\beta^{-1}\exp\left(\frac{\beta^2}{2\alpha}\right)\alpha^{-u}M_{-u,v}\left(\frac{\beta^2}{\alpha}\right) \end{aligned} \tag{C.1.6}$$

where $M_{u,v}(\cdot)$ is the Whittaker function. Hence, by using another the identity [75, eq. (07.44.03.0041.01)]

$$M_{\frac{m-1}{2},\frac{m}{2}}(z) = \exp\left(-\frac{z}{2}\right)z^{\frac{1-m}{2}}m!\left(\exp(z)-\sum_{k=0}^{m-1}\frac{z^k}{k!}\right), m \geq 0 \tag{C.1.7}$$

we can represent (C.1.5) as (12). In our derivation, the integral identity (C.1.3) requires that $(\alpha - \beta) \notin \mathbb{Z}$, and the integral identity (C.1.6) requires that the summation index j in (C.1.5) must be lower than or equal to $J = \lfloor \gamma^2 - \alpha \rfloor$, where $\lfloor x \rfloor$ denotes the largest integer not greater than x. Such truncation method is also used in [12] to estimate the BER of systems over the Gamma-Gamma channels with Hoyt distributed pointing error. Due to the truncation of the infinite series and the constraint on the number of terms $j \leq \lfloor \gamma^2 - \alpha \rfloor$, our series PDF in (12) may not converge to the exact PDF for weak turbulence. However, beyond certain threshold of transmit power P_t (shown in Appendix F), the approximate BER is accurate since the PDF $f_{GG}(h)$ near the origin can be accurately described by (12).

C.2 PDF Near the Origin

To obtain the power series expansion of the Gamma-Gamma composite PDF near the origin, we can express $W(h)$ as

$$\lim_{h\to 0} W(h) = \frac{\pi \left(\frac{\alpha\beta}{A_0 h_l} \exp\left(\frac{2x^2}{w_{z_{eq}}^2} \right) \right)^{-\frac{\alpha-\beta}{2}}}{2\sin(\pi(\alpha-\beta))\Gamma(-(\alpha-\beta)+1)} h^{\beta-1} + g_{\beta-1}(h). \tag{C.2.1}$$

From (C.2.1) and (C.1.2), we can derive the PDF near the origin as

$$\begin{aligned}\lim_{h\to 0} f_{GG}(h) =& \frac{\gamma^2 \pi \left(\frac{\alpha\beta}{A_0 h_l} \right)^{\beta} \exp\left(-\frac{s^2}{2\sigma_s^2} - \frac{s^2\gamma^2/\sigma_s^2}{2\beta - 2\gamma^2} \right) \sin^{-1}((\alpha-\beta)\pi)}{\Gamma(\alpha)\Gamma(\beta)\Gamma(-(\alpha-\beta)+1)|-(\beta-\gamma^2)|} h^{\beta-1} \\ &+ g_{\beta-1}(h).\end{aligned} \tag{C.2.2}$$

Appendix D

Bound on approximation error

By applying an upper bound $\text{erfc}(x) < \exp(-x^2)$ to (4.15), we can upper bound R_B as

$$\begin{aligned} &R_B < \\ &\frac{\gamma^2 u_c}{4} \exp\left(u_a - \gamma^2 u_b\right) \\ &\times \int_B^\infty \exp\left(\gamma^2 u_c x - x^2 - \frac{P_t^2}{2\sigma_n^2} A_0^2 h_l^2 \exp(u_c x - b)\right) dx \\ &< \frac{\gamma^2 u_c}{4} \exp\left(u_a - \gamma^2 u_b\right) \int_B^\infty \exp\left(\gamma^2 u_c x - x^2\right) dx. \end{aligned} \tag{D.0.1}$$

Using an integral identity [87, Eq.(2.33.1)]

$$\begin{aligned} &\int \exp(-(ax^2 + 2bx + c))dx = \\ &\frac{1}{2}\sqrt{\frac{\pi}{a}} \exp\left(\frac{b^2 - ac}{a}\right) \text{erf}\left(\sqrt{a}x + \frac{b}{\sqrt{a}}\right) \end{aligned} \tag{D.0.2}$$

we derive the upper bound for R_B as

$$\begin{aligned} &R_B < \\ &\frac{\sqrt{\pi}\gamma^2 u_c}{8} \exp\left(u_a - \gamma^2\left(u_b - \frac{\gamma^2 u_c^2}{4}\right)\right) \text{erfc}\left(B - \frac{\gamma^2 u_c}{2}\right). \end{aligned} \tag{D.0.3}$$

For different R_B, the required values of B, which are calculated by (D.0.3), are shown in Table D.1, where we set $w_z/a = 10, s/a = 1.0, \sigma_s/a = 1.0$. It is found that the approximation error R_B decreases rapidly with increasing B, and therefore we can adjust the value of B to make R_B arbitrarily small.

Table D.1: Values of B for different R_B values

Parameters	$R_B = 10^{-6}$	$R_B = 10^{-8}$	$R_B = 10^{-10}$
$\sigma_R^2 = 0.05$	7.60	8.18	8.69
$\sigma_R^2 = 0.1$	9.28	9.86	10.36
$\sigma_R^2 = 0.2$	11.65	12.22	12.73

Appendix E

Proof of convergence of series

The series in (4.20) contains the expression

$$P_S = \frac{2}{\sqrt{\pi}} \sum_{j=0}^{\infty} \frac{(-1)^j}{j!(2j+1)} \left(\frac{P_t A_0 h_l}{\sqrt{2}\sigma_n} \right)^{2j+1} \frac{\exp(-u_b(2j+1))}{(2j+1+\gamma^2)u_c} S_j. \tag{E.0.1}$$

We now use the ratio test to assess the convergence of this series. The absolute ratio between two consecutive terms is

$$\left| \frac{a_{j+1}}{a_j} \right| = \frac{(2j+1)\left(\frac{P_t A_0 h_l}{\sqrt{2}\sigma_n}\right)^2 \exp(-2u_b)(2j+1+\gamma^2)}{(j+1)(2j+3)(2j+3+\gamma^2)} \cdot \frac{S_{j+1}}{S_j}. \tag{E.0.2}$$

By applying the bounds of the erfc$(\cdot)$ function [88]

$$\frac{1}{\sqrt{\pi}x}\left(1 - \frac{1}{2x^2}\right)\exp(-x^2) < \operatorname{erfc}(x) < \frac{1}{\sqrt{\pi}x}\exp(-x^2) \tag{E.0.3}$$

to S_{j+1} (upper bound) and S_j (lower bound), we have

$$\frac{S_{j+1}}{S_j} < \frac{\frac{1}{B} + \frac{1}{(\gamma^2+2j+3)\frac{u_c}{2} - B}\exp(2Bu_c)}{\frac{1}{B}\left(1 - \frac{1}{2B^2}\right) + \frac{1}{(\gamma^2+2j+1)\frac{u_c}{2} - B}\left(1 - \frac{1}{2((\gamma^2+2j+1)\frac{u_c}{2} - B)^2}\right)}. \tag{E.0.4}$$

Applying the limit operation to both sides of (E.0.4) and noting that S_j and S_{j+1} are positive, we have

$$0 < \lim_{j\to\infty} \frac{S_{j+1}}{S_j} < \frac{1}{1 - \frac{1}{2B^2}}. \tag{E.0.5}$$

For the rest of the terms in (E.0.2), we have

$$\lim_{j\to\infty} \frac{(2j+1)\left(\frac{P_t A_0 h_l}{\sqrt{2}\sigma_n}\right)^2 \exp(-2u_b)(2j+1+\gamma^2)}{(j+1)(2j+3)(2j+3+\gamma^2)} = 0. \tag{E.0.6}$$

Since limits in (E.0.5) and (E.0.6) both exist, we have

$$\begin{aligned}\lim_{j\to\infty}\left|\frac{a_{j+1}}{a_j}\right| &= \lim_{j\to\infty} \frac{(2j+1)\left(\frac{P_t A_0 h_l}{\sqrt{2}\sigma_n}\right)^2 (2j+1+\gamma^2)}{\exp(2u_b)(j+1)(2j+3)(2k+3+\gamma^2)} \cdot \lim_{j\to\infty}\frac{S_{j+1}}{S_j} \\ &= 0.\end{aligned} \tag{E.0.7}$$

Thus, we have $\lim_{j\to\infty}\left|\frac{a_{j+1}}{a_j}\right| = 0$. We conclude that the series P_S in (4.20) is convergent.

Appendix F

Approximation error

After the numerical evaluation of the approximation error in (4.23) under different system parameters, we find our series solutions in (4.23) and (4.34) may not approach to the exact results when P_t is small. This is a limitation of the series approach. In Table F.1, we show the minimum required P_t that can guarantee the relative error $\frac{\varepsilon(P_e)}{P_e} < 10^{-6}$ and $\frac{\varepsilon(P_{out})}{P_{out}} < 10^{-6}$ for three representative turbulence conditions. From Table F, we observe that the minimum required P_t becomes larger with increasing boresight or jitter.

Table F.1: Minimum Required P_t(dBm) for $\frac{\varepsilon(P_e)}{P_e} < 10^{-6}$ and $\frac{\varepsilon(P_{out})}{P_{out}} < 10^{-6}$

Parameters	$s/a = 1.0$, $\sigma_s/a = 1.0$	$s/a = 1.0$, $\sigma_s/a = 1.5$	$s/a = 2.0$, $\sigma_s/a = 1.5$
$\sigma_R^2 = 0.6$; $\alpha = 5.41$, $\beta = 3.78$	-14, -18	-1, -5	9, 5
$\sigma_R^2 = 2.0$; $\alpha = 3.99$, $\beta = 1.70$	-19, -23	-8, -12	6, 2
$\sigma_R^2 = 4.0$; $\alpha = 4.34$, $\beta = 1.31$	-19, -23	-13, -17	-9, -12

Appendix G

PDF of received instantaneous SNR of multiple-branch system

G.1 MRC

G.1.1 Dual Branch

In order to obtain the joint PDF of received instantaneous SNR (For simplicity here, we assume $\gamma = h^2$) of system having channel state z_1, z_2 in (6.24), we first introduce the PDF of a product of two independent RVs $Z = X \cdot Y$:

$$f_Z(z) = \int_{-\infty}^{\infty} f_X(x) f_Y\left(\frac{z}{x}\right) \frac{1}{|x|} dx \tag{G.1.1}$$

where X, Y are two independent, continuous random variables, described by probability density functions $f_X(x)$ and $f_Y(y)$. Therefore using (6.7), (6.25) and (G.1.1), we can obtain the joint PDF of the received SNRs γ_1, γ_2 as

$$f_{\gamma_1,\gamma_2}(\gamma_1, \gamma_2) = \int_0^{\infty}\int_0^{\infty} f_{Y_1}\left(\frac{\gamma_1}{x_1}\right) f_{Y_2}\left(\frac{\gamma_2}{x_2}\right) f_{X_1,X_2}(x_1, x_2) \frac{1}{x_1 x_2} dx_1 dx_2 \tag{G.1.2}$$

where we have used the fact that γ_1 and γ_2 are both positive variables. The MRC has the combiner output instantaneous SNR $\gamma = \gamma_1 + \gamma_2$, which has

the following PDF

$$\begin{aligned} f_{\gamma}(\gamma) &= \int_0^{\gamma} f_{\gamma_1,\gamma_2}(\gamma - a, a)da \\ &= \int_0^{\gamma}\int_0^{\infty}\int_0^{\infty} f_{Y_1}\left(\frac{\gamma-a}{x_1}\right) f_{Y_2}\left(\frac{a}{x_2}\right) f_{X_1,X_2}(x_1,x_2)\frac{1}{x_1x_2}dx_1dx_2da \\ &= \int_0^{\gamma}\int_0^{\infty}\int_0^{\infty} \frac{m^{2m}\exp\left(-m\left(\frac{\gamma-a}{x_1}+\frac{a}{x_2}\right)\right)}{\Gamma(m)^2}\left(\frac{\gamma-a}{x_1}\right)^{m-1}\left(\frac{a}{x_2}\right)^{m-1} \\ &\qquad \times f_{X_1,X_2}(x_1,x_2)\frac{1}{x_1x_2}dx_1dx_2da. \end{aligned} \tag{G.1.3}$$

For the PDF near the origin, we have the asymptotic PDF when $\gamma \to 0$ as

$$\begin{aligned} &f_{\gamma,\text{asym}}(\gamma) = \\ &\int_0^{\gamma}\int_0^{\infty}\int_0^{\infty} \frac{m^{2m}}{\Gamma(m)^2}\left(\frac{\gamma-a}{x_1}\right)^{m-1}\left(\frac{a}{x_2}\right)^{m-1} f_{X_1,X_2}(x_1,x_2)\frac{1}{x_1x_2}dx_1dx_2da. \end{aligned} \tag{G.1.4}$$

Using a binomial expansion theorem, we can simplify the asymptotic PDF in (G.1.4) to

$$\begin{aligned} &f_{\gamma,\text{asym}}(\gamma) \\ &= \int_0^{\infty}\int_0^{\infty} \frac{m^{2m}}{\Gamma(m)^2}\left(\sum_{i=0}^{m-1}(-1)^i\frac{\binom{m-1}{i}}{m+i}\right)\gamma^{2m-1} f_{X_1,X_2}(x_1,x_2)\frac{1}{x_1^m x_2^m}dx_1dx_2 \\ &= \frac{m^{2m}}{\Gamma(m)^2}\left(\sum_{i=0}^{m-1}(-1)^i\frac{\binom{m-1}{i}}{m+i}\right)\gamma^{2m-1}\int_0^{\infty}\int_0^{\infty} f_{X_1,X_2}(x_1,x_2)\frac{1}{x_1^m x_2^m}dx_1dx_2 \end{aligned} \tag{G.1.5}$$

where the double integral in (G.1.5) can be expressed by the MGF of a multivariate Gaussian distribution, which has two normal variables being the natural logarithm of x_1, x_2 in (6.24). Therefore the asymptotic PDF

near the origin can be further simplified to

$$\begin{aligned} & f_{\gamma,\text{asym}}(\gamma) \\ &= \frac{m^{2m}}{\Gamma(m)^2}\left(\sum_{i=0}^{m-1}(-1)^i\frac{\binom{m-1}{i}}{m+i}\right)\gamma^{2m-1}M_{\log(x_1),\log(x_2)}(-m,-m) \\ &= \frac{m^{2m}}{\Gamma(m)^2}\left(\sum_{i=0}^{m-1}(-1)^i\frac{\binom{m-1}{i}}{m+i}\right)\gamma^{2m-1}\exp\left(\frac{m}{2}(m+1)(\sigma_1^2+\sigma_2^2)+m^2\rho\sigma_1\sigma_2\right). \end{aligned} \tag{G.1.6}$$

G.1.2 Multiple-Branch

Following the derivation of the two-branch case, we can write the joint PDF of L-branch received instantaneous SNR as

$$\begin{aligned} & f_{\gamma_1,\cdots,\gamma_L}(\gamma_1,\cdots,\gamma_L) = \\ & \int_0^\infty\cdots\int_0^\infty f_{Y_1}\left(\frac{\gamma_1}{x_1}\right)\cdots f_{Y_L}\left(\frac{\gamma_L}{x_L}\right)\frac{f_{X_1,\cdots,X_L}(x_1,\cdots,x_L)}{x_1\cdots x_L}dx_1\cdots dx_L. \end{aligned} \tag{G.1.7}$$

The output instantaneous SNR of MRC has the PDF

$$\begin{aligned} & f_\gamma(\gamma) = \\ & \int_0^\gamma\int_0^{a_1}\cdots\int_0^{a_{L-2}} f_{\gamma_1,\gamma_2,\cdots,\gamma_L}(\gamma-a_1,a_1-a_2,\cdots,a_{L-1})da_1da_2\cdots da_{L-2}da_{L-1}. \end{aligned} \tag{G.1.8}$$

When $\gamma\to 0$, we can get the asymptotic PDF from (G.1.8) as

$$\begin{aligned} f_{\gamma,\text{asym}}(\gamma) = & \int_0^\gamma\cdots\int_0^{a_{L-2}}\int_0^\infty\cdots\int_0^\infty\frac{m^{Lm}}{\Gamma(m)^L}\left(\frac{\gamma-a_1}{x_1}\right)^{m-1}\cdots\left(\frac{a_L}{x_L}\right)^{m-1} \\ & \times\frac{f_{X_1,\cdots,X_L}(x_1,\cdots,x_L)}{x_1\cdots x_L}dx_1\cdots dx_Lda_1\cdots da_{L-1} \end{aligned} \tag{G.1.9}$$

which can be simplified to

$$\begin{aligned}
&f_{\gamma,\text{asym}}(\gamma) \\
&= \frac{m^{Lm}}{\Gamma(m)^L} \int_0^{\infty} \cdots \int_0^{\infty} (\gamma - a_1)^{m-1} \cdots (a_L)^{m-1} da_1 \cdots da_{L-1} \\
&\times \int_0^{\gamma} \cdots \int_0^{a_{L-2}} \frac{f_{X_1,\cdots,X_L}(x_1,\cdots,x_L)}{x_1^m \cdots x_L^m} dx_1 \cdots dx_L \qquad \text{(G.1.10)} \\
&= \frac{m^{Lm}}{\Gamma(m)^L} \int_0^{\infty} \cdots \int_0^{\infty} (\gamma - a_1)^{m-1} \cdots (a_L)^{m-1} da_1 \cdots da_{L-1} \\
&\qquad \times M_{\log(x_1),\cdots,\log(x_L)}(-m,\cdots,-m)
\end{aligned}$$

where $M_{x_1,\cdots,x_L}(t_1,\cdots,t_L)$ is the MGF of a multivariate distribution function $f_{X_1,\cdots,X_L}(x_1,\cdots,x_L)$. Since $x_i's, i = 1,\cdots,L$ follow the lognormal distribution, we have

$$M_{\log(x_1),\cdots,\log(x_L)}(t_1,\cdots,t_L) = \exp\left(\mu^T t + \frac{1}{2} t^T \Sigma t\right) \qquad \text{(G.1.11)}$$

where T denotes matrix transpose, $\mu = [\mu_1,\cdots,\mu_L]^T$, $t = [t_1,\cdots,t_L]^T$ and Σ denotes the covariance matrix of $\log(x_1),\cdots,\log(x_L)$. Substituting (G.1.11) into (G.1.10) and using a binomial expansion theorem, we can obtain the asymptotic PDF as

$$\begin{aligned}
&f_{\gamma,\text{asym}}(\gamma) \\
&= \frac{m^{Lm}}{\Gamma(m)^L} \left(\sum_{i=0}^{m-1} \frac{(-1)^i \binom{m-1}{i}}{Lm+i}\right) \left(\sum_{i=0}^{m-1} \frac{(-1)^i \binom{m-1}{i}}{(L-1)m+i}\right) \cdots \left(\sum_{i=0}^{m-1} \frac{(-1)^i \binom{m-1}{i}}{m+i}\right) \\
&\quad \times \gamma^{Lm-1} M_{\log(x_1),\cdots,\log(x_L)}(-m,\cdots,-m) \\
&= \frac{m^{Lm}}{\Gamma(m)^L} \left(\prod_{j=1}^{L-1} \left(\sum_{i=0}^{m-1} \frac{(-1)^i \binom{m-1}{i}}{jm+i}\right)\right) \\
&\quad \times \gamma^{Lm-1} \exp\left(\frac{1}{2} m \left(\left(\sum_{i=1}^{L} \sigma_i^2\right) + m||\Sigma||_1\right)\right) \\
&= \frac{m^{Lm}}{\Gamma(m)^L} \left(\prod_{j=1}^{L-1} S_{1,j}\right) \gamma^{Lm-1} \exp\left(\frac{1}{2} m \left(\left(\sum_{i=1}^{L} \sigma_i^2\right) + m||\Sigma||_1\right)\right).
\end{aligned} \qquad \text{(G.1.12)}$$

G.2 EGC

The asymptotic PDF of instantaneous SNR can be obtained by following derivation similar to the MRC case. In EGC, the received instantaneous SNR has the form

$$\gamma = \frac{(h_1 + h_2 + \cdots + h_L)^2}{L} \tag{G.2.1}$$

where $h_i's$ are channel states following the lognormal-Nakagami distribution. The instantaneous SNR in the MRC case is

$$\gamma = h_1^2 + h_2^2 + \cdots + h_L^2. \tag{G.2.2}$$

From (G.2.1) and (G.2.2), we can see that instantaneous SNR of EGC is the scaled squared of the summation of lognormal-Nakagami RVs, while the output instantaneous SNR of MRC is the summation of lognormal-Gamma RVs (lognormal-Nakagami squared). Substituting the lognormal-Nakagami distribution into (G.1.8) and, after some mathematica manipulation, we can obtain the asymptotic PDF as

$$f_{\gamma,\mathrm{EGC,asym}}(\gamma) = \frac{2^{L-1}(Lm)^{Lm}}{\Gamma(m)^L} \prod_{i=1}^{L-1} S_{2,2i} \gamma^{Lm-1} \exp\left(\frac{1}{2} m \left(\left(\sum_{i=1}^{L} \sigma_i^2\right) + m||\Sigma||_1\right)\right). \tag{G.2.3}$$

G.3 SC

For the SC system, we can first derive the cumulative density function (CDF) of received instantaneous SNR and then obtain the PDF using the CDF or outage probability. The outage probability of L-branch SC system over the correlated lognormal-Nakagami channels can be expressed as

$$P_{out,\mathrm{asym}} = Pr(\gamma_1 < \gamma_{th}, \gamma_2 < \gamma_{th}, \cdots, \gamma_L < \gamma_{th}). \tag{G.3.1}$$

Using (G.1.7), we have

$$\begin{aligned} P_{out,\mathrm{asym}} =& \int_0^{\gamma_{th}} \cdots \int_0^{\gamma_{th}} f_{\gamma_1,\cdots,\gamma_L}(\gamma_1, \cdots, \gamma_L) d\gamma_1 \cdots d\gamma_L \\ =& \frac{m^{L(m-1)}}{\Gamma(m)^L} \left(\frac{\gamma_{th}}{\bar{\gamma}}\right)^{Lm} \exp\left(\frac{1}{2} m \left(\left(\sum_{i=1}^{L} \sigma_i^2\right) + m||\Sigma||_1\right)\right). \end{aligned} \tag{G.3.2}$$

From (G.3.2), we can obtain the PDF of instantaneous SNR at the output of SC as

$$f_{\gamma,\mathrm{SC,asym}}(\gamma) = \frac{Lm^{L(m-1)+1}}{\Gamma(m)^L}\gamma^{Lm-1}\exp\left(\frac{1}{2}m\left(\left(\sum_{i=1}^{L}\sigma_i^2\right) + m||\Sigma||_1\right)\right). \tag{G.3.3}$$

Appendix H

ARDO of MRC

From the PDF in (G.1.12), we observe that the Nakagami parameter m and the number of branch L determine the diversity order, while the parameters in lognormal PDF only appear in the exponential component. The diversity order is dominated by the Nakagami RV because the lognormal PDF has undefined diversity order near its origin. Therefore the information of lognormal PDF is only contained in the exponential component in (G.1.12). In order to obtain the ARDO of MRC combined lognormal channel states, we have to compensate the impact of the Nakagami variable on the diversity order of the system. Therefore we can set $m_1 = Lm_L$, which makes the Nakagami contributed diversity order to be identical for single-branch and multiple-branch systems. Then we can cancel out the contribution of the Nakagami variable by setting $m_L \to \infty$, and obtain the ARDO as

$$\begin{aligned} ARDO = & \lim_{m_L \to \infty} \frac{\left(\frac{1}{2} L m_L \left(\sigma_1^2 + L m_L \sigma_1^2\right)\right)}{\frac{1}{2} m_L \left(\left(\sum_{i=1}^{L} \sigma_i^2\right) + m_L ||\Sigma||_1\right)} \\ = & \frac{L^2 \sigma_1^2}{||\Sigma||_1}. \end{aligned} \tag{H.0.1}$$